DISSERTATION ZUR ERLANGUNG DES DOKTORGRADES
DER FAKULTÄT FÜR CHEMIE UND PHARMAZIE
DER LUDWIG – MAXIMILIANS - UNIVERSITÄT MÜNCHEN

DEVELOPMENT AND CHARACTERIZATION OF IN-VITRO MODELS FOR FILAGGRIN ASSOCIATED SKIN DISEASES

Kay Strüver

aus

Leipzig

2018

ERKLÄRUNG

Diese Dissertation wurde im Sinne von §7 der Promotionsordnung vom 28. November 2011 von Herrn Prof. Dr. Wolfgang Frieß betreut.

EIDESSTATTLICHE VERSICHERUNG

Diese Dissertation wurde eigenständig und ohne unerlaubte Hilfe erarbeitet.

Berlin, den 24.10.2018

Kay Strüver

Dissertation eingereicht am: 04.09.2018

1. Gutachter: Prof. Dr. Wolfgang Frieß

2. Gutachter: Prof. Dr. Sarah Hedtrich

Mündliche Prüfung am: 23.10.2018

Für Karsten und Simone

DANKSAGUNG

Die vorliegende Doktorarbeit wurde in im Zeitraum von Juli 2012 bis April 2016 im Department Pharmazie an der Ludwig-Maximilians-Universität (LMU) in München, am Lehrstuhl für Pharmazeutische Technologie und Biopharmazie, angefertigt. Die Anfertigung der Arbeit erfolgte in Zusammenarbeit mit dem Institut für Pharmazie der Freien Universität Berlin, Fachbereich Pharmakologie und Toxikologie.

Gleichermaßen möchte ich deshalb meinem Doktorvater und Betreuer Professor Dr. Wolfgang Frieß und meiner Betreuerin Professorin Dr. Sarah Hedtrich (geb. Küchler) für die Möglichkeit zum Durchführen dieser Arbeit, für die Mitarbeit in ihren Arbeitskreisen und die hervorragende wissenschaftliche Betreuung bedanken. Besonders für die Möglichkeit zum interdisziplinären Austausch während diverser Forschungsaufenthalte am Institut für Pharmazie der Freien Universität Berlin, bin ich ihnen sehr dankbar. Ohne diese Forschungsaufenthalte wäre die Anfertigung dieser Arbeit in dieser Form nicht möglich gewesen.

Bedanken möchte ich ebenfalls bei Dr. Stefan Schreml und Dr. Robert Meier von der Universität Regensburg für die zusammen durchgeführten pH-Messungen an Hautmodellen. Genauso möchte ich mich bei Dominica für die sehr gute methodische Einarbeitung bedanken.

Großer Dank gebührt auch meinen beiden Masterstudenten Frida und Ramona für die Unterstützung und den wissenschaftlichen Beitrag.

Spezieller Dank geht an meine Laborpartnerin Madeleine für die wissenschaftliche Hilfestellung in der Anfangszeit und die Durchführung der UCA/PCA-Messungen, sowie an die beiden wunderbaren Laborpartner Verena und Christoph für die gemeinsame Zeit.

An dieser Stelle möchte ich mich ganz ausdrücklich bei allen Kollegen der Arbeitsgruppen von Professor Frieß, Professor Winter, Professorin Merkel, Professorin Schäfer-Korting, Professor Weindl und Professorin Hedtrich für die exzellente Zusammenarbeit, die wissenschaftlichen Diskussionen und die Freizeitaktivitäten, welche weit über ein rein berufliches Verhältnis hinausgingen, bedanken.

Explizit bedanken muss und vor allem möchte ich mich dabei bei Kerstin und Laura für die moralische Unterstützung und Hilfe in den schwierigen Zeiten, sowie bei Leo, Stefan und Guy für die nicht aufzuwiegende Unterstützung während der letzten Jahre.

Besonderer Dank gebührt natürlich Matze, welcher mich seit dem ersten Tag meiner akademischen Laufbahn begleitet hat und auch maßgeblich zu meiner Bewerbung in München beigetragen hat. Neben dem wissenschaftlichen Austausch möchte ich mich vor allem für seine Freundschaft bedanken.

Zu guter Letzt möchte ich der absoluten Dankbarkeit gegenüber meiner Eltern Ausdruck verleihen. Vielen Dank für die Hilfe, Förderung und Liebe.

TABLE OF CONTENT

LIST OF TABLES

LIST OF FIGURES

LIST OF ABBREVIATIONS

AD	ATOPIC DERMATITIS
AS	α-HYDROXY SPHINGOSINE
ATR	ATTENUATED TOTAL REFLECTANCE
BSA	BOVINE SERUM ALBUMIN
Cer	CERAMIDE
Chol	CHOLISTEROL
CholS	CHOLESTEROL SULFATE
EDC	EPIDERMAL DIFFERENTIATION COMPLEX
EOS	CERAMIDE 1
FFA	FREE FATTY ACIDS
FLG	FILAGGRIN
FTIR	FOURIER TRANSFORM INFRARED
GCer	GLUCOCERAMIDE
GCerase	β-GLUCOCEREBROSIDASE
GSph	GLUCOSYLSPHINGOSINE
H&E	HEMATOXYLIN-EOSIN
IL	INTERLEUKIN
IV	ICHTHYOSIS VULGARIS
KD	KNOCK DOWN
NHE-1	SODIUM HYDROGEN EXCHANGER 1
NP	PHYTOCERAMIDE
NS	NON-HYDROXY SPHINGOSINE
PBS	PHOSPHATE-BUFFERED SALINE
PCA	PYRROLIDON-5-CARBOXYLIC ACID
PL	PHOSPHOLIPID
RHE	RECONSTRUCTED HUMAN EPIDERMIS
RT-PCR	REVERSE TRANSCRIPTION POLYMERASE CHAIN REACTION
SC	STRATUM CORNEUM
SM	SPHINGOMYELIN
SMase	SPHINGOMYELINASE
SPC	SPHINGOSYLPHOSPHORYLCHOLIN
sPLA	SECRETED PHOSPHOLIPASES A
TSLP	THYMIC STROMAL LYMPHOPOIETIN
UCA	UROCANIC ACID

1 GENERAL INTRODUCTION

1.1 SKIN

1.1.1 STRUCTURE AND FUNCTION

Knowledge of the skin's exact structure and function is crucial to understand skin diseases and to develop new therapeutic options. In general, skin has the extremely important function to provide a barrier between body and the environment. Skin protects us from environmental factors such as pathogens, chemicals, noxious physical and mechanical insults. It is necessary to regulate the body temperature and to prevent excessive loss of water. Furthermore, the skin is an enormous sensory organ with millions of different nerve endings that let our body feel touch, pain or heat [1,2]. To fulfill these function, the skin has a specific structure. In general, skin or cutis is divided into two main layers: the epidermis and dermis (Fig. 1). The underlying subcutis does not belong morphologically to the actual skin, although its fatty tissue supports the skin's function [3].

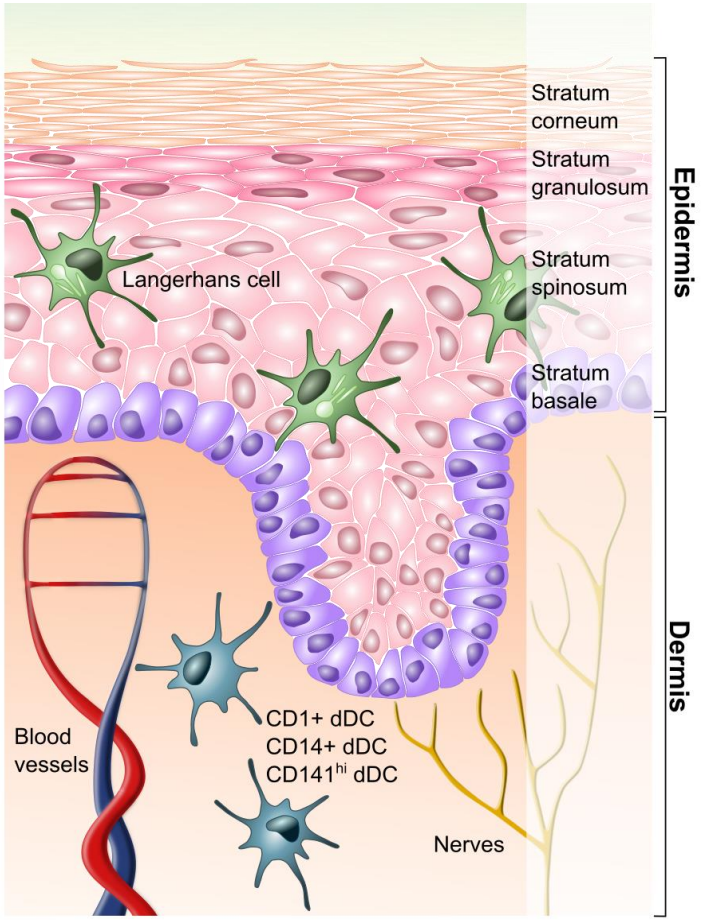

Figure 1-1 *Structure of the skin including antigen presenting cells. Taken from Engelke et al., 2015 [4].*

The epidermis – the outer stratum of the skin – is an avascular and multilayered epithelium. Adnexa like hairs, glands and nails belong to the epidermis. The thickness varies between 40 µm and 700 µm that may vary with mechanical exposure. For example, palms and soles have a pronounced epidermis with an additional layer – the stratum lucidum – and a depth of up to 700 µm while the skin of eyelids, on the other hand, exhibit the thinnest epidermis with a thickness of approximately 40 µm [5]. The epidermis consists to up to 95% of keratinocytes.

Other cells are melanocytes, Langerhans cells, Merkel cells and occasionally inflammatory cells [3,6]. The multilayered structure of the epidermis is based on the keratinocytes differentiation process of the keratinocytes. Starting from the outermost layer, the epidermis consists of the stratum corneum, stratum granulosum, stratum spinosum and stratum basale (see Figure 1) [1,3]. The stratum corneum (SC) is the main barrier of the skin.

Fully differentiated, cornified, anucleated and flattened keratinocytes – also called corneocytes – are surrounded by a lipid multilayer, which in a healthy state, provide a very effective barrier. The intracellular lipids consist of 30% ceramides, 30% free fatty acids (FFA) plus cholesterol and its derivatives. Important to structural integrity are the long-chained ceramide esters [7]. Initially, Elias stated the brick and mortar model to describe the structure and function of the stratum corneum [8]. However, during the last two decades this model was revised. Four major structures contribute to the barrier function of the skin. First, cavities of corneocytes jam the corneocytes into each other. The second important structure are corneodesmosomes, transmembrane proteins that rivet corneocytes together. The corneocytes with cavities and the corneodesmosome connections form an intercellular scaffold for the highly ordered lipid bilayer, the third structure. Finally, tight junctions attach the SC to the viable part of the epidermis [9].

The stratum lucidum only occurs on the sole of the foot and the palm of the hand. This additional layer has the function to reduce shear forces and friction on these very stressed body parts [3]. The stratum granulosum consists of two to four layers of keratinocytes that exhibit microscopically visible granules. These granules contain precursors of the lipid lamellae of the stratum corneum. The stratum spinosum contains the daughter cells of the basal layer, which show a polygonal form. Usually, the dimension of the stratum spinosum includes four to eight layers of keratinocytes. Langerhans cells are also present within the stratum granulosum and spinosum. The Langerhans cells have a dendritic shape and are part of the immune system. They absorb invading antigens and then present these to the immune system [1,3]. The regeneration of the epidermis occurs in the stratum basale. This layer is made of cylindric keratinocytes with ovoid nuclei. Besides the regeneration, the stratum basale is also involved in melanin production. In between the keratinocytes are dendritic melanocytes, which produce melanin and eumelanin. Melanin pigments serve as an

UV light filter and protect the body from UV radiation, converting 99.9% of the harmful radiation harmless heat. In addition, the basal layer also contains Merkel cells. This cell type is associated with unmyelinated nerve endings and is responsible for sensory perception [3].

The dermis is located underneath the stratum basale. The connection of the dermal-epidermal junction is also called basement membrane. Keratinocytes from the basal layer are attached to this basement membrane by the anchoring filaments of hemidesmosomes that consist of integrins. The dermal side is connected to the basement membrane via collagen type VII filaments [10].

The dermis is a connective tissue and consists mostly of fibroblasts surrounded by collagen, elastic fibers, hyaluronic acid and proteoglycans. The dermis can also be distinguished by distinct layers. The top lying papillary dermis is relatively thin and is composed of a loose and fine meshwork of fibers. The lower reticular dermis is much thicker and denser with fibers arranged in parallel to the skin surface. In contrast to the epidermis, the dermis is a vascularized tissue and supplies the epidermis with nutrients, water and partly oxygen via diffusion [3,11].

1.1.2 Skin Differentiation

To achieve the described multilayer structure of the skin, the epidermis undergoes a complex process of proliferation and differentiation. The so called epidermal differentiation complex (EDC) plays a major role in this genetically driven process of skin differentiation [12–14]. The EDC is a region on the chromosome 1q21, which contains multiple genes responsible for skin differentiation. The precise regulation of this gene cassette is crucial for the proper maintenance of the skin barrier. The over 50 different EDC genes can be clustered in 3 families, the cornified envelope precursor family, the S100 protein family and the S100 fused type protein family [14,15].

Stem cell keratinocytes, which are mitotically active, preserve the self-renewing capability of the skin. Following mitosis, their daughter cells detach from the stratum basale and start an ordered process of differentiation. The keratinocytes become flatter, larger and take on a polyhedral form. Gene expression changes during their

migration through the epidermis. While in the stratum basale the proteins keratin 5, 14 and 15 are present in keratinocytes, the transcription of keratins 1 and 10 is favourer in the spinous layer. Later, keratin 2 also accrues in the stratum spinosum [15]. In the stratum granulosum, the keratins built in the spinous layer remain present and the keratinocytes flatten further. Basophilic keratohyalin granules are microscopically visible in the cytoplasm. They contain keratin filaments, loricrin and the polyprotein profilaggrin (see Fig. 2) [16].

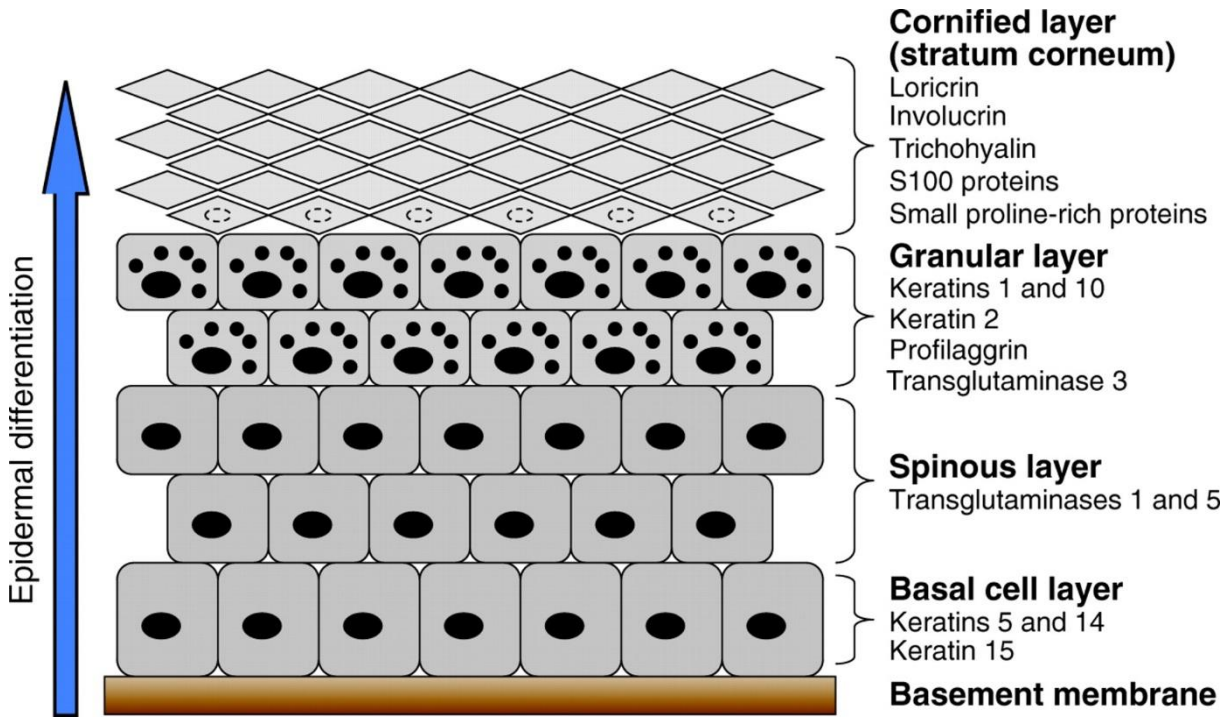

Figure 1-2 *Epidermal differentiation. Taken from Sandilands et al., 2009 [17].*

The proteins filaggrin and its precursor profilaggrin play a major role in skin differentiation. Profilaggrin consist of a S100-like calcium binding domain and a nuclear localization domain at the N-terminus, 10 to 12 similar filaggrin monomers in the middle of the polyprotein, and a specific C-terminal domain [18]. The calcium binding domain enables the regulation of terminal skin differentiation via calcium dependent events. The nuclear localization domain facilitates entry in to the nucleus and plays a role during enucleation. The domain at the C-terminus contributes to the processing of profilaggrin to filaggrin. The overall molecular weight of profilaggrin is over 400 kDa. The histidine rich protein filaggrin is released after dephosphorylation and degradation [18]. By assembling keratin filament aggregates, filaggrin, profilaggrin, involucrin, loricrin and further structural proteins and subsequently crosslinking these with disulfide bonds, the cornified envelope is created. In addition, skin lipids are accumulated within the lamellar bodies. In the final step, the disintegration of the nuclei, the cell membrane and further organelles takes place. The lamellar bodies release the lipids into intercellular space, forming an ordered lipid matrix. Together with the linked corneocytes, this forms the skin barrier [18,19].

Besides the cornified envelope, filaggrin further contributes to the skin’s barrier function. In the upper SC, filaggrin is degraded to release amino acids; mostly histidine. The amino acids are part of the skin’s natural moisturizing factor. The released histamine is partly metabolized to trans urocanic acid (UCA) and pyrolidone-5-carboxylic acid (PCA). The cis-enantiomer of UCA has an immunomodulatory effect in keratinocytes and leucocytes, and UCA and PCA contribute to UV photoprotection [18]. In addition, the participation of UCA and PCA to skin acidification is discussed [20–23] and detailed investigations are part of this thesis. The described functions of profilaggrin and filaggrin have a strong influence on a sound skin function and barrier. Notably reduced amounts of filaggrin are linked to skin disorders and diseases.

1.2 Filaggrin-related Skin Diseases

1.2.1 Ichthyosis Vulgaris

Ichthyosis vulgaris (IV), also known as autosomal dominant ichthyosis, is the most common form of ichthyosis. Phenotypic characteristics of IV are palmar hyper-linearity, lichen pilaris and fine scales over the lower abdomen, arms, and legs. IV is a single gene disorder and caused by filaggrin null mutations [24,25]. More than 40 truncating *FLG* mutations are described in literature, including Asian- and European-specific mutations. The most common loss-of-function *FLG* mutations in Europe are R501X and 2282del4 [26]. Heterozygous mutation of R501X or 2282del4 leads to a mild form of IV, while homozygous mutations lead to severe forms of IV. Heterozygous R501X/2282del4 mutations are also known and lead to severe cases of IV [27].

As the polyprotein profilaggrin is the major component of those granules found in the granular layer of the epidermis, the histological absence of this layer in severe forms of profilaggrin null IV is not surprising [24,25,28]. Furthermore, the lack of profilaggrin and coherent filaggrin leads to a disordered lamellar bilayer in the SC that in turn causes the impaired barrier function often found in patients with IV [27].

1.2.2 Atopic Dermatitis

Atopic dermatitis (AD) or atopic eczema is a highly pruritic, chronic inflammatory skin disorder and a very common dermatological disease. Its prevalence is up to 20 % in children [29] and up to 7 % in adults [30] with particular prevalence in in industrialized countries. The onset of AD occurs earlier than at the age of 5 in more than 70% of all cases, and the intensity of the disease symptoms often diminish with age, frequently vanishing by adolescence. Furthermore, 40% of patients with AD exhibit systemic atopic comorbidities such as allergic rhinitis, asthma or IgE related food allergies [26,31]. AD varies from mild acute forms to severe chronic forms with high impact on quality of life. This occurs owing to the multifactorial disease pattern of AD in which genetic, environmental and immunological factors all play prominent roles [32,33]. FLG null mutation is the major predisposing factor for AD but, notably, not all patients with AD carry mutations in the *FLG* gene.

Despite the high and still increasing prevalence of AD, its pathogenesis remains poorly understood. One decade ago, there was a change in basic assumptions. Whereas previously AD was thought to be an immune-mediated disorder, the fact that skin barrier deficiencies play a prominent role required re-evaluation of the disease [34]. The immunological constituent, associated with elevated levels of IgE, caused mainly by the T-cell cytokines IL-4 and IL-13, was well established [35,36]. This progression starts with elevated levels of Th17 associated cytokines followed by increased levels of Th2 cytokine family members like the aforementioned IL-4 and IL-13. The contribution of increased thymic stromal lymphopoietin (TSLP) levels was also recognized [37]. Since then, barrier function impairment has come into focus as a primary cause for AD [34,38,39]. Nevertheless, TSLP and further cytokines like IL-33 and IL-25 strongly contribute to the atopic diseases and drive the progression from AD to asthma [40]. In 2006, Palmer and colleagues described loss-of-function variants of FLG such as caused by the null mutations R501X and 2282del4, as the main predisposing factors for AD, with up to 40% of all patient with AD having loss-of-function variants of FLG [25,41]. The impaired barrier function of the skin leads to enhanced trans-epidermal water loss and the entry of allergens and irritants through the epidermis. Those allergens and irritants in turn trigger the Th2 and Th22 immune response. The following inflammation of the skin decreases the barrier function even further.

Besides the *FLG* null mutations, further genetic factors can contribute to AD. Polymorphisms of desmosomes or, for example, mutations of the serine peptidase inhibitor Kazal type 5 (SPINK5) can also lead to an impaired skin barrier. Relevant single nucleotide polymorphisms in the Th2 cytokine family can also lead to higher expression rates of IL-4 and IL-13, which trigger the immune-mediated part of the disease [42,43]. In addition, IL-4 and IL-13 also themselves reduce the expression rate of *FLG* and helps explains the reduce FLG amounts in all AD patients, independent from the genomic aberrations [44,45].

The lack of filaggrin and its impact on skin disease like IV and AD were a major focus of this thesis. For this purpose, reconstructed skin models, including new skin disease models, were to be investigated and developed.

1.3 *IN VITRO* SKIN MODELS

1.3.1 GENERAL OVERVIEW

Various *in vitro* test systems are available to investigate skin physiology, skin diseases and drug application routes through the skin [46]. The general complexity of *in vitro* skin models increases with higher relevance for research and drug development (Figure 3) [47]. For example, monolayer cell culture of keratinocytes is used for basic drug substance response investigations and comparison of cytokine profiles from healthy and unsound donors [48]. More complex formats like co-culturing of keratinocytes and fibroblast enable insights into cellular crosstalk and improves the significance of those models. Two decades ago, Sato et. al already showed the benefits of keratinocyte-fibroblast coculturing [49]. Nevertheless, 2D cell culture technique has obvious limitations, e.g. investigation of the barrier function or permeability of active compounds or allergens [50].

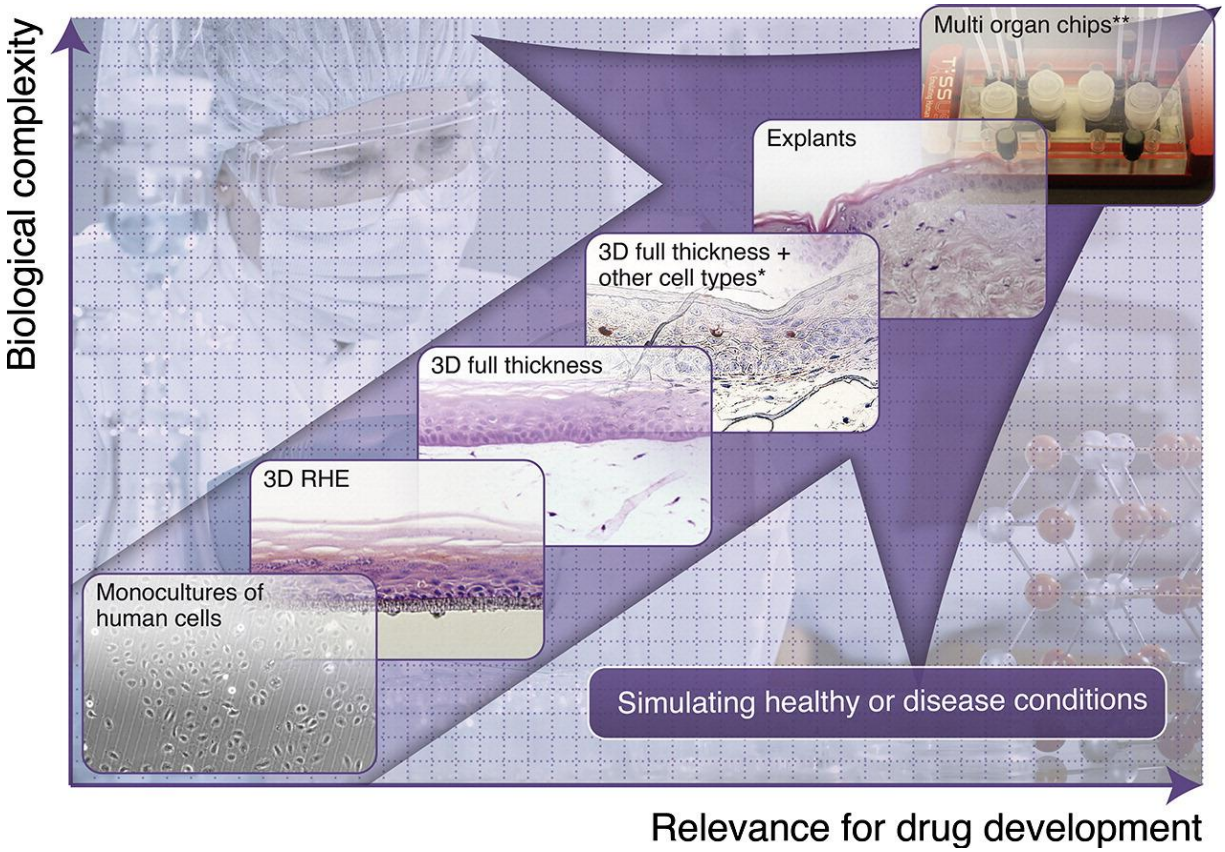

Figure 1-3 *General correlation of in vitro model complexity and relevance for drug development (RHE – reconstructed human epidermis). Taken from Mathes et al., 2014 [47].*

The more complex reconstructed human epidermis (RHE) models and full thickness skin models mimic the physiology of human skin adequately and are partly validated for skin irritation, corrosions and phototoxicity tests [51–54]. RHE models were one of the earliest skin models based on tissue engineering. The development derived from skin grafts to treat chronic or burn wounds. As the name already indicates, these models consist of differentiated keratinocytes. To generate these models, it is possible to use primary keratinocytes as well as keratinocyte cell lines. Usually primary cells or immortalized cells are cultivated and proliferated with standard cell culture procedures [55]. The cultivated cells are then transferred to special inserts. After overnight incubation, these inserts are lifted to an air-liquid interface and the medium is changed from a growing medium to a differentiation medium. Caused by the medium and the air contact, keratinocytes start to differentiate. After seven to 14 days, all layers of the epidermis are visible in a microscope section.

RHE models are useful for different applications, including drug permeation studies and investigations on the impact of genetic modifications on the barrier function [56]. Pendaries et al. used mRNA interference in RHE models to investigated the influence of filaggrin on skin differentiation to further conclude about the pathophysiology of AD [57]. Furthermore, Danso et al. used cytokine treated RHE models to mimic AD and an impaired skin barrier [58]. Possible application for those models are screening tests for new AD treatments.

Full-thickness models further contains a dermis equivalent with incorporated fibroblasts. These advanced models offer the benefit of fibroblasts attachment together with surrounding polymers as well as growing and differentiation of the keratinocytes [59,60]. One further advantage is the possibility to include additional cells in the skin model. For example, the incorporation of immune cells can help to mimic the multifactorial disease pattern of AD. Engelhart et al. included activated T-cells in reconstructed full-thickness skin models and could reproduce atopic hallmarks in reconstructed skin [61]. Wallmeyer et al. even combined genetically modified filaggrin deficient models with the exposure of activated T-cell to gain new insights into AD, like the roll of TSLP [62].

Nevertheless, reconstructed skin models exhibit several limitations and disadvantages. In general, the permeability of reconstructed skin models is higher, and their

mechanical resistance lower as compared to human or animal skin [63]. This can be explained by an inferior lipid organization, altered ceramide profiles and lower expression of skin differentiation markers. Furthermore, the characteristics are strongly dependent on the culture conditions of the generated models. In contrast to human or animal tissue, reconstructed skin lacks mechanical stimuli associated with daily activities of living. Bioreactors for skin models are a promising tool to overcome those obstacles.

1.3.2 Bioreactors for Skin models

Bioreactors are a promising tool to provide a complex growing environment to further improve the concept of tissue engineering [64]. The term bioreactor comprises multiple laboratory tissue-engineering devices. They are designed to introduce an active and controllable growing environment to improve the tissue properties [65]. In general, bioreactors can help to reduce manual tasks, to speed up cell expansion, decrease costs and standardize growing conditions. For example, bioreactors introduce a laminar flow of medium, diffusion limitations can be reduced, and the mass transport of nutrients is optimized. In addition, mechanical forces, like stretching or shear stress, increase cell density and tissue robustness. This is caused by modulation of the cell physiology and by increasing the biosynthetic activity of cells [66]. For example, osteoblasts exhibit higher amounts of specific cross-linked proteins like actin or filamin after exposure to fluid shear stress [67]. The exact physiological process by applying fluid shear stress is not completely understood.

The pioneers of bioreactors for skin are found in anaplasty. To treat ulcers or burn wounds, plastic surgeons often use split-thickness skin grafts. However, the expansion of skin comes along with the lack of elasticity, contraction, and scarring. To overcome those obstacles, bioreactors were used to improve the growing conditions and finally the quality of skin grafts [68,69].

Applications for bioreactors in tissue engineering of skin constructs are cell expansion or the generation and maturation of the construct [63]. Today, the most common bioreactors for the maturation phase are designed like flow-through platforms. While the skin construct can grow at an air-liquid interphase, a medium flow is applied below

the construct [68,70]. Often these flow-through platforms are connected to peristaltic pumps and the whole assembly is stored in a common cell culture incubator to maintain general growing conditions like temperature, humidity, and carbon dioxide concentration.

The combination of tissue engineering, genetic modifications and bioreactors enables the development of highly complex skin disease models, which more closely resemble the characteristics of *in-vivo* models. Step by step it is possible to gain new insights in skin disease and to avoid animal models, which come with ethical concerns.

1.4 REFERENCES

1 Proksch E, Brandner JM, Jensen JM: The skin: An indispensable barrier. Exp Dermatol 2008;17:1063–1072.

2 Montagna W, Parakkal PF: 1 – An Introduction to Skin; in : The Structure & Function of Skin. 1974, pp 1–17.

3 Vaupel P, Schaible H-G, Mutschler E: Anatomie, Physiologie, Pathophysiologie des Menschen. ed 6th Wissenschaftliche Verlagsgesellschaft, 2007.

4 Engelke L, Winter G, Hook S, Engert J: Recent insights into cutaneous immunization: How to vaccinate via the skin. Vaccine 2015;33:4663–4674.

5 Lee Y, Hwang K: Skin thickness of Korean adults. Surg Radiol Anat 2002 Jan 1;24:183–189.

6 Montagna W, Parakkal PF: 2 – The Epidermis; in : The Structure & Function of Skin. 1974, pp 18–74.

7 Neubert, R. H. H., Wohlrab, W. A., Marsch WA: Dermopharmazie. Stuttgart, Wiss. Verlagsges. GmbH, 2001.

8 Elias PM: The permeability barrier in mammalian epidermis. J Cell Biol 1975 Apr 1;65:180–191.

9 Pfeiffer S, Vielhaber G, Vietzke J-P, Wittern K-P, Hintze U, Wepf R: High-Pressure Freezing Provides New Information on Human Epidermis: Simultaneous Protein Antigen and Lamellar Lipid Structure Preservation. Study on Human Epidermis by Cryoimmobilization. J Invest Dermatol 2000 May;114:1030–1038.

10 Briggaman RA, Dalldorf FG, Wheeler CE: Formation and origin of basal lamina and anchoring fibrils in adult human skin. J Cell Biol 1971;51:384–395.

11 Montagna W, Parakkal PF: 4 – The Dermis; in : The Structure & Function of Skin. 1974, pp 96–141.

12 Mischke D, Korge BP, Marenholz I, Volz A, Ziegler A: Genes Encoding Structural Proteins of Epidermal Cornification and S100 Calcium-Binding Proteins Form a Gene Complex (“Epidermal Differentiation Complex”) on Human Chromosome 1q21. J Invest Dermatol 1996 May;106:989–992.

13 Hoffjan S, Stemmler S: On the role of the epidermal differentiation complex in ichthyosis vulgaris, atopic dermatitis and psoriasis. Br J Dermatol 2007 Sep;157:441–449.

14 Kypriotou M, Huber M, Hohl D: The human epidermal differentiation complex: cornified envelope precursors, S100 proteins and the “fused genes” family. Exp Dermatol 2012 Sep;21:643–9.

15 Elias PM, Largman C: Epidermal Differentiation 1999;796–801.

16 Steinert PM, Marekov LN: The proteins elafin, filaggrin, keratin intermediate filaments, loricrin, and small proline-rich proteins 1 and 2 are isodipeptide cross-linked components of the human epidermal cornified cell envelope. J Biol Chem 1995 Jul 28;270:17702–11.

17 Sandilands A, Sutherland C, Irvine AD, McLean WHI: Filaggrin in the frontline: role in skin barrier function and disease. J Cell Sci 2009 May 1;122:1285–1294.

18 Brown SJ, McLean WHI: One remarkable molecule: filaggrin. J Invest Dermatol 2012 Mar;132:751–62.

19 Nemes Z, Steinert PM: Bricks and mortar of the epidermal barrier. Exp Mol Med 1999 Mar 31;31:5–19.

20 Fluhr JW, Elias PM: Stratum corneum pH: Formation and Function of the “Acid Mantle.” Exog Dermatology 2002;1:163–175.

21 Hachem J-P, Crumrine D, Fluhr J, Brown BE, Feingold KR, Elias PM: pH directly regulates epidermal permeability barrier homeostasis, and stratum corneum integrity/cohesion. J Invest Dermatol 2003 Aug;121:345–53.

22 Fluhr JW, Behne MJ, Brown BE, Moskowitz DG, Selden C, Mao-Qiang M, et al.:

Stratum corneum acidification in neonatal skin: secretory phospholipase A2 and the sodium/hydrogen antiporter-1 acidify neonatal rat stratum corneum. J Invest Dermatol 2004 Feb;122:320–9.

23 Fluhr JW, Elias PM, Man M-Q, Hupe M, Selden C, Sundberg JP, et al.: Is the filaggrin-histidine-urocanic acid pathway essential for stratum corneum acidification? J Invest Dermatol 2010 Aug;130:2141–4.

24 Smith FJD, Irvine AD, Terron-Kwiatkowski A, Sandilands A, Campbell LE, Zhao Y, et al.: Loss-of-function mutations in the gene encoding filaggrin cause ichthyosis vulgaris. Nat Genet 2006;38:337–342.

25 Palmer CN, Irvine AD, Terron-Kwiatkowski A, Zhao Y, Liao H, Lee SP, et al.: Common loss-of-function variants of the epidermal barrier protein filaggrin are a major predisposing factor for atopic dermatitis. Nat Genet 2006 Apr;38:441–6.

26 Irvine AD, McLean WHI, Leung DYM: Filaggrin Mutations Associated with Skin and Allergic Diseases. N Engl J Med 2011 Oct 6;365:1315–1327.

27 Thyssen JP, Godoy-Gijon E, Elias PM: Ichthyosis vulgaris: the filaggrin mutation disease. Br J Dermatol 2013 Jun;168:1155–66.

28 Blunder S, Rühl R, Moosbrugger-Martinz V, Krimmel C, Geisler A, Zhu H, et al.: Alterations in Epidermal Eicosanoid Metabolism Contribute to Inflammation and Impaired Late Differentiation in FLG-Mutated Atopic Dermatitis. J Invest Dermatol 2017 Mar;137:706–715.

29 Asher MI, Montefort S, Björkstén B, Lai CK, Strachan DP, Weiland SK, et al.: Worldwide time trends in the prevalence of symptoms of asthma, allergic rhinoconjunctivitis, and eczema in childhood: ISAAC Phases One and Three repeat multicountry cross-sectional surveys. Lancet 2006 Aug;368:733–743.

30 Silverberg JI: Public Health Burden and Epidemiology of Atopic Dermatitis. Dermatol Clin 2017 Jul;35:283–289.

31 Williams HC: Clinical practice. Atopic dermatitis. N Engl J Med 2005 Jun 2;352:2314–24.

32 Brown SJ: Atopic eczema. Clin Med 2016 Feb;16:66–9.

33 Williams HC: Is the prevalence of atopic dermatitis increasing? Clin Exp Dermatol 1992 Nov;17:385–91.

34 Elias PM, Hatano Y, Williams ML: Basis for the barrier abnormality in atopic dermatitis: outside-inside-outside pathogenic mechanisms. J Allergy Clin Immunol 2008 Jun;121:1337–43.

35 He J-Q, Chan-Yeung M, Becker AB, Dimich-Ward H, Ferguson AC, Manfreda J, et al.: Genetic variants of the IL13 and IL4 genes and atopic diseases in at-risk children. Genes Immun 2003 Jul;4:385–9.

36 Liu X, Nickel R, Beyer K, Wahn U, Ehrlich E, Freidhoff LR, et al.: An IL13 coding region variant is associated with a high total serum IgE level and atopic dermatitis in the German multicenter atopy study (MAS-90). J Allergy Clin Immunol 2000 Jul;106:167–70.

37 Brandt EB, Sivaprasad U: Th2 Cytokines and Atopic Dermatitis. J Clin Cell Immunol 2011 Aug 10;2. DOI: 10.4172/2155-9899.1000110

38 Boguniewicz M, Leung DYM: Atopic dermatitis: a disease of altered skin barrier and immune dysregulation. Immunol Rev 2011 Jul;242:233–46.

39 Novak N, Leung DYM: Advances in atopic dermatitis. Curr Opin Immunol 2011 Dec;23:778–83.

40 Han H, Roan F, Ziegler SF: The atopic march: current insights into skin barrier dysfunction and epithelial cell-derived cytokines. Immunol Rev 2017 Jul;278:116–130.

41 Rodríguez E, Baurecht H, Herberich E, Wagenpfeil S, Brown SJ, Cordell HJ, et al.: Meta-analysis of filaggrin polymorphisms in eczema and asthma: Robust risk factors in atopic disease. J Allergy Clin Immunol 2009 Jun;123:1361–1370.e7.

42 Broussard JA, Getsios S, Green KJ: Desmosome regulation and signaling in disease. Cell Tissue Res 2015 Jun;360:501–12.

43 Walley AJ, Chavanas S, Moffatt MF, Esnouf RM, Ubhi B, Lawrence R, et al.: Gene polymorphism in Netherton and common atopic disease. Nat Genet 2001 Oct;29:175–8.

44 Howell MD, Kim BE, Gao P, Grant A V, Boguniewicz M, Debenedetto A, et al.: Cytokine modulation of atopic dermatitis filaggrin skin expression. J Allergy Clin Immunol 2007 Jul;120:150–5.

45 Hönzke S, Wallmeyer L, Ostrowski A, Radbruch M, Mundhenk L, Schäfer-Korting M, et al.: Influence of Th2 Cytokines on the Cornified Envelope, Tight Junction Proteins, and ß-Defensins in Filaggrin-Deficient Skin Equivalents. J Invest Dermatol 2016 Mar;136:631–9.

46 Küchler S, Strüver K, Friess W: Reconstructed skin models as emerging tools for drug absorption studies. Expert Opin Drug Metab Toxicol 2013 Oct 5;9:1255–63.

47 Mathes SH, Ruffner H, Graf-Hausner U: The use of skin models in drug development. Adv Drug Deliv Rev 2014 Apr;69–70:81–102.

48 Giustizieri ML, Mascia F, Frezzolini A, De Pità O, Chinni LM, Giannetti A, et al.: Keratinocytes from patients with atopic dermatitis and psoriasis show a distinct chemokine production profile in response to T cell–derived cytokines. J Allergy Clin Immunol 2001 May;107:871–877.

49 Sato T, Kirimura Y, Mori Y: The Co-Culture of Dermal Fibroblasts with Human Epidermal Keratinocytes Induces Increased Prostaglandin E2 Production and Cyclooxygenase 2 Activity in Fibroblasts. J Invest Dermatol 1997 Sep;109:334–339.

50 Löwa A, Jevtic M, Gorreja F, Hedtrich S: Alternatives to animal testing in basic and preclinical research of atopic dermatitis. Exp Dermatol 2018 Jan 22; DOI: 10.1111/exd.13498

51 Ponec M, Boelsma E, Gibbs S, Mommaas M: Characterization of reconstructed skin models. Skin Pharmacol Appl Skin Physiol 2002 Jan;15 Suppl 1:4–17.

52 Auxenfans C, Fradette J, Lequeux C, Germain L, Kinikoglu B, Bechetoille N, et al.: Evolution of three dimensional skin equivalent models reconstructed in vitro by tissue engineering. Eur J Dermatol 2009;19:107–13.

53 Küchler S, Henkes D, Eckl K-M, Ackermann K, Plendl J, Korting H-C, et al.: Hallmarks of atopic skin mimicked in vitro by means of a skin disease model based on FLG knock-down. Altern Lab Anim 2011 Oct;39:471–80.

54 Bellas E, Seiberg M, Garlick J, Kaplan DL: In vitro 3D full-thickness skin-equivalent tissue model using silk and collagen biomaterials. Macromol Biosci 2012 Dec;12:1627–36.

55 Pruniéras M, Régnier M, Woodley D: Methods for cultivation of keratinocytes with an air-liquid interface. J Invest Dermatol 1983 Jul;81:28s–33s.

56 Netzlaff F, Lehr C-M, Wertz PW, Schaefer UF: The human epidermis models EpiSkin, SkinEthic and EpiDerm: an evaluation of morphology and their suitability for testing phototoxicity, irritancy, corrosivity, and substance transport. Eur J Pharm Biopharm 2005 Jul;60:167–78.

57 Pendaries V, Malaisse J, Pellerin L, Le Lamer M, Nachat R, Kezic S, et al.: Knockdown of filaggrin in a three-dimensional reconstructed human epidermis impairs keratinocyte differentiation. J Invest Dermatol 2014 Dec 13;134:2938–46.

58 Danso MO, van Drongelen V, Mulder A, van Esch J, Scott H, van Smeden J, et al.: TNF-α and Th2 Cytokines Induce Atopic Dermatitis–Like Features on Epidermal Differentiation Proteins and Stratum Corneum Lipids in Human Skin Equivalents. J Invest Dermatol 2014 Jul;134:1941–1950.

59 Smola H, Stark H-J, Thiekötter G, Mirancea N, Krieg T, Fusenig NE: Dynamics of Basement Membrane Formation by Keratinocyte–Fibroblast Interactions in Organotypic Skin Culture. Exp Cell Res 1998 Mar;239:399–410.

60 MacNeil S: Progress and opportunities for tissue-engineered skin. Nature 2007 Feb 22;445:874–80.

61 Engelhart K, El Hindi T, Biesalski H-K, Pfitzner I: In vitro reproduction of clinical hallmarks of eczematous dermatitis in organotypic skin models. Arch Dermatol Res 2005 Jul 15;297:1–9.

62 Wallmeyer L, Dietert K, Sochorová M, Gruber AD, Kleuser B, Vávrová K, et al.: TSLP is a direct trigger for T cell migration in filaggrin-deficient skin equivalents. Sci Rep 2017 Dec 4;7:774.

63 Schäfer-Korting M, Bock U, Gamer A, Haberland A, Haltner-Ukomadu E, Kaca M, et al.: Reconstructed human epidermis for skin absorption testing: results of the German prevalidation study. Altern Lab Anim 2006 Jun;34:283–94.

64 Hansmann J, Groeber F, Kahlig A, Kleinhans C, Walles H: Bioreactors in tissue engineering-principles, applications and commercial constraints. Biotechnol J 2013;8:298–307.

65 Freed LE, Guilak F, Guo XE, Gray ML, Tranquillo R, Holmes JW, et al.: Advanced tools for tissue engineering: scaffolds, bioreactors, and signaling. Tissue Eng 2006 Dec;12:3285–305.

66 Martin I, Wendt D, Heberer M: The role of bioreactors in tissue engineering. Trends Biotechnol 2004;22:80–86.

67 Jackson WM, Jaasma MJ, Tang RY, Keaveny TM: Mechanical loading by fluid shear is sufficient to alter the cytoskeletal composition of osteoblastic cells. Am J Physiol Physiol 2008 Oct;295:C1007–C1015.

68 Sun T, Norton D, Haycock JW, Ryan AJ, MacNeil S: Development of a closed bioreactor system for culture of tissue-engineered skin at an air-liquid interface. Tissue Eng 2005;11:1824–31.

69 Ladd MR, Lee SJ, Atala A, Yoo JJ: Bioreactor Maintained Living Skin Matrix. Tissue Eng Part A 2009 Apr;15:861–868.

70 Ataç B, Wagner I, Horland R, Lauster R, Marx U, Tonevitsky AG, et al.: Skin and hair on-a-chip: in vitro skin models versus ex vivo tissue maintenance with dynamic perfusion. Lab Chip 2013 May 14; DOI: 10.1039/c3lc50227

2 AIM OF THE THESIS

The aim of the present thesis was to gain detailed insights into the role of FLG in FLG related skin disease like AD. Based on the knowledge about the lack of FLG in IV and AD, the focus of this thesis was to characterize and further develop *in vitro* models for FLG related skin disease. Significant disease models are crucial to improve the understanding of the pathophysiology and to establish new therapeutic strategies.

First, the overall impact of FLG mutations in AD was to be investigated, including an intensive characterization of the previously for this purpose established FLG knock-down models. Skin surface pH, gene expression of relevant proteins, skin lipid profiles and the barrier function were to be analyzed in detail comparing sound and disease models. The gained knowledge should help to distinguish between barrier related and immune related pathogenic factors in AD.

Based on the results, the interplay between the different contributors to the acidic surface pH of the skin was to be further analyzed. Beside the FLG knock down model, the goal was the establishment of a NHE-1 knock down and a FLG/NHE-1 double knock down model and to carry out a comparison of the surface pH between all these models.

Developing the reconstructed *in vitro* skin models demonstrated the need for further improvement. Amongst other differences, the models exhibit less mechanical resistance and a weaker barrier function compared to *in-vivo* skin. Therefore, the goal for the last part was to develop a perfusion bioreactor for skin cultivation and to carry out a detailed characterization of the obtained dynamic models regarding barrier function and expression of relevant skin differentiation factors.

3 Filaggrin Deficiency Leads to Impaired Lipid Profile and Altered Acidification Pathways in a 3 D Skin Construct

The following section has been published in the Journal of Investigative Dermatology and appears in this thesis with the journal`s permission:

Project idea: S. Hedtrich (née Küchler)
Design of experiments: S. Hedtrich (née Küchler), K. Vávrová, D. Henkes, K. Strüver
Performed experiments: D. Henkes, K. Strüver, M. Witting, B. Skolova, M. Sochorova, S. Schreml, R.J. Meier
Data analysis: S. Hedtrich (née Küchler), K. Vávrová, D. Henkes, J.W. Fluhr, W. Friess, M. Schäfer-Korting
Manuscript writing: S. Hedtrich (née Küchler), K. Vávrová
Manuscript revision: S. Hedtrich (née Küchler), K. Vávrová

Personal contribution: The UCA and PCA determination in a time depended manner was carried by me with the help of Madeleine Wittig. All PCR studies for the days 4 and 7 were carried out by me, for day 14 by Dominika Henkes and me. All pH measurements were performed by me with the help of Robert Meier. Furthermore, I performed the skin penetration studies.

3.1 ABSTRACT

Mutations in the *FLG* gene are strongly associated with common dermatological disorders such as AD. However, the exact underlying pathomechanism is still ambiguous. Here, we investigated the impact of FLG on skin lipid composition, organization and skin acidification using a *FLG* knock down (*FLG*-) skin construct. Initially, NHE-1 activity was sufficient to maintain the acidic pH (5.5) of the reconstructed skin. At day 7, the FLG degradation products UCA and PCA were significantly decreased in the *FLG*- but the skin surface pH was still physiological due to an upregulation of NHE-1. At day 14, secretory phospholipase A_2 ($sPLA_2$) IIA, which is converting phospholipids to fatty acids, was significantly more activated in the *FLG*- than in *FLG*+. Although NHE-1 and $sPLA_2$ were able to compensate the FLG deficiency, maintain the skin surface pH and ensured ceramide processing (no differences detected), an accumulation of FFA (twofold increase) led to less ordered intercellular lipid lamellae and higher permeability of the *FLG*- constructs. The interplay of the UCA/PCA and the $sPLA_2$/NHE-1 acidification pathways of the skin and the impact of FLG insufficiency on skin lipid composition and organization in reconstructed skin, to our knowledge previously unreported, are described.

3.2 INTRODUCTION

FLG loss-of-function mutations contribute to several dermatological disorders such as IV and AD [1,2]. Mutations in the *FLG* gene are the most-widely occurring genetic risk factors for AD known to date and have been identified in up to 20-40 % of the patients [2–4]. Although *FLG* mutations are the most common mutations in these skin disorders, still the overall impact on the pathogenesis is not understood in full.

FLG is crucial for the adequate development of the epidermal structure and barrier function [1]. It is ultimately degraded to its component amino acids including histidine. These amino acids are highly hygroscopic and are the major components of the "natural moisturizing factor" which is crucial for epidermal hydration and barrier function [5]. Histidine is of particular importance as it is eventually metabolized to UCA and PCA which contribute to the acidification of the SC via the "histidine-to-UCA/PCA pathway" [6,7]. Furthermore, due to the importance of the acidic pH for the formation of the 'acidic mantle' other pathways contribute to its formation [8]. This includes the NHE-1 and the "phospholipid (PL)-to-FFA pathway" via secreted phospholipases ($sPLA_2$) [6,9]. However, until now the interplay and impact of the single pathways on the formation of the acidic skin surface pH remains unclear. The acidic mantle is a prerequisite for the formation of ceramides (Cer), i.e., the most important lipid class in the SC intercellular lipid matrix, and, thus, directly influences the skin barrier development: In the SC the ß-glucocerebrosidase (GCerase) and acid sphingomyelinase (SMase) metabolize glycosylceramides (GCer) and sphingomyelin (SM) to Cer. Both enzymes require an acidic environment of pH ≤ 5.5 for their optimal activity [10]. Thus, a decreased production of UCA/PCA due to a lack of FLG could result in an increase of SC pH and, consequently, to a decreased Cer content. This assumption was underlined by the reduced Cer levels found in AD patients [11–15].

We have previously described a *FLG*- skin construct which exhibits disturbed epidermal maturation and differentiation, increased susceptibility to irritants and altered drug absorption [16]. In this study, we investigated how the lack of FLG influences the composition and organization of the SC lipids generated in *FLG*- constructs in comparison to normal skin constructs and isolated human SC and how skin absorption is influenced. Additionally, we determined the amount of UCA/PCA, the expression of

various $sPLA_2$ subtypes and of the sodium-hydrogen antiporter NHE-1, $sPLA_2$ activity and the skin surface pH in a time dependent manner to gain deeper insights in the mechanisms of skin acidification.

3.3 RESULTS

3.3.1 FLG- CONSTRUCTS CONTAIN SIGNIFICANTLY LESS UCA AND PCA COMPARED TO HEALTHY SKIN MODELS

The knock down efficiency of our *FLG*- constructs was 75.7 ± 2.83 % (n = 10, Figure S5). As expected, *FLG* knock down decreased the levels of the histidine degradation products PCA (*FLG*+ 0.45 ± 0.05 mmol/g protein; *FLG*- 0.22 ± 0.04 mmol/g protein) and UCA (*FLG*+ 0.018 ± 0.003 mmol/g protein; *FLG*- 0.011 ± 0.002 mmol/g protein) at day 14 (Supplementary Figure S1). Similar differences were detected at day 7, but *not* at day 4 (Figure S4). In comparison to human skin (UCA 0.210 ± 0.045 mmol/g protein; PCA 2.65 ± 0.42 mmol/g protein), PCA and UCA levels were reduced.

3.3.2 *FLG*- CONSTRUCTS SHOW SIGNIFICANT UPREGULATION OF NHE-1 AND sPLA$_2$ IIA

We found a significant upregulation of NHE-1 in the *FLG*- constructs compared to *FLG*+ starting at day 7. No significant differences were seen at day 4 on the mRNA (Figure 1 a) and protein level. sPLA$_2$ IIA was only found at day 14 in the constructs, its relative expression being significantly higher in the *FLG*- construct (Figure 1 a). The upregulation of sPLA$_2$ IIA and NHE-1 was further confirmed on the protein level (Figure 1 b). sPLA$_2$ -IB, -IIF, -V and -XIIA were detected, too, some of them are only expressed at day 14 and without statistically significant differences between *FLG*+ and *FLG-,* respectively (Supplementary Figure S2). Because of the relatively small difference in sPLA$_2$ IIA on mRNA level, we also checked for the activity of the enzyme detecting an about 55 % increased sPLA$_2$ activity in *FLG*- (36.28 ± 10.70 units/ml) compared to *FLG*+ (23.38 ± 7.70 units/ml).

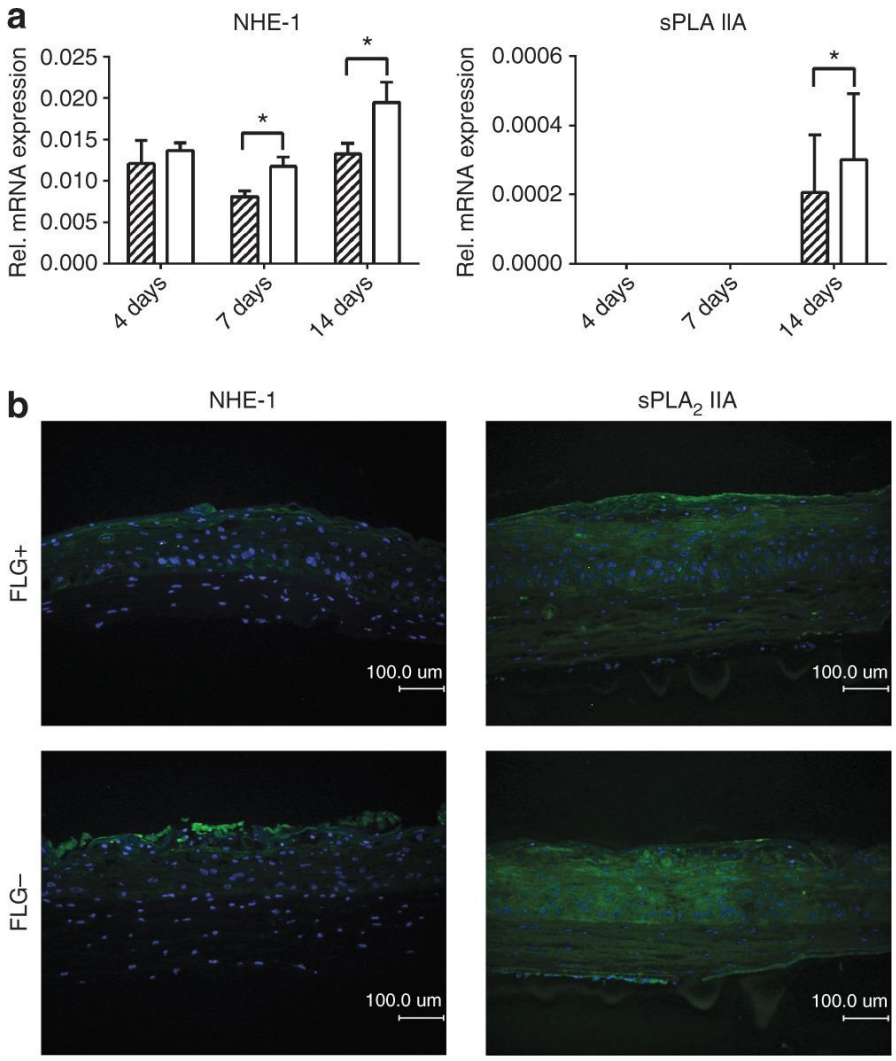

Figure 3-1 *Sodium/hydrogen antiporter (NHE-1) and secretory phospholipase A2 (sPLA2) IIA expression.*

a *Relative mRNA expression of NHE-1 and sPLA2 IIA in FLG+ (striped bars) and FLG- (white bars) constructs at days 4, 7 and 14 quantified using RT-PCR. Mean ± SEM, n = 10, * p ≤ 0.05*

b *Protein expression in FLG+ and FLG- constructs; the expression of NHE-1 and sPLA2 IIA at day 14 is clearly increased (green fluorescence). The nuclei were stained with DAPI (blue fluorescence) (bar = 100µm).*

3.3.3 NO DIFFERENCES OF SKIN SURFACE PH WERE FOUND IN FLG+ AND FLG-

Interestingly, we measured a physiological skin surface around pH 5.5 from day 4 through 14 of tissue cultivation. No differences were detected between the *FLG+* and *FLG-* constructs. The respective absolute values are given in Figure 2.

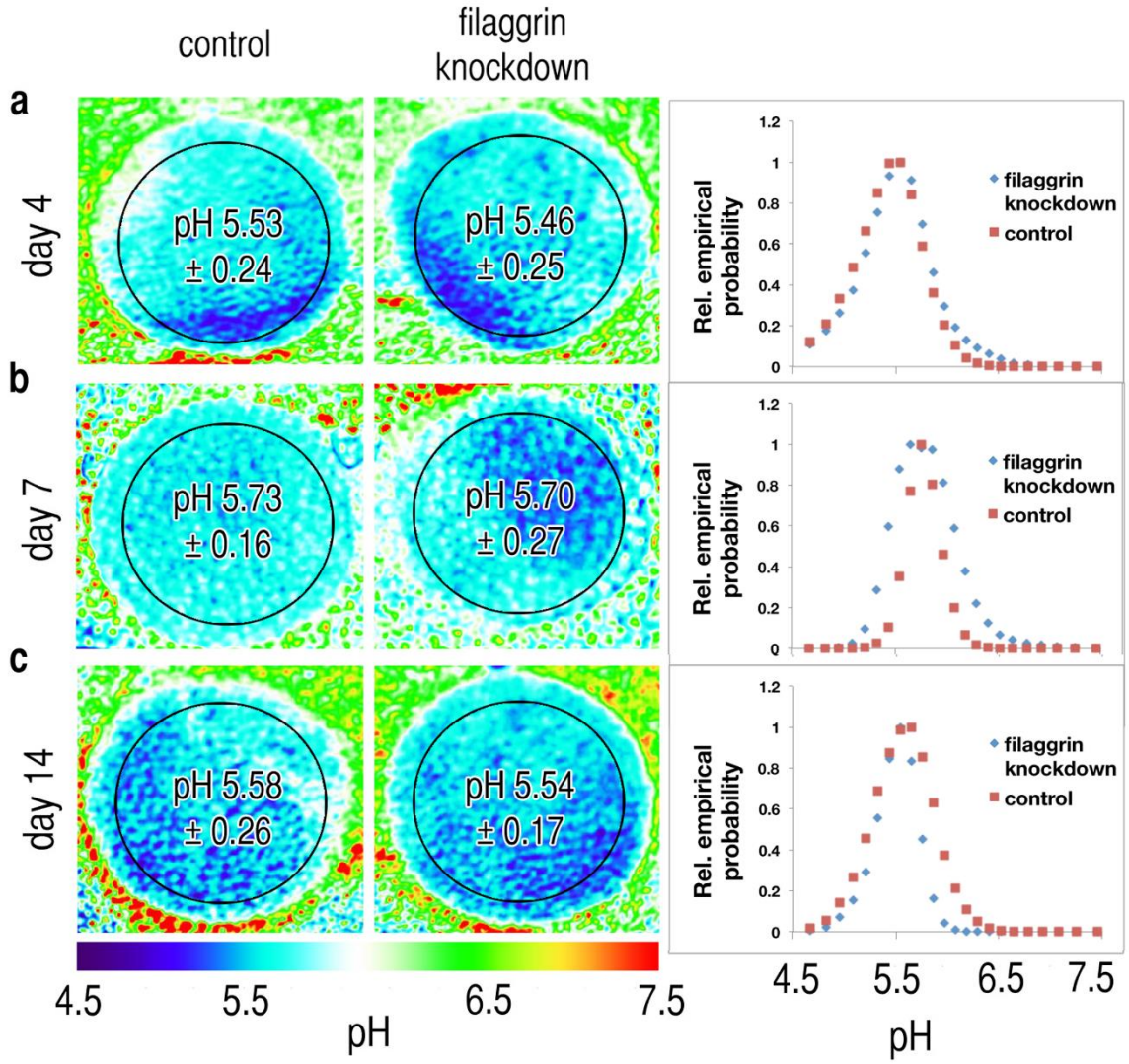

Figure 3-2 *Skin surface pH of FLG+ (control) and FLG- (FLG knock down) constructs at day 4, 7 and 14 of tissue cultivation and a histographical analysis of the spatial surface pH value distributions of the skin constructs using RGB-imaging luminescent 2D-imaging.*

Regions of interest are marked with circles, and the respective mean pH values ± SD are given. No differences were observed between FLG+ and FLG- at day 4 (n=2), day 7 (n=4) and day 14 (n=4), respectively.

3.3.4 FLG KNOCK DOWN LEADS TO LESS ORDERED SKIN LIPID BARRIER

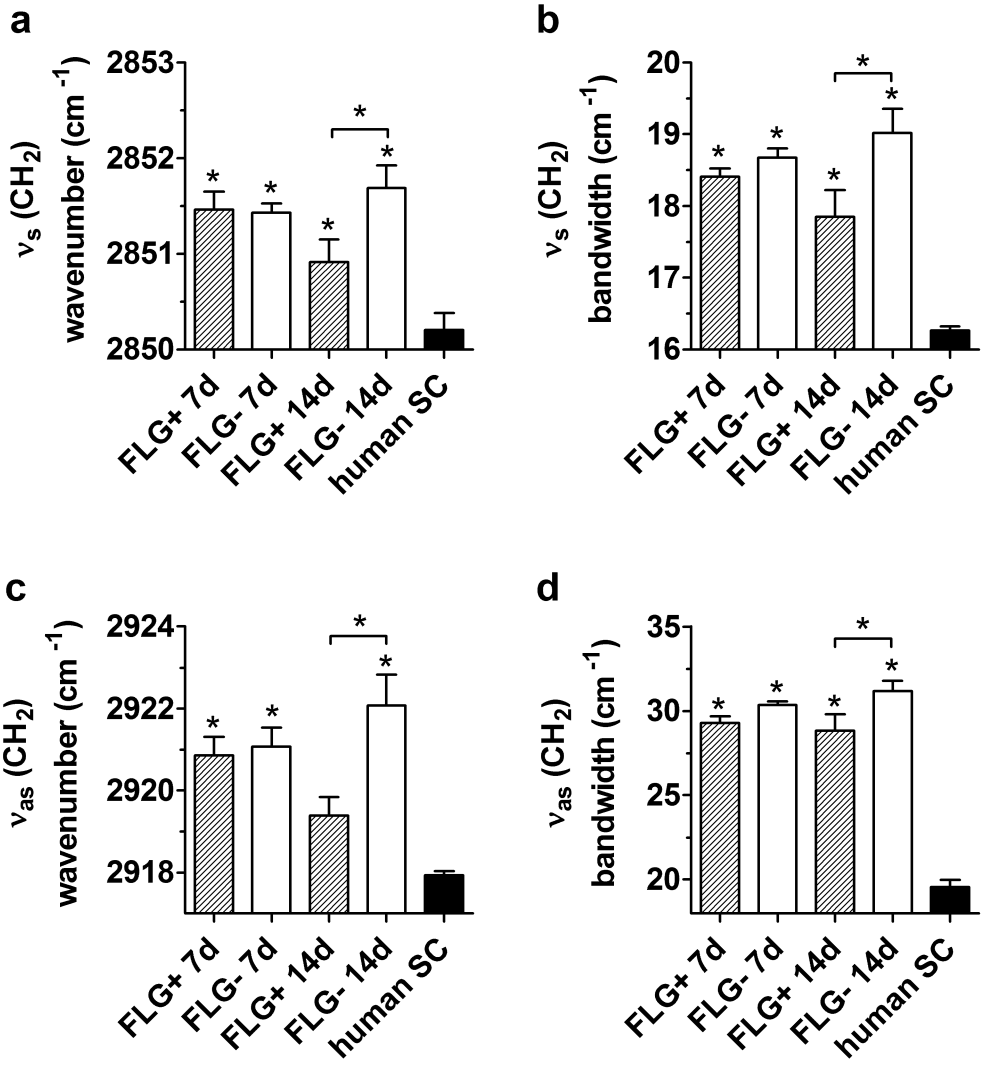

Figure 3-3 *Stratum corneum (SC) lipid chain order as indicated by the wavenumbers of the IR methylene symmetric (ν_s) and asymmetric (ν_{as}) stretching vibrations (panels a and c, respectively) and their corresponding bandwidths (panels b and d) of the hydrated SC.*

*Samples from FLG+ and FLG- skin models grown for 7 and 14 d compared to isolated human SC. The hydrated SC samples were examined by ATR-FTIR spectroscopy by co-addition of 256 scans at 4 cm^{-1} resolution at 23 °C. Mean ± SEM, n = 8, * indicates statistically significant differences compared to human SC or as indicated at $p \leq 0.05$.*

The lipid chain order in the SC sheets from normal and *FLG*- constructs was examined by ATR-FTIR spectroscopy and compared to hydrated human SC. Cultivated for 7 d, the constructs displayed more disordered lipid chains than the human SC as indicated by the shift of both the methylene symmetric and asymmetric stretching vibrations towards slightly higher wavenumbers (over 2851 cm^{-1} and ~2921 cm^{-1}, respectively, compared to 2850 cm^{-1} and 2918 cm^{-1} in human SC) and significant broadening of both bands due to incorporation of more *gauche* conformers into the lipid chains [17] (Figure 3). No differences were found between *FLG*+ and *FLG*- cultures at day 7.

In contrast, cultivation for 14 d led to significant differences between the lipid chain conformations of the constructs. While the normal cultures showed a trend towards improving the lipid chain order reflected by lower wavenumbers of methylene stretching bands and decreased bandwidths, the opposite was found for *FLG*-. The methylene symmetric stretching in the *FLG*- construct reached ~2852 cm^{-1}, indicating a higher proportion of a liquid ordered phase [18] where the lipid chains are still more ordered than in the fluid phase but display greater lateral and rotational freedom. This is consistent with the character of the methylene scissoring mode, which appeared as a single band at around 1466 cm^{-1} indicating a laterally disordered phase. The relative amounts of lipids, determined as the corrected area under the C-H stretching vibration, and also the lipid/protein ratios, were similar in both models.

3.3.5 FLG- CONSTRUCTS CONTAIN MORE FFA COMPARED TO NORMAL CONSTRUCTS

The total lipid content was very similar in both *FLG- and FLG*+ constructs (approximately 100 µg/mg of dry SC). No differences were found between the 7 d models consistently with the FTIR results and [19]. After 14 d cultivation of *FLG*+ constructs, the amounts of the major barrier lipids FFA (11.3 ± 2.1 µg), Chol (12.5 ± 2.1 µg), Cer (21.1 ± 3.7 µg) and CholS (1.3 ± 0.5 µg) per mg of SC (Figure 4 a) correspond to a roughly equimolar mixture of FFA, Chol, and Cer, which is in agreement with previous studies [20]. Yet, the amount of these barrier lipids was significantly lower in either construct than in human SC (Figure 4 a). In the skin models, significant amounts of more polar lipid precursors including SM, GCer and PL were

detected explaining the lower lipid chain order of the *in vitro* constructs compared to human SC.

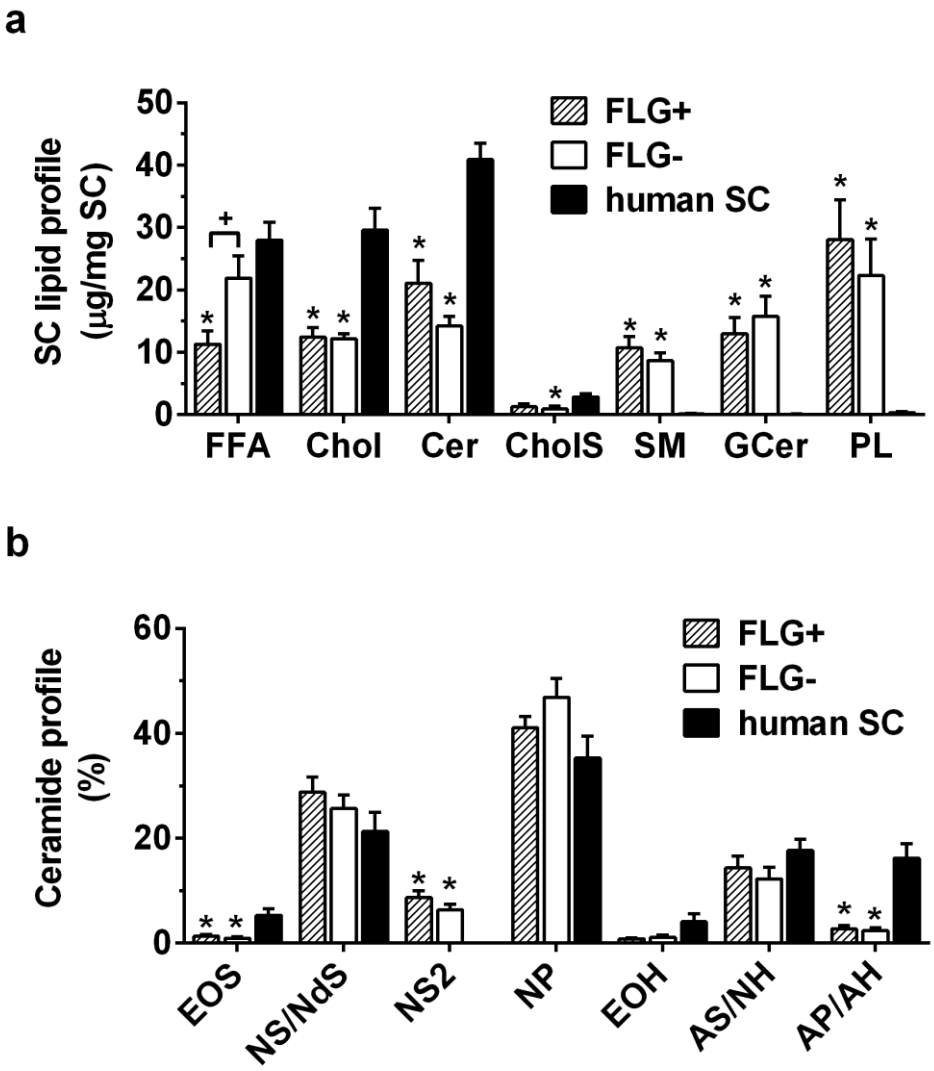

Figure 3-4 *The SC lipid content (panel a) and Cer profiles (panel b) in FLG+ and FLG- reconstructed skin grown for 14 d compared to human SC.*

*The analyses were performed on silica gel 60 HPTLC plates and quantitated by densitometry after dipping in 7.5% $CuSO_4$, 8% H_3PO_4, and 10% MeOH in water for 10 s and heating at 160 °C for 30 min. Cer, FFA, and Chol were separated using chloroform/methanol/acetic acid 190:9:1.5 (v/v/v) twice to the top of the plate. The other lipids were separated using chloroform/methanol/acetic acid/water 65:25:6:3 by volume. Mean ± SEM, n > 17, * indicates statistically significant differences compared to human SC at $p < 0.05$, $^+$ indicates statistically significant differences between FLG+ and FLG- skin models at $p < 0.05$.*

In *FLG*- cultivated for 14 d, all these lipid classes were found, too. The only significant difference between *FLG- and FLG*+ was an almost twofold increase in FFA (21.9 ± 3.6 µg/mg) accompanied by slightly less PL (22.3 ± 5.8 µg/mg) (Figure 4 a), suggesting an increased PL processing into FFA by $sPLA_2$. Importantly, neither glucosylsphingosine (GSph) nor sphingosylphosphorylcholine (SPC), i.e. the degradation products of SM and GCer found previously in AD [21], was detected.

3.3.6 FLG- CONSTRUCTS DISPLAY SIMILAR CER PROFILES COMPARED TO FLG+ CONTROL

The overall Cer profiles were similar in both *in vitro* skin models (Figure 4 b). The major Cer species in the skin constructs were Cer NS and NP (28.8 ± 0.3 % and 41.1 ± 2.1 %), which is similar to native human SC, where these Cer species accounted for 21.3 ± 3.6 % and 35.3 ± 4.2 %, respectively. The band below Cer NS was assigned to its shorter analog (8.7 ± 1.3 %, labeled as Cer NS2). Such a subfraction of Cer NS was not present in human SC but was detected in reconstructed epidermal models previously [22,23]. The more polar Cer bands attributed to hydroxylated Cer AS/NH and Cer AP/AH, constituted 14.4 ± 2.3 % and 2.7 ± 0.6 % of the Cer mass compared to 17.7 ± 2.1 % and 16.2 ± 2.7 % in human SC, respectively. The AcylCer species, *i.e.,* EO-type Cer, were found in some but not all lipid models. The mean levels were around 1% for either EOS or EOH, which is lower than in human SC, where they comprised 4 to 5 %. Cer EOP concentrations were below the detection limit. The highest amounts of Cer EOS and EOH detected were 4.9 % and 3.4 % with no significant differences between the skin constructs.

Notably, the percentages of all sphingosine-based Cer (i.e., CerEOS, NS, NS2, and AS) were slightly lower in the *FLG*- constructs but without statistical significance.

3.3.7 SKIN PERMEABILITY IS INCREASED IN FLG- FOR LIPOPHILIC AGENTS

We also determined the permeability of the skin constructs. Testosterone (logP = 3.47) served as lipophilic, caffeine (logP = -0.08) as a hydrophilic model drug. At day 7, neither for testosterone nor caffeine significant differences in skin permeability were found in *FLG*+ and *FLG*-. For testosterone, mean apparent permeability coefficients (P_{app}) ± SEM were 5.01 ± 0.37 x 10^{-6} (*FLG+)* and 5.13 ± 0.31 x 10^{-6} cm/s (*FLG-)*. For caffeine, P_{app} values were 9.33 ± 0.51 x 10^{-6} for *FLG*+ and 10.03 ± 0.93 x10^{-6} cm/s for *FLG*-. At day 14, significantly higher skin permeability was found for testosterone in *FLG*- in our previous work, while no differences were detected for caffeine [16].

3.4 DISCUSSION

The association of FLG mutations with ichthyosis vulgaris and AD is well established [1]. However, the exact mechanisms leading from genetic defects to clinical manifestation and the overall impact of these mutations are still ambiguous [1]. To investigate the impact of FLG on the skin barrier formation we developed an *in vitro* FLG deficient skin construct by knocking down its expression in primary, human keratinocytes using siRNA [16]. In this study, we elucidated the influence of FLG on the skin lipid formation and composition and the acidification mechanism in FLG deficient constructs in a time dependent manner. The advantage of *in vitro* FLG knock down constructs is that we are able to investigate the influence of FLG alone without other possibly contributing factors.

In terms of skin lipid organization, we found less ordered intercellular lipid lamellae in FLG- constructs compared to the normal constructs at day 14 indicating a decreased viscosity and higher degree of freedom of mobility of the lipid chains. A similar decrease in lipid chain order was found in non-lesional SC from patients with AD and psoriasis [24]. This disorder was accompanied by a significantly higher permeability for lipophilic drugs in FLG- skin construct at day 14 [16], which is in agreement with [25]. These results correspond well with the observed changes in sPLA activity (upregulation at day 14), fatty acid level (increase at day 14) and skin lipid order (decreased at day 14) in FLG-. In contrast, no differences in permeability were found at day 7.

When considering the lipid chain packing, electron diffraction showed a higher proportion of hexagonal compared to orthorhombic lateral chain packing in AD patients [26]. However, we were unable to confirm this finding as our *in vitro* constructs generally did not form the orthorhombic lipid lattice. This is well in accordance with findings from other skin constructs [27].

First, we assumed that the changes in the lipid chain order must be related to a decrease in Cer levels in the FLG- constructs. Such a lack of Cer was described repeatedly in AD patients [11,12,14,28]. The lack of FLG and, thus, the impairment of the UCA/PCA acidification pathway may affect the activity of the Cer-generating enzymes GCerase and SMase that need an acidic pH [6]. On the other hand,

comparable Cer levels in AD and healthy skin were also found in vivo [29]. Although our lipid analyses showed lower levels of Cer in the FLG- constructs, this was neither statistically significant nor consistently found in the individual tissues. Therefore, there must be additional mechanism independent of FLG mutations leading to Cer deficiency. This is in agreement with recent reports [30,31]. The ability to generate Cer from their precursors can be explained by increased $sPLA_2$ and/or NHE-1 activity which acidify the SC in the absence of UCA/PCA and, thus, ensure the activity of GCerase and SMase [8].

The Cer profiles were similar in both constructs; we only found a slight decrease in total sphingosine-based Cer in FLG- compared to FLG+. This seems to be contradictory to the lower abundances in Cer NP and total Cer EO in AD patients [31]. However, in that study, patients with the most prevalent FLG mutations were excluded suggesting that those changes were FLG independent. Unfortunately, only some of our constructs contained detectable amounts of the EO-type Cer; thus, we could not study whether FLG knock down contributes to the decrease of these extremely long acylCer found previously in AD [15]. Notably, neither GCer nor SPC were detected in the skin constructs. These lysolipids are formed from GCer and SM, respectively, by the action of GCer-SM-deacylase, which is highly expressed in the skin of AD patients. The breakdown of these Cer precursors leads to Cer deficiency and barrier disruption [21,32]. Our data suggest that there is no link between FLG and GCer-SM-deacylase in AD, both can independently contribute to skin lipid barrier abnormalities.

The most striking feature in the SC lipid profiles of our skin constructs was the almost twofold increase of the FFA fraction in FLG- compared to FLG+ at day 14 strongly suggesting an involvement of $sPLA_2$ as an alternative acidification pathway. Indeed, at day 14 we observed a significant increase of $sPLA_2$ IIA in FLG- constructs and an about 55 % increased $sPLA_2$ activity explaining the high amounts of FFA. This is in line with previous in vivo findings: twice higher FFA levels were found in atopic epidermis (1.30 +/- 0.74 mg/g wet weight) compared to healthy epidermis (0.61 +/- 0.14 mg/g) [33]. Furthermore, Tarroux et al., found significantly increased sPLA activity in atopic skin and a decrease in activity upon treatment [34]. The increased production of FFA due to $sPLA_2$ IIA upregulation not only disturbs the lipid ratio and lipid order in the skin barrier but also directly contributes to inflammatory processes [9].

Because these changes were detected only at day 14, we further investigated the time course of the pH values of the skin constructs. Interestingly, we found a physiological pH of about 5.5 from day 4 through 14 of tissue cultivation in both constructs suggesting that other mechanisms than FLG maintain the SC acidity in the absence of FLG. Initially, at day 4, the basal activity of NHE-1 is fully sufficient to maintain the acidic pH. This idea is substantiated by the high abundance of NHE-1 in the skin constructs already at day 4. This result is in good agreement with previous findings that FLG-UCA/PCA pathway is not essential for SC acidification [8] and that NHE-1 is the primary source of acidic microdomains activating lipid processing enzymes [35].

At day 7 the lack of FLG becomes apparent as UCA/PCA values are significantly lower in FLG- constructs. NHE-1 is still able to maintain an acidic pH but is significantly upregulated in FLG-, which is likely a compensatory mechanism of the decreased UCA/PCA-based acidity. At this time point, FLG+ and FLG- constructs are still very similar as also indicated by the skin lipid arrangement and permeability being in a good agreement with [19], who cultivated their models for 7 days. The most pronounced consequences of FLG deficiency appear at later time points due to the progressive differentiation and maturation of the skin constructs. At day 14, NHE-1 is still upregulated in FLG- constructs but now another acidification mechanism is activated: the PL-FFA conversion by $sPLA_2$. The importance of NHE-1 and $sPLA_2$ for skin acidification has been demonstrated before [36,37]. While this happens in both FLG- and FLG+ constructs, the expression and activity of $sPLA_2$ are significantly higher in the FLG-. Thus, although the time-course of NHE-1 and FFA-based acidification pattern of the skin constructs is not affected by deficient FLG, these two pathways are upregulated to compensate for the lack of FLG-His-UCA/PCA.

The question is what exactly is the trigger activating the other acidification pathways. As we did not detect any differences in pH between FLG+ and FLG-, it seems that these compensatory mechanisms are activated by very small or localized pH changes that we are not able to measure. Another possibility is that pH does not control acidification itself but by the levels of products or intermediates of other acidification pathways. The latter possibility would be more advantageous as it would prevent pH changes rather than correct them.

Nevertheless, we cannot exclude that there are other key players involved in the acidification process which have not yet been identified as also suggested by [35]. Our findings are well in line with [8] and substantiate the idea of compensatory mechanism between different pathways to ensure skin acidification.

In conclusion, the decreased levels of UCA/PCA accompanied by an increase of NHE-1 and later $sPLA_2$ IIA in FLG- constructs demonstrate an interplay between different skin acidification pathways. Fig. 5 displays the suggested processes of skin acidification. Additionally, using *in vitro* skin constructs we showed that FLG deficiency directly influences the skin lipid orientation by increasing the amount of FFA and, thus, affecting skin permeability. Our results considerably contribute to the understanding of skin acidification and the impact of FLG deficiency on skin barrier dysfunction. To our best knowledge, these direct interdependencies have not been described before.

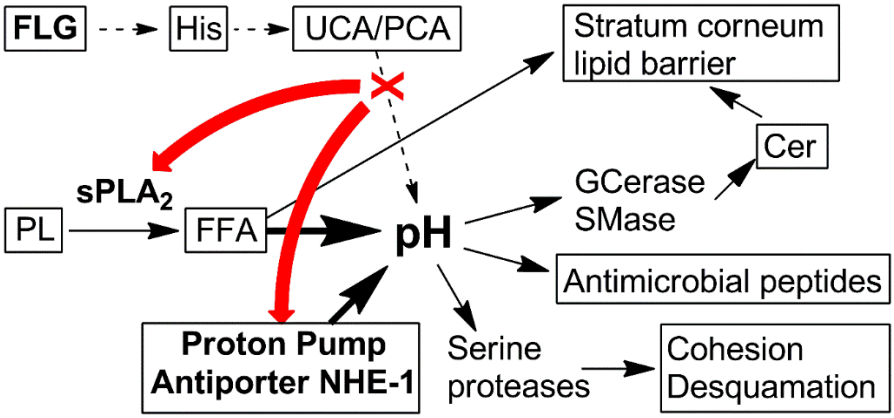

Figure 3-5 *Stratum corneum pH unifying concept. In FLG deficiency, NHE-1 and sPLA2 are upregulated to maintain the acidic pH needed for a variety of skin functions. Adapted and modified from Fluhr et al., 2001 [37].*

3.5 MATERIALS AND METHODS

Non-hydroxy and α-hydroxy sphingosine-based ceramides (Cer NS and AS), GCer, SM, GSph, and SPC were purchased from Avanti Polar Lipids (Alabaster, USA). Phytoceramide (Cer NP) was prepared by acylation of phytosphingosine with lignoceric acid as described previously [38,39]. The structure and purity of the prepared Cer NP were confirmed by ^{1}H and ^{13}C NMR spectra (Varian Mercury-Vx BB 300 instrument, operating at 300 MHz for ^{1}H, 75 MHz for ^{13}C), MS (Agilent 500 Ion Trap LC/MS), and infrared spectra (Nicolet 6700 FT-IR spectrophotometer). Chol and all other chemicals were from Sigma-Aldrich (Schnelldorf, Germany). Radiolabelled 1,2,6,7-^{3}H-testosterone was from Amersham, Freiburg, Germany. Radiolabelled 1-methyl-^{14}C-caffeine was from Arc Inc., St. Louis, USA.

3.5.1 PREPARATION OF SKIN CONSTRUCTS

The skin constructs (*FLG*+ and *FLG*-) have been generated according to [16,40]. SC was isolated after 4, 7 and 14 days. The constructs were placed on a filter paper soaked in 0.5 % trypsin in phosphate-buffered saline (PBS, pH 7.4) (Kligman and Christophers, 1963). The isolated SC sheets were washed with PBS and any remaining keratinocytes were removed with a cotton swab. Subsequently, SC sheets were washed with acetone to remove surface contaminants, vacuum-dried and stored at -20°C. Isolated human SC served as control.

3.5.2 FOURIER TRANSFORM INFRARED (FTIR) SPECTROSCOPY

IR spectra of the samples were collected on a Nicolet 6700 FT-IR spectrometer (Thermo Scientific, USA) equipped with a single-reflection MIRacle attenuated total reflectance (ATR) germanium crystal at 23 °C. The spectra were generated by co-addition of 256 scans collected at 4 cm^{-1} resolution and analyzed with the Bruker OPUS software. The exact peak positions were determined from second derivative spectra and by peak fitting if needed.

3.5.3 Isolation of SC Lipids

For the extraction of the SC intercellular lipids, a modified [41] method was used. The SC samples were extracted with 1 ml $CHCl_3$/MeOH 2:1 (v/v) per mg of SC for 1.5 h, filtered, separated and concentrated under a stream of nitrogen. The lipids were dried and stored at -20°C under argon.

3.5.4 HPTLC Lipid Analysis

The lipid analysis was performed on silica gel 60 HPTLC plates (20 × 10 cm, Merck, Darmstadt, Germany). The extracted SC lipids were dissolved in 100 µl $CHCl_3$/MeOH 2:1. 10 µl of each lipid sample was sprayed on the plate using a Linomat IV (Camag, Muttenz, Switzerland). Standard lipids were dissolved in $CHCl_3$/MeOH 2:1 (v/v) (Cer NS, AS, NP, Chol, and palmitic acid), $CHCl_3$/MeOH 1:1 (v/v) (CholS, GCer and SM), and MeOH (GSph and SPC), respectively, at 1 mg/ml. They were first analyzed separately during method development and then mixed at 50 µg/ml and applied on a HPTLC plate together with the analyzed samples to generate calibration curves from 50 ng to 7.5 µg. The major skin barrier lipids (Cer, FFA and Chol) were separated using $CHCl_3$/MeOH/acetic acid 190:9:1.5 (v/v/v) mobile phase twice to the top of the plate (Bleck *et al.*, 1999). The Cer precursors (GlcCer and SM), their degradation products (GSph and SPC) and CholS were separated using a more polar mobile phase ($CHCl_3$/MeOH/acetic acid/H_2O 65:25:6:3). The lipids were visualized by dipping in a derivatization reagent (7.5% $CuSO_4$, 8% H_3PO_4, 10% MeOH in water) for 10 s and heating at 160 °C for 30 min and quantitated by densitometry using TLC scanner 3 and WinCats software (Camag, Muttenz, Switzerland).

3.5.5 Determination of FLG, sPLA_2 and NHE-1 Expression

For isolation of RNA the constructs were harvested at day 14 and punched to discs (10 mm). Epidermis was frozen using liquid nitrogen and then milled for 30 s at 25 Hz using a TissueLyzer (Qiagen, Hilden, Germany). Subsequently, RNA was isolated using NucleoSpin® RNA II according to the manufacturer's instructions. For cDNA

synthesis RevertAid™ First Strand cDNA Synthesis Kit was used according to manufacturer's instruction.

For relative quantification of FLG, NHE-1 and $sPLA_2$ isoforms expression reverse transcription polymerase chain reaction (RT-PCR) was performed using the SYBR Green I Masterplus kit (Roche, Penzberg, Germany). For primer sequences see Tab. S2. The house-keeping gene YWHAZ served as control.

3.5.6 Skin surface pH measurements

Luminescent 2D-imaging of pH [42,43] was performed via RGB-imaging [42] of pH sensor foils consisting of a hydrogel layer containing pH-indicator microparticles (fluorescein isothiocyanate bound to aminoethylcellulose) and reference particles [ruthenium(II)-tris(4,7-diphenyl-1,10-phenanthroline) incorporated in polyacrylonitrile]. Sensor foils were gently applied to 3D skin construct surfaces and they were allowed to slowly adapt by adhesion forces. Calculations and pseudocolor image processing were done with ImageX software (Microsoft Corporation) and ImageJ (http://rsbweb.nih.gov/ij/). For details see Supplemental methods.

3.5.7 Immunohistochemistry

After 14 days, the constructs were embedded in tissue freezing medium (Leica Microsystems, Nussloch, Germany) and frozen using liquid nitrogen. After overnight storage at -80°C, the constructs were cut to vertical slices (5 µm) with a freeze microtome (Leica Microsystems, Nussloch, Germany). After fixation, they were washed with PBS containing 1% bovine serum albumin (BSA) and blocked with normal goat serum (1:20 in PBS). The sections were incubated for one hour with primary rabbit antibodies specific against NHE-1 and $sPLA_2$-IIA (Abcam, Cambridge, UK) diluted in PBS containing 1% BSA (1:400 and 1:200, respectively) and subsequently with goat-anti-rabbit IgG DyLight 488 antibody (Dianova, Hamburg, Germany). After washing, the sections were embedded in antifading mounting medium (Dianova, Hamburg, Germany) and analyzed with a fluorescence microscope (BZ-8000, Keyence, Neu-Isenburg, Germany).

3.5.8 Skin permeability testing

The skin permeability was evaluated according to validated test procedures (Schäfer-Korting *et al.*, 2008). Briefly, stock solutions of testosterone (40 µg/ml, 2% [v/v] Igepal® CA-630) and caffeine (1 mg/ml) were spiked with an appropriate amount of the radiolabelled compound to achieve a total radioactivity of 2 µCi/ml. Permeation studies were performed at day 7 using a static setup (Franz type diffusion cells, diameter 15 mm, volume 12 ml, Permegear, Bethlehem, USA).

3.5.9 Statistical Analysis

Wilcoxon signed rank test or t-test were used when comparing two different conditions according to the results of D'Agostino-Pearson normality test. When comparing three or more conditions, a one-way analysis of variance (ANOVA) with a Bonferroni post-hoc test or Friedman plus Dunn's tests were performed using SigmaStat for Windows 3.5 (SPSS, U.S.A.). $p \leq 0.05$ was considered significant. The data are presented as means ± SEM.

3.6 ACKNOWLEDGEMENT

We thank Dr. Hans Christian Hennies (Center of Genomics, University of Cologne) and Dr. Katja Martina Eckl (Center of Genomics, University of Cologne) for their help with the reconstructed skin models and the related scientific discussions. This work was supported by the Czech Science Foundation (project No. 207/11/0365) and Charles University (SVV 267 001).

3.7 REFERENCES

1 Brown SJ, McLean WHI: One remarkable molecule: filaggrin. J Invest Dermatol 2012 Mar;132:751–62.

2 Palmer CN, Irvine AD, Terron-Kwiatkowski A, Zhao Y, Liao H, Lee SP, et al.: Common loss-of-function variants of the epidermal barrier protein filaggrin are a major predisposing factor for atopic dermatitis. Nat Genet 2006 Apr;38:441–6.

3 Jung T, Stingl G: Atopic dermatitis: Therapeutic concepts evolving from new pathophysiologic insights. J Allergy Clin Immunol 2008 Dec;122:1074–1081.

4 O'Regan GM, Sandilands A, McLean WHI, Irvine AD: Filaggrin in atopic dermatitis. J Allergy Clin Immunol 2009 Sep;124:R2–R6.

5 Rawlings A V, Harding CR: Moisturization and skin barrier function. Dermatol Ther 2004;17 Suppl 1:43–8.

6 Fluhr JW, Elias PM: Stratum corneum pH: Formation and Function of the "Acid Mantle." Exog Dermatology 2002;1:163–175.

7 Krien PM, Kermici M: Evidence for the Existence of a Self-Regulated Enzymatic Process Within the Human Stratum Corneum –An Unexpected Role for Urocanic Acid. J Invest Dermatol 2000 Sep;115:414–420.

8 Fluhr JW, Elias PM, Man M-Q, Hupe M, Selden C, Sundberg JP, et al.: Is the filaggrin-histidine-urocanic acid pathway essential for stratum corneum acidification? J Invest Dermatol 2010 Aug;130:2141–4.

9 Chan A, Mauro T: Acidification in the epidermis and the role of secretory phospholipases. Dermatoendocrinol 2011 Apr;3:84–90.

10 Feingold KR: Thematic review series: Skin Lipids . The role of epidermal lipids in cutaneous permeability barrier homeostasis: Fig. 1. J Lipid Res 2007 Dec;48:2531–2546.

11 Bleck O, Abeck D, Ring J, Hoppe U, Vietzke J-P, Wolber R, et al.: Two Ceramide Subfractions Detectable in Cer(AS) Position by HPTLC in Skin Surface Lipids of

Non-Lesional Skin of Atopic Eczema. J Invest Dermatol 1999 Dec;113:894–900.

12 Di Nardo, P Wertz, A Giannetti, S S A: Ceramide and cholesterol composition of the skin of patients with atopic dermatitis. Acta Derm Venereol 1998 Jan 20;78:27–30.

13 Imokawa G, Abe A, Jin K, Higaki Y, Kawashima M, Hidano A: Decreased Level of Ceramides in Stratum Corneum of Atopic Dermatitis: An Etiologic Factor in Atopic Dry Skin? J Invest Dermatol 1991 Apr;96:523–526.

14 Ishikawa J, Narita H, Kondo N, Hotta M, Takagi Y, Masukawa Y, et al.: Changes in the Ceramide Profile of Atopic Dermatitis Patients. J Invest Dermatol 2010 Oct;130:2511–2514.

15 Park Y-H, Jang W-H, Seo JA, Park M, Lee TR, Park Y-H, et al.: Decrease of ceramides with very long-chain fatty acids and downregulation of elongases in a murine atopic dermatitis model. J Invest Dermatol 2012 Feb;132:476–9.

16 Küchler S, Henkes D, Eckl K-M, Ackermann K, Plendl J, Korting H-C, et al.: Hallmarks of atopic skin mimicked in vitro by means of a skin disease model based on FLG knock-down. Altern Lab Anim 2011 Oct;39:471–80.

17 Mendelsohn R, Moore DJ: Infrared determination of conformational order and phase behavior in ceramides and stratum corneum models. Methods Enzymol 2000;312:228–47.

18 Velkova V, Lafleur M: Influence of the lipid composition on the organization of skin lipid model mixtures: An infrared spectroscopy investigation. Chem Phys Lipids 2002 Aug;117:63–74.

19 Mildner M, Jin J, Eckhart L, Kezic S, Gruber F, Barresi C, et al.: Knockdown of filaggrin impairs diffusion barrier function and increases UV sensitivity in a human skin model. J Invest Dermatol 2010 Sep;130:2286–94.

20 Wertz PW: Lipids and barrier function of the skin. Acta Derm Venereol Suppl (Stockh) 2000;208:7–11.

21 Hara J, Higuchi K, Okamoto R, Kawashima M, Imokawa G: High-Expression of Sphingomyelin Deacylase is an Important Determinant of Ceramide Deficiency Leading to Barrier Disruption in Atopic Dermatitis1. J Invest Dermatol 2000 Sep;115:406–413.

22 Pappinen S, Hermansson M, Kuntsche J, Somerharju P, Wertz P, Urtti A, et al.: Comparison of rat epidermal keratinocyte organotypic culture (ROC) with intact human skin: lipid composition and thermal phase behavior of the stratum corneum. Biochim Biophys Acta 2008 Apr;1778:824–34.

23 Ponec M: Skin constructs for replacement of skin tissues for in vitro testing. Adv Drug Deliv Rev 2002 Nov 1;54 Suppl 1:S19-30.

24 Wohlrab J, Vollmann A, Wartewig S, Marsch WC, Neubert R: Noninvasive characterization of human stratum corneum of undiseased skin of patients with atopic dermatitis and psoriasis as studied by Fourier transform Raman spectroscopy. Biopolymers 2001;62:141–146.

25 Potts RO, Francoeur ML: Lipid biophysics of water loss through the skin. Proc Natl Acad Sci U S A 1990 May;87:3871–3.

26 Pilgram GSK, Vissers DCJ, van der Meulen H, Koerten HK, Pavel S, Lavrijsen SPM, et al.: Aberrant Lipid Organization in Stratum Corneum of Patients with Atopic Dermatitis and Lamellar Ichthyosis. J Invest Dermatol 2001 Sep;117:710–717.

27 Thakoersing VS, Danso MO, Mulder A, Gooris G, El Ghalbzouri A, Bouwstra JA: Nature versus nurture: does human skin maintain its stratum corneum lipid properties in vitro ? Exp Dermatol 2012 Nov;21:865–870.

28 Imokawa G: A possible mechanism underlying the ceramide deficiency in atopic dermatitis: expression of a deacylase enzyme that cleaves the N-acyl linkage of sphingomyelin and glucosylceramide. J Dermatol Sci 2009 Jul;55:1–9.

29 Farwanah H, Raith K, Neubert RHH, Wohlrab J: Ceramide profiles of the uninvolved skin in atopic dermatitis and psoriasis are comparable to those of healthy skin. Arch Dermatol Res 2005 May;296:514–21.

30 Jakasa I, Koster ES, Calkoen F, McLean WHI, Campbell LE, Bos JD, et al.: Skin barrier function in healthy subjects and patients with atopic dermatitis in relation to filaggrin loss-of-function mutations. J Invest Dermatol 2011 Feb;131:540–2.

31 Janssens M, van Smeden J, Gooris GS, Bras W, Portale G, Caspers PJ, et al.: Lamellar lipid organization and ceramide composition in the stratum corneum of patients with atopic eczema. J Invest Dermatol 2011 Oct;131:2136–8.

32 Ishibashi M, Arikawa J, Okamoto R, Kawashima M, Takagi Y, Ohguchi K, et al.: Abnormal Expression of the Novel Epidermal Enzyme, Glucosylceramide Deacylase, and the Accumulation of its Enzymatic Reaction Product, Glucosylsphingosine, in the Skin of Patients with Atopic Dermatitis. Lab Investig 2003 Mar;83:397–408.

33 Schäfer L, Kragballe K: Abnormalities in epidermal lipid metabolism in patients with atopic dermatitis. J Invest Dermatol 1991 Jan;96:10–5.

34 Tarroux R, Assalit MF, Licu D, Périé JJ, Redoulès D: Variability of enzyme markers during clinical regression of atopic dermatitis. Skin Pharmacol Appl Skin Physiol15:55–62.

35 Behne MJ, Meyer JW, Hanson KM, Barry NP, Murata S, Crumrine D, et al.: NHE1 regulates the stratum corneum permeability barrier homeostasis. Microenvironment acidification assessed with fluorescence lifetime imaging. J Biol Chem 2002 Dec 6;277:47399–406.

36 Fluhr JW, Behne MJ, Brown BE, Moskowitz DG, Selden C, Mao-Qiang M, et al.: Stratum corneum acidification in neonatal skin: secretory phospholipase A2 and the sodium/hydrogen antiporter-1 acidify neonatal rat stratum corneum. J Invest Dermatol 2004 Feb;122:320–9.

37 Fluhr JW, Kao J, Jain M, Ahn SK, Feingold KR, Elias PM: Generation of free fatty acids from phospholipids regulates stratum corneum acidification and integrity. J Invest Dermatol 2001 Jul;117:44–51.

38 Novotný J, Janůsová B, Novotný M, Hrabálek A, Vávrová K: Short-chain ceramides decrease skin barrier properties. Skin Pharmacol Physiol

2009;22:22–30.

39 Novotný J, Pospěchová K, Hrabálek A, Čáp R, Vávrová K: Synthesis of fluorescent C24-ceramide: Evidence for acyl chain length dependent differences in penetration of exogenous NBD-ceramides into human skin. Bioorg Med Chem Lett 2009 Dec;19:6975–6977.

40 Eckl K-M, Alef T, Torres S, Hennies HC: Full-thickness human skin models for congenital ichthyosis and related keratinization disorders. J Invest Dermatol 2011 Sep;131:1938–42.

41 Bligh EG, Dyer WJ: A RAPID METHOD OF TOTAL LIPID EXTRACTION AND PURIFICATION. Can J Biochem Physiol 1959 Jan;37:911–917.

42 Meier RJ, Schreml S, Wang X, Landthaler M, Babilas P, Wolfbeis OS: Simultaneous photographing of oxygen and pH in vivo using sensor films. Angew Chem Int Ed Engl 2011 Nov 11;50:10893–6.

43 Schreml S, Meier RJ, Wolfbeis OS, Maisch T, Szeimies R-M, Landthaler M, et al.: 2D luminescence imaging of physiological wound oxygenation. Exp Dermatol 2011 Jul;20:550–4.

4 ESTABLISHMENT OF A DOUBLE KNOCKDOWN SKIN MODEL TO INVESTIGATE THE IMPACT OF FILAGGRIN AND SODIUM/HYDROGEN ANTIPORTER 1 ON SKIN ACIDIFICATION

4.1 ABSTRACT

An acidic skin surface pH is crucial for correct skin homeostasis. While many common skin diseases such as atopic dermatitis demonstrate increased skin surface pH values, the underlying mechanism is still elusive. Here we establish a sodium/hydrogen exchanger 1 *(NHE-1)* knockdown (KD) and a filaggrin *(FLG)*/ *NHE-1* double KD in reconstructed skin models to gain deeper insight into the impact of intrinsic contributors to the acidic skin surface. NHE-1 KD leads to slightly elevated pH values, while the KD of both *NHE-1* and *FLG* did not result in further pH increase. NHE-1 KD alone resulted in decreased *FLG* expression. Overall, contributors like NHE-1 or secretory phospholipases seem to be more important for pH maintenance than the structural protein filaggrin and its degradation products. Other, yet unknown pathways likely take part in the regulation of skin surface pH. In general, reconstructed skin models in combination with RNA interference are a suitable tool to access the impact of single genes and proteins on a complex issue like skin surface pH.

4.2 INTRODUCTION

The acidic pH of the skin surface (pH 5.5) is pivotal to the homeostasis and integrity of the human skin [1–3]. The outermost layer of human skin, the stratum corneum (SC), consists of tightly packed corneocytes embedded within organized lipid lamellae composed of free fatty acids, cholesterol and ceramides, forming an essential barrier against the entry of xenobiotics and microorganism, as well as against extensive water loss from the body [4]. Ceramides are generated from β-D-glucosylceramides or sphingomyelins by β-glucocerebrosidase and acidic sphingomyelinase catalysed hydrolysis, enzymes that exhibit activity maximums at acidic pH values [5–7]. Skin diseases such as ichthyosis vulgaris and atopic dermatitis are often associated with increased skin surface pH [8–10], which in turn may diminish enzymatic activities resulting in reduced ceramide levels and hampered formation of the SC lamellar lipid bilayers [7,10]. The underlying reasons for these increased pH values is still not fully understood, nor are the exact mechanisms that maintain and regulate the surface pH of skin. Though it was once hypothesized that acidic surface pH resulted from sebaceous and eccrine gland secretions and/or bacterial byproducts like lactic acid, it is now known that three intrinsic mechanisms are significantly contributing : [1] free fatty acids generated from phospholipids by secretory phospholipases A_2, [2] expression of sodium/hydrogen exporter 1 (NHE-1) and [3] the filaggrin-histidine-urocanic acid/pyrrolidonic acid pathway [11,12]. Mutations in the filaggrin gene (*FLG*) are the underlying cause of ichthyosis vulgaris (IV) and a major predisposing factor for the manifestation of atopic dermatitis (AD) [13,14]. Hence, the increased skin surface pH in patients suffering from IV or AD is often linked to a lack of filaggrin [15]. However, it has been demonstrated that FLG deficiency alone does not result in increased skin surface pH [16,17]. This might be explained by the recent identification of a feedback mechanism that compensates for a lack of FLG by upregulating NHE-1 expression and increasing sPLA2 activity [17]. Nevertheless, ultimate impact of NHE-1 on the skin surface pH is unclear.

Thus, the aim of this study was to establish a *NHE-1* KD skin model and a *FLG*/*NHE-1* double KD model using RNA interference, so as to investigate the interdependencies between FLG and NHE-1 on skin acidification. Moreover, to the best of our knowledge, the feasibility of establishing a double KD skin model for basic research has yet to be

demonstrated and as such, systematic optimizations of those conditions required for efficient double gene KD in skin models were performed. Following successful establishment, KD efficiency was assessed at the mRNA and protein level, and the impact these had on skin model physiology investigated by histology and assessment secretory phospholipases expression and measurement of skin surface pH.

4.3 METHODS

4.3.1 CELL CULTURE

Primary human fibroblasts and keratinocytes were isolated from juvenile foreskin (with written consent). Briefly, foreskins were cut into small pieces and incubated overnight with Dispase II (Roche Diagnostics, Mannheim, Germany). The epidermis and dermis were separated using forceps. For keratinocyte isolation, the epidermis was further treated with trypsin/EDTA solution for 5 min at 37°C (Biochrome, Berlin, Germany). Afterwards, keratinocytes were cultured in keratinocyte growth medium (Lonza, Cologne, Germany). The dermis was cultured in DMEM (Sigma-Aldrich, Taufkirchen, Germany) containing 5 mM L-glutamine and 10% FBS (Biochrome, Berlin, Germany) until outgrowth of the fibroblasts occurred. Media changes were performed every other day. For all experiments, cell passages 2 or 3 were used.

4.3.2 NHE-1 KD

To identify optimal KD conditions, three different NHE-1-specific siRNAs (siRNA 1, HSS109888, siRNA 2 HSS109889, siRNA 3 HSS109889, Life Technologies, Darmstadt, Germany) were tested in primary human keratinocytes at concentrations ranging from 10 to 50 nM. HiPerfect (Qiagen, Hilden, Germany) served as transfection reagent, and was used at concentrations ranging from 1.5 to 4.5 µl/ml. KD efficiencies were assessed 24 h and 48 h post transfection. A non-coding siRNA served as negative control (Life Technologies, Darmstadt, Germany).

4.3.3 CONSTRUCTION OF SKIN MODELS

In vitro skin models were generated according to previously published procedures [18,19]. Briefly, bovine collagen (Cellsytems, Troisdorf, Germany) was mixed with 10-fold Hanks balanced salt solution (Life Technologies, Darmstadt, Germany) and brought to a neutral pH. Afterwards, 2.5 x 10^5 fibroblasts (per skin model) were added and 2.5 ml of the mixture was poured into 6-well cell culture inserts (VWR, Ismaning, Germany). After solidification at 37° C for 2h, 4.2 x 10^6 normal or transfected

keratinocytes were added to the top of the collagen matrix. 24h on, the skin models were lifted to the air-liquid interface and the medium changed to a differentiation medium. Skin models were cultivated for up to 14 days with a media change every other day.

To generate *FLG* KD skin models, keratinocytes were transfected prior to seeding using *FLG*-specific siRNAs (HSS177192, Life Technologies, Darmstadt, Germany) [19]. KD efficiency was determined by quantitative reverse transcription polymerase chain reaction (RT-PCR).

4.3.4 RT-PCR

Skin constructs were punched to 10 mm discs, and the viable epidermis gently peeled-off, frozen and then milled. Subsequently, RNA was isolated using the NucleoSpin® RNA II kit (Macherey-Nagel, Düren, Germany) according to the manufacturer's instructions. For cDNA synthesis, RevertAidTM First Strand cDNA Synthesis Kit (Thermo Scientific, Waltham, MA, USA) was used. For relative gene expression quantification, RT-PCR was performed using the Power SYBR® Green PCR Master Mix (Life Technologies, Darmstadt, Germany). The primer sequences are listed in supplementary Table 4-1. YWHAZ served as house-keeping gene.

Table 4-1 *Primer sequences for PCR analysis*

Gene	Primer sense 5'-3'	Primer antisense 5'-3
YWHAZ	AGACGGAAGGTGCTGAGAAA	GAAGCATTGGGGATCAAGAA
FLG	AAGGAACTTCTGGAAAAGGAATTTC	TTGTGGTCTATATCCAAGTGATCCAT
NHE-1	AGATCCAGGCTTCTCCCGGAC	CCATGTGCCTGGTACCCCTGGT
sPLA$_2$-IB	GCAATCACCTGTAGCAGCAA	GTCCAGGTTCTTGTGTGCCT
sPLA$_2$-IIA	ACCCTCCCTCCCTACCCTAAC	AATCTGCTGGATGTCTCATTCTGG
sPLA$_2$-IIF	GACCCACACCCTCTCTCC	GATGCTCTCCCTGCTTACG
sPLA$_2$-V	CTGCCTGGTTCCTGAGAGAG	CAACCCTGAGTTGGAGGAGA
sPLA$_2$-XIIA	TAGCTGTCGGCATCTCCTTT	GGCATGTGAAACAACAGTGG

4.3.5 WESTERN BLOT

For Western blot analysis of FLG and NHE-1, skin models or keratinocytes were lysed in RIPA buffer containing proteases inhibitor (New England Biolabs, Frankfurt/Main, Germany), centrifuged for 30 min at 14,000 × g and the supernatant subsequently stored at -80°C until use. The total amount of protein was quantified via BCA protein assay (Thermo Scientific, Waltham, USA). 30 µg of each protein sample was incubated at 95°C in standard SDS-PAGE buffer and separated via 10% SDS polyacrylamide gel electrophoresis (Bio-Rad, Munich, Germany). Gels were blotted onto Immobilon P nitrocellulose membranes (Carl Roth, Karlsruhe, Germany) via Trans-Blot® Turbo™ Transfer System (Bio-Rad, Munich, Germany). After blocking with 5% non-fat dry milk in tris-buffered saline -Tween 20 (0.1%) for 1 h, the membranes were incubated with primary antibodies (filaggrin antibody ab81468, NHE-1 antibody ab67313, Abcam, Cambridge, UK) overnight. Subsequently, the membranes were washed and incubated with anti-rabbit horseradish-peroxidase-conjugated secondary antibody (Cell Signaling, Frankfurt/Main, Germany) at room temperature for 1 h. All blots were

developed with SignalFire™ ECL reagent (Cell Signaling, Frankfurt/Main, Germany) and visualized by a PXi/PXi Touch gel imaging system (Syngene, Cambridge, UK).

4.3.6 Hematoxylin-eosin (H&E) staining and immunofluorescence

Skin constructs were embedded in tissue freezing medium (Leica Microsystems, Nussloch, Germany) and shock-frozen using liquid nitrogen. Afterwards, vertical cryosections (5 µm) were prepared using a cryotome (Leica Microsystems, Nussloch, Germany). For histological analysis, H&E staining was performed according to standard procedures. For immunostaining against FLG and NHE-1 the skin sections were stained with filaggrin antibody ab81468 (1:200) or NHE-1 antibody ab67313 (1:400), (Abcam, Cambridge, UK) respectively, and counterstained with DAPI. Sections were analyzed using the fluorescence microscope BZ-8000 (Keyence, Neu-Isenburg, Germany).

4.3.7 Skin surface pH measurements

For surface pH measurements of the skin models, optical sensor foils containing pH-indicator microparticles (fluorescein isothiocyanate) and reference microparticles (ruthenium(II)-tris(4,7-diphenyl-1,10-phenanthroline)) were applied onto the skin models [17,20]. The luminophores were excited with a 460-nm LED array and a RGB image was recorded using a commercial camera. The red channel contained the reference signal, while the green channel recorded the pH depended signal. Channel intensity ratios enabled the calculation of the pH at every pixel in the image with ImageX software (Microsoft Corporation) and ImageJ (http://rsbweb.nih.gov/ij/). Reported values were averaged from 4 separate skin models.

4.3.8 Statistical analysis

The data were statistically analyzed using ANOVA and one-sample t-test and $p \leq 0.05$ was defined as the level of significance.

4.4 RESULTS

4.4.1 ESTABLISHMENT OF NHE-1 AND FILAGGRIN/NHE-1 DOUBLE KD SKIN MODELS

To achieve a sound *NHE-1* KD, the efficacies of different siRNA concentrations in combination with different transfection agent concentrations were evaluated in primary human keratinocytes. Exemplary transfection with siRNA 2 is shown in Figure 4-1 A. The combination of 50 nM siRNA and 4.5 µl/ml HiPerfect yielded the best silencing (≥ 77 ± 9.5%). No KD was observed after transfection with 50nM non-coding siRNA and 4.5 µl/ml HiPerFect at mRNA (Fig. 4-1 B) and protein level (Fig. 4-1 C).

All three *NHE-1* specific siRNA sequences, alone or in combination, were tested at 50 nM with 4.5 µl/ml HiPerFect (Fig. 4-2 A). While distinct *NHE-1* KD was observed in all instances, siRNA 2 and 3 were superior to siRNA 1, with KD rates of 75.2 ± 4.1%, 86.9 ± 6.2% and 45.2 ± 1.5%, respectively. Combination of all three siRNAs produced no further improvements to KD efficiency. Concordant data were observed at the protein level, where siRNA 2 produced the most effective KD of NHE-1 (Fig. 4-2 B). Subsequently 50nM siRNA 2 (HSS 109889) with 4.5 µl HiPerFect was chosen for further experiments.

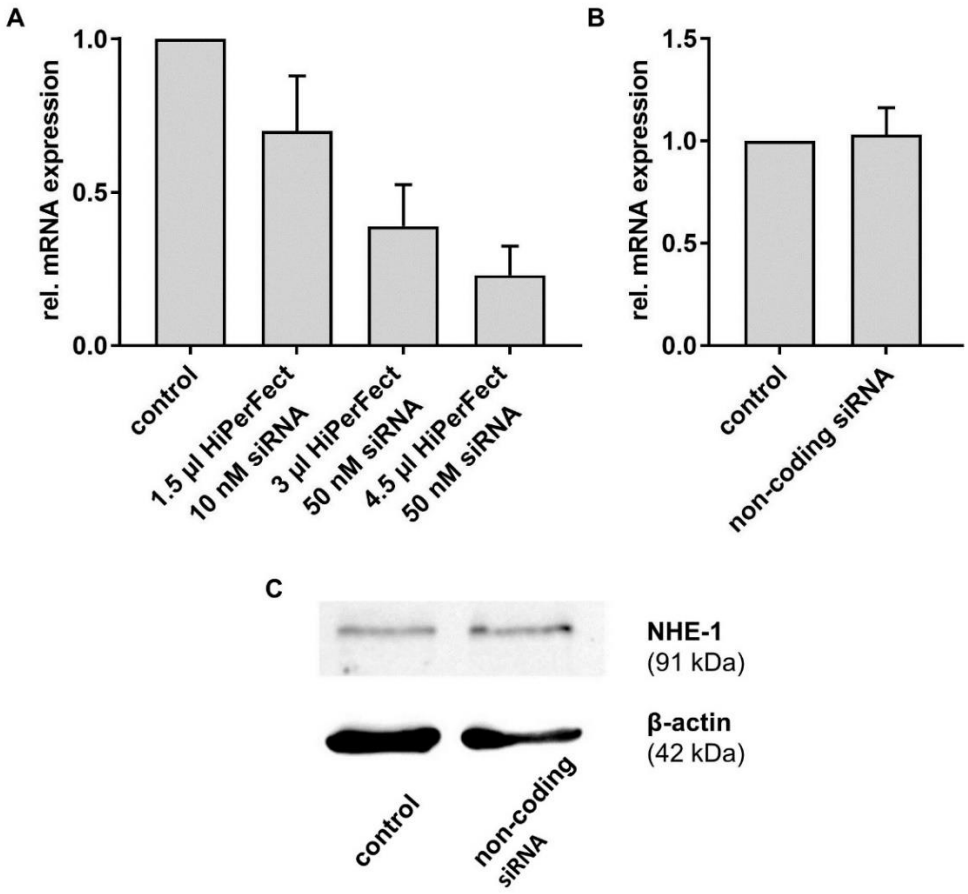

Figure 4-1 *Relative mRNA expression of NHE-1 in normal human keratinocytes 48 h after (A) siRNA 2 and (B) non-coding siRNA transfection quantified by RT-PCR, mean ± SEM, n = 3. (C) Protein expression of NHE-1 and β-actinin in normal human keratinocytes untreated and non-coding siRNA transfected.*

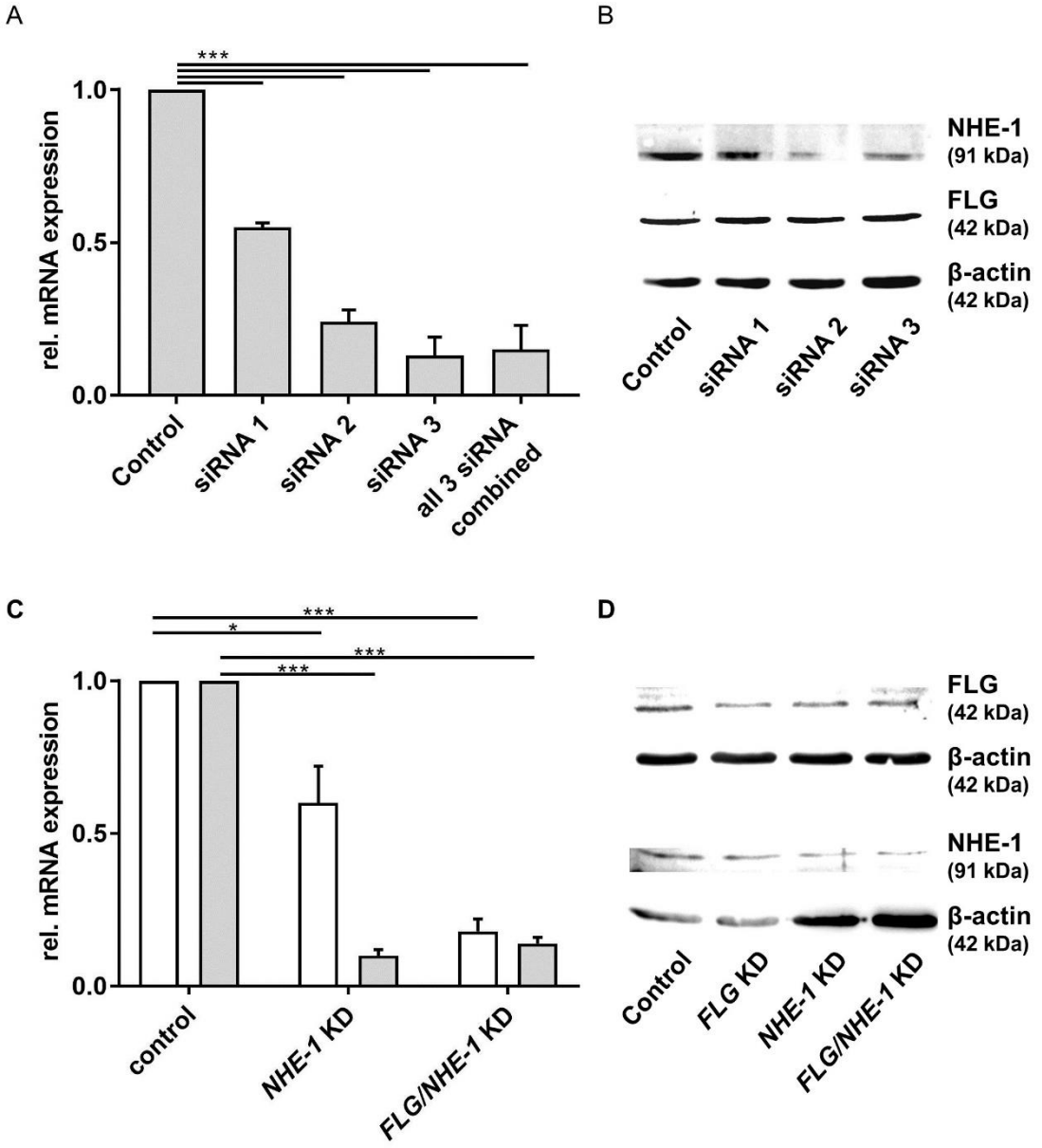

Figure 4-2 *(A) Relative mRNA expression of NHE-1 and (B) protein expression of NHE-1, FLG and β-actin in normal human keratinocytes 48 h post transfection. (C) Relative mRNA expression of FLG (white) and NHE-1(grey bars) and (D) protein expression of NHE-1, FLG and β-actin in skin models. Relative mRNA expression quantified by RT-PCR; mean ± SEM, n = 3, *p ≤ 0.05, ***p ≤ 0.001.*

For disease skin model generation, keratinocytes were transfected with *FLG*- (HSS177192) or *NHE-1*- (HSS109889) specific siRNA sequences alone or in combination *NHE-1* and *FLG* KDs were performed 48h and 24h prior seeding, respectively. In the fully formed skin models, a KD efficiency of 90.5 ± 3.1% for *NHE-1* was achieved (Fig. 4-2 C), and KD efficiencies of 81.6 ± 4.1% and 86.3 ± 1.8% for *NHE-1* and *FLG* respectively in the double KD skin models. KDs were confirmed by western blot and immunostaining (Fig. 4-2 D and Fig. 4-3 E-H). Unexpectedly, a slight reduction in *FLG* expression, both at the mRNA and protein level, was seen in the *NHE-1* KD models (Fig. 4-3).

4.4.2 SKIN MODEL CHARACTERIZATION

In line with previous publications, the *FLG* deficient skin model was characterized by disturbed epidermal maturation and differentiation as compared with the normal skin model (Fig. 4-3 B) [19]. These effects were even more pronounced in the *NHE-1* and *FLG/NHE-1* KD skin models (Fig. 4-3 C, D).

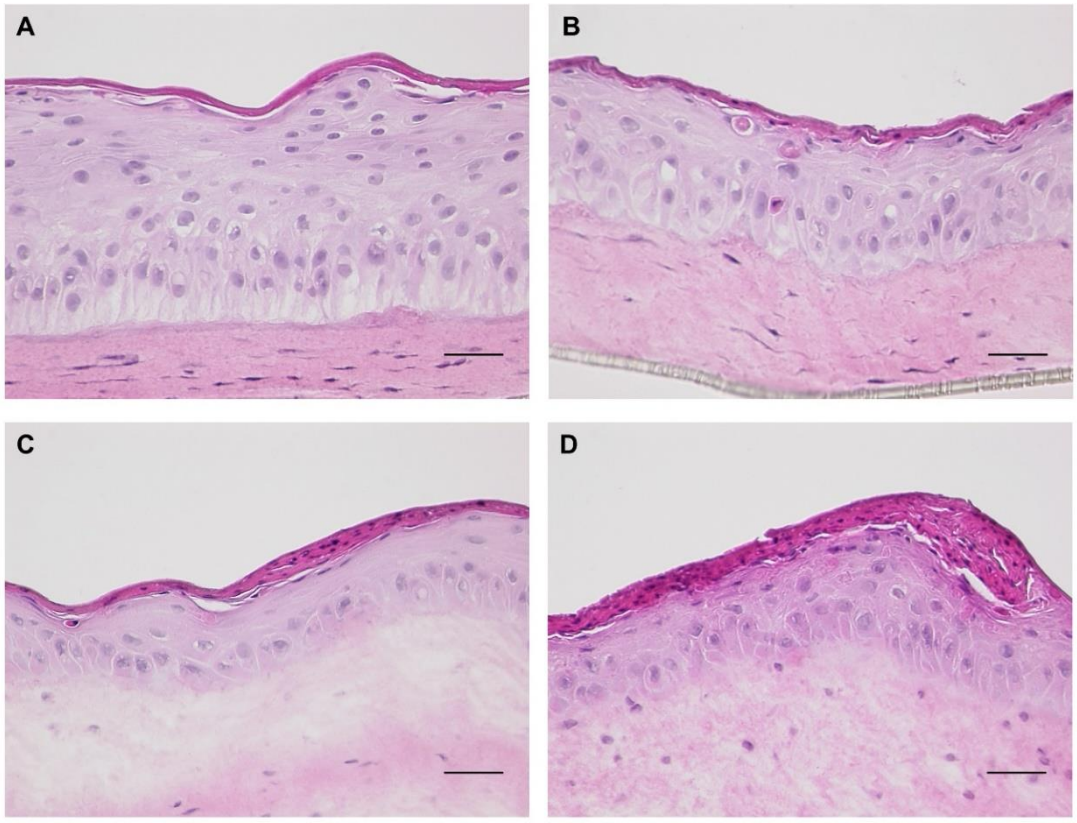

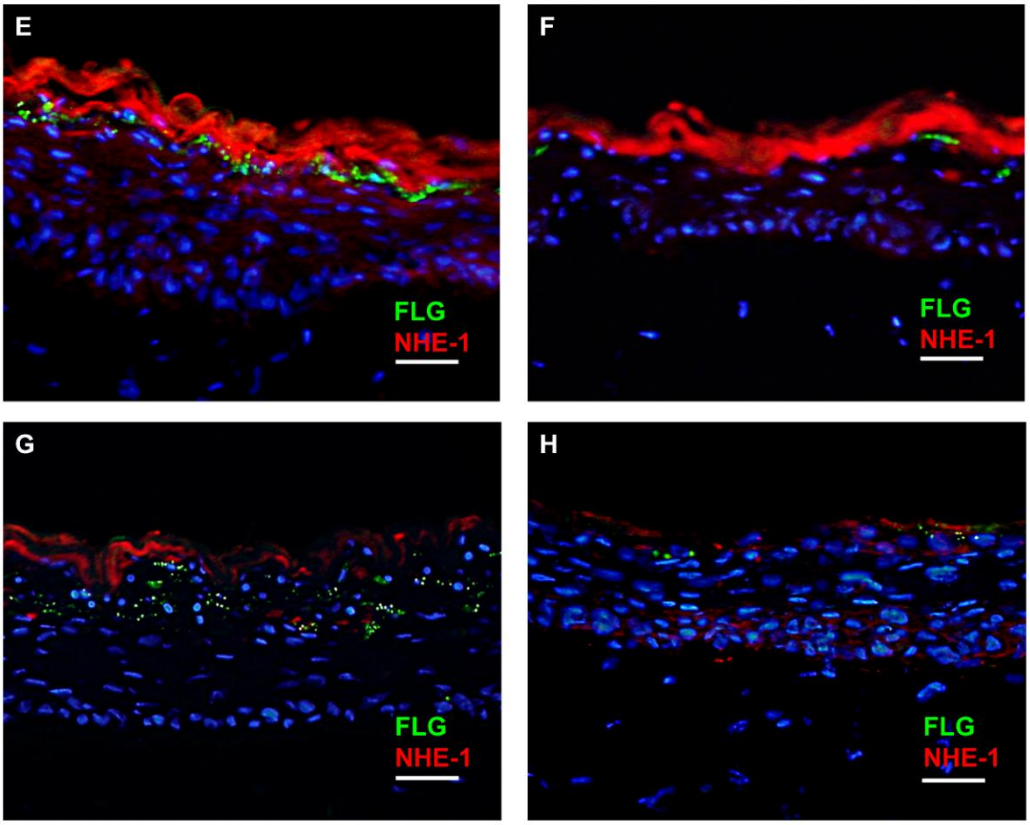

Figure 4-3 *Representative histological pictures of (A) normal, (B) FLG KD, (C) NHE-1 KD and (D) FLG/NHE-1 KD models after 14 days cultivation. Immunostaining against filaggrin (green) and NHE-1 (red) in (E) normal, (F) FLG KD, (G) NHE-1 KD and (H) FLG/NHE-1 KD models. The cell nuclei were counterstained with DAPI (blue fluorescence), 20× magnification, scale bar = 50 µm.*

4.4.3 SKIN SURFACE PH MEASUREMENTS

Normal skin models exhibited a skin surface pH of 5.45 ± 0.1. No significant differences between normal and filaggrin-deficient skin models were detected. *NHE-1*-deficient models showed a significant increased to pH 5.66 ± 0.1 (n=4, *p < 0.05). Similarly, *FLG/NHE-1* KD models demonstrated a surface pH of 5.62 ± 0.1. Representative images of the skin surface pH measurements are shown in Figure 4-4.

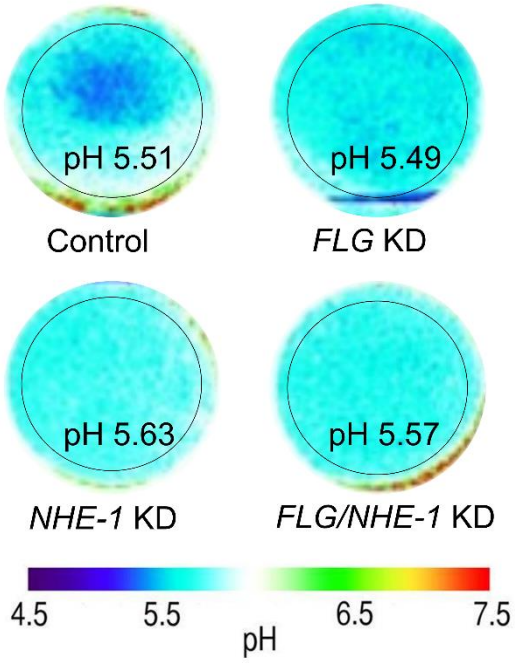

Figure 4-4 *Representative skin surface pH of skin models at day 14 of tissue cultivation using RGB-imaging luminescent 2D-imaging.*

4.4.4 SPLA$_2$ EXPRESSION

To investigate the influence of filaggrin and NHE-1 deficiencies on the expression of different sPLA$_2$ subtypes, relative mRNA expressions of sPLA$_2$ IB, IIF, IIA, V, X and XIIA were analyzed. No significant differences between the normal, *NHE-1* or *FLG/NHE-1* deficient skin models were detected for sPLA$_2$ IB, IIF, V, X and XIIA (Fig. 4-5). The expression of sPLA$_2$ IIA was too low to be assessed.

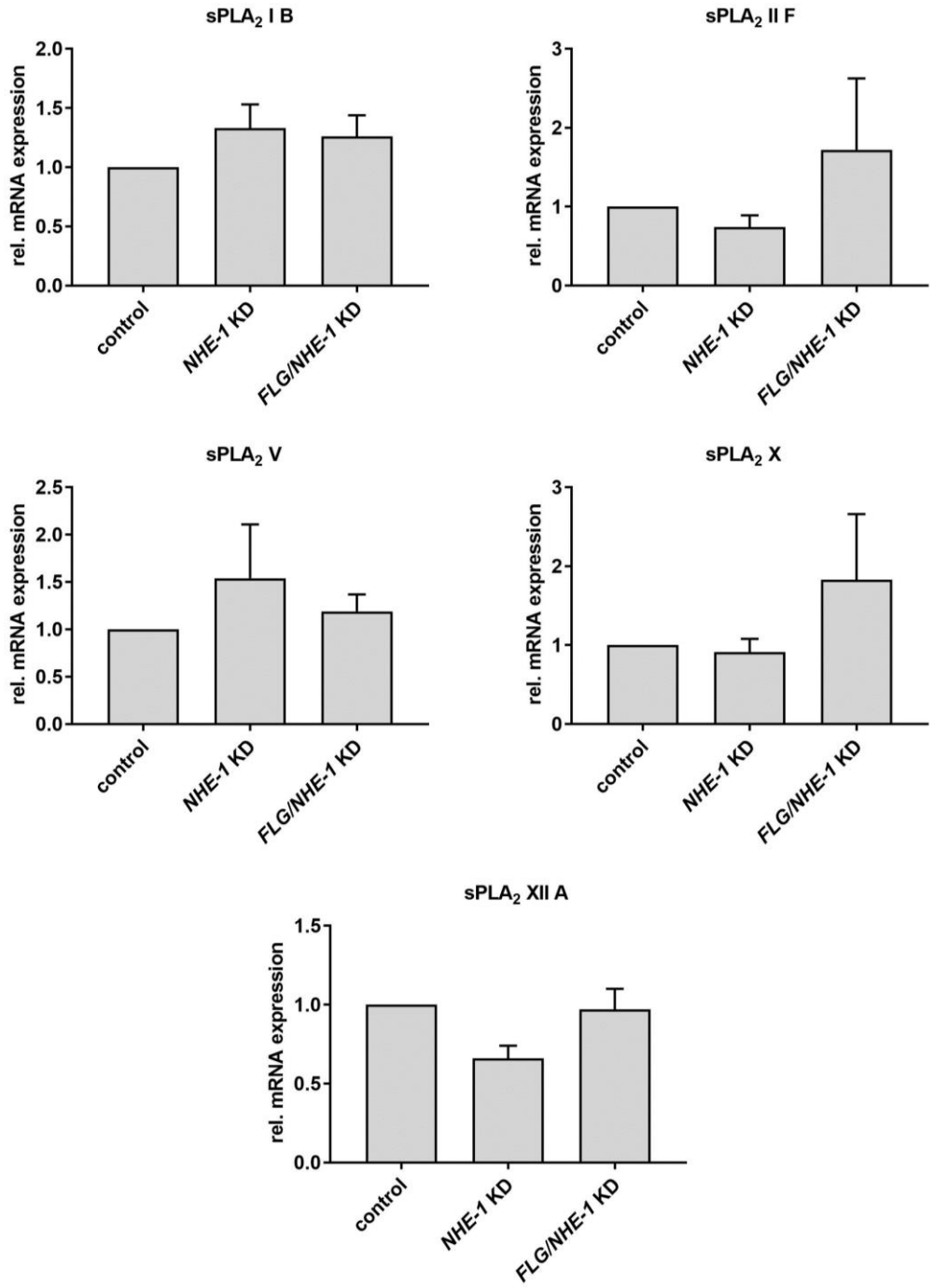

Figure 4-5 *Relative mRNA expression of sPLA2 1B, 2F, V, X and IIA in NHE-1 and FLG/NHE-1 KD skin models quantified by RT-PCR; mean ± SEM, n = 4.*

4.5 DISCUSSION

Skin models are important tools for the investigation of complex physiological and pathophysiological processes [21,22]. Using RNA interference, specific genes of interest can be knocked down in order to study their impact on skin homeostasis. The aim of the present study was to develop and characterize a *FLG/NHE-1* double KD skin model to the feasibility of a double KD approach, and to investigate the impact of filaggrin and NHE-1 deficiencies on the skin surface pH.

Filaggrin is an important structural protein in the human epidermis, where mutations in *FLG* are known to cause ichthyosis vulgaris and act as a major predisposing risk factor to the manifestation of atopic dermatitis [14]. The hypothesis that filaggrin degradation is essential for skin acidification was recently challenged by several groups [16,17,23]. NHE-1, the only sodium hydrogen antiporter isoform expressed in keratinocytes, regulates intracellular pH, cellular volume and acidifies extracellular 'microdomains' of the upper epidermis [12,24]. Moreover, it is upregulated in instances of FLG deficiency [17]. While an important role for NHE-1 in skin acidification has been suggested, its exact role has remained elusive.

In the present study, *NHE-1* KD resulted in a moderate but statistically significant increase in the surface pH of skin models (Fig. 4). Whilst it was clear *NHE-1* KD reduced the NHE-1 protein expression, it is still unknown exactly how many active proton pumps are required to maintain skin surface pH. Residual NHE-1 levels post KD may be sufficient for substantial acidification and could explain the moderate increase in skin surface pH. The increase in skin surface pH is concordant with previously published work, where topical treatment with a specific NHE-1 inhibitor led to only slight pH elevations in neonatal rats [23], and *NHE-1* knockout mice displayed similarly mild increased in surface pH compared to wild-type [12]. In contrast to these studies, the data presented here was acquired by an *in vitro* approach, avoiding animal experiments. The use of human primary keratinocytes also ensures the absence of interspecies disparities.

Interestingly, the double KD of *FLG* and *NHE-1* resulted in similar pH values as the single *NHE-1* KD. We previously identified a compensatory upregulation of NHE-1 in filaggrin deficient skin, indicating a feedback mechanism to maintain the skin surface

pH [17]. The deficiency of both, however, did not further increase the pH. Comparable results were described by Fluhr et al., where inhibition of NHE-1 or $sPLA_2$ slightly increased the pH values and delayed postnatal SC acidification, but simultaneous inhibition of both did not lead to further detrimental effects [25]. A similar scenario is suggested for NHE-1 and filaggrin. Beyond that, *NHE-1* KD led to reduced amounts of FLG in skin models, which might provide a further explanation why the *NHE-1* KD and the *FLG/NHE-1* KD do not relevant differ. The reduced amount of FLG in *NHE-1* KD models may originate from an impaired skin differentiation.

Furthermore, if inhibition of the known contributors to skin acidification such NHE-1 does not lead to a shift to the near neutral surface pH, other thus far undiscovered pathways may well be involved.

In conclusion, we have shown that it is possible to knock down the two genes, *FLG* and *NHE-1*, at the same time in reconstructed skin models. Furthermore, we confirmed that NHE-1 is important for the formation and maintenance of epidermis and contributes to the skin acidification. The contribution of FLG to the acidity of the skin is inferior, also when NHE-1 is lacking.

4.6 ACKNOWLEDGEMENTS

We greatly acknowledge the assistance with the pH measurements of Robert J. Meier (University Regensburg) and the scientific support of Priv. Doz. Dr. Joachim Fluhr (Charité Berlin).

4.7 REFERENCES

1 Behne MJ, Barry NP, Hanson KM, Aronchik I, Clegg RW, Gratton E, et al.: Neonatal development of the stratum corneum pH gradient: localization and mechanisms leading to emergence of optimal barrier function. J Invest Dermatol 2003 Jun;120:998–1006.

2 Hachem J-P, Crumrine D, Fluhr J, Brown BE, Feingold KR, Elias PM: pH directly regulates epidermal permeability barrier homeostasis, and stratum corneum integrity/cohesion. J Invest Dermatol 2003 Aug;121:345–53.

3 Schreml S, Szeimies R-M, Karrer S, Heinlin J, Landthaler M, Babilas P: The impact of the pH value on skin integrity and cutaneous wound healing. J Eur Acad Dermatol Venereol 2010 Apr;24:373–8.

4 Proksch E, Brandner JM, Jensen JM: The skin: An indispensable barrier. Exp Dermatol 2008;17:1063–1072.

5 Holleran WM, Ginns EI, Menon GK, Grundmann JU, Fartasch M, McKinney CE, et al.: Consequences of beta-glucocerebrosidase deficiency in epidermis. Ultrastructure and permeability barrier alterations in Gaucher disease. J Clin Invest 1994 Apr;93:1756–64.

6 Takagi Y, Kriehuber E, Imokawa G, Elias PM, Holleran WM: Beta-glucocerebrosidase activity in mammalian stratum corneum. J Lipid Res 1999;40:861–869.

7 Holleran WM, Takagi Y, Uchida Y: Epidermal sphingolipids: Metabolism, function, and roles in skin disorders. FEBS Lett 2006;580:5456–5466.

8 Rippke F, Schreiner V, Doering T, Maibach HI: Stratum corneum pH in atopic dermatitis: impact on skin barrier function and colonization with Staphylococcus Aureus. Am J Clin Dermatol 2004 Jan;5:217–23.

9 Schmid-Wendtner M-H, Korting HC: The pH of the skin surface and its impact on the barrier function. Skin Pharmacol Physiol 2006 Jan;19:296–302.

10 Jungersted JM, Scheer H, Mempel M, Baurecht H, Cifuentes L, Høgh JK, et al.: Stratum corneum lipids, skin barrier function and filaggrin mutations in patients with atopic eczema. Allergy 2010;65:911–918.

11 Fluhr JW, Kao J, Jain M, Ahn SK, Feingold KR, Elias PM: Generation of free fatty acids from phospholipids regulates stratum corneum acidification and integrity. J Invest Dermatol 2001 Jul;117:44–51.

12 Behne MJ, Meyer JW, Hanson KM, Barry NP, Murata S, Crumrine D, et al.: NHE1 regulates the stratum corneum permeability barrier homeostasis. Microenvironment acidification assessed with fluorescence lifetime imaging. J Biol Chem 2002 Dec 6;277:47399–406.

13 Smith FJD, Irvine AD, Terron-Kwiatkowski A, Sandilands A, Campbell LE, Zhao Y, et al.: Loss-of-function mutations in the gene encoding filaggrin cause ichthyosis vulgaris. Nat Genet 2006;38:337–342.

14 Palmer CN, Irvine AD, Terron-Kwiatkowski A, Zhao Y, Liao H, Lee SP, et al.: Common loss-of-function variants of the epidermal barrier protein filaggrin are a major predisposing factor for atopic dermatitis. Nat Genet 2006 Apr;38:441–6.

15 Brown SJ, McLean WHI: One remarkable molecule: filaggrin. J Invest Dermatol 2012 Mar;132:751–62.

16 Fluhr JW, Elias PM, Man M-Q, Hupe M, Selden C, Sundberg JP, et al.: Is the filaggrin-histidine-urocanic acid pathway essential for stratum corneum acidification? J Invest Dermatol 2010 Aug;130:2141–4.

17 Vávrová K, Henkes D, Strüver K, Sochorová M, Skolová B, Witting MY, et al.: Filaggrin deficiency leads to impaired lipid profile and altered acidification pathways in a 3D skin construct. J Invest Dermatol 2014 Mar;134:746–53.

18 Eckl K-M, Alef T, Torres S, Hennies HC: Full-thickness human skin models for congenital ichthyosis and related keratinization disorders. J Invest Dermatol 2011 Sep;131:1938–42.

19 Küchler S, Henkes D, Eckl K-M, Ackermann K, Plendl J, Korting H-C, et al.: Hallmarks of atopic skin mimicked in vitro by means of a skin disease model based on FLG knock-down. Altern Lab Anim 2011 Oct;39:471–80.

20 Schreml S, Meier RJ, Weiß KT, Cattani J, Flittner D, Gehmert S, et al.: A sprayable luminescent pH sensor and its use for wound imaging in vivo. Exp Dermatol 2012 Dec;21:951–3.

21 Pendaries V, Malaisse J, Pellerin L, Le Lamer M, Nachat R, Kezic S, et al.: Knockdown of filaggrin in a three-dimensional reconstructed human epidermis impairs keratinocyte differentiation. J Invest Dermatol 2014 Dec 13;134:2938–46.

22 Küchler S, Strüver K, Friess W: Reconstructed skin models as emerging tools for drug absorption studies. Expert Opin Drug Metab Toxicol 2013 Oct 5;9:1255–63.

23 Fluhr JW, Behne MJ, Brown BE, Moskowitz DG, Selden C, Mao-Qiang M, et al.: Stratum corneum acidification in neonatal skin: secretory phospholipase A2 and the sodium/hydrogen antiporter-1 acidify neonatal rat stratum corneum. J Invest Dermatol 2004 Feb;122:320–9.

24 Sarangarajan R, Shumaker H, Soleimani M, Le Poole C, Boissy RE: Molecular and functional characterization of sodium--hydrogen exchanger in skin as well as cultured keratinocytes and melanocytes. Biochim Biophys Acta 2001 Mar 9;1511:181–92.

25 Choi E-H, Man M-Q, Xu P, Xin S, Liu Z, Crumrine D a, et al.: Stratum corneum acidification is impaired in moderately aged human and murine skin. J Invest Dermatol 2007 Dec;127:2847–56.

5 DEVELOPMENT OF A PERFUSION PLATFORM FOR DYNAMIC CULTIVATION OF IN VITRO SKIN MODELS

The following section has been published in Skin Pharmacology and Physiology and appears in this thesis with the journal`s permission:

Project idea: K. Strüver
Design of experiments: K. Strüver, S. Hedtrich, W. Friess
Performed experiments: K. Strüver
Data analysis: K. Strüver, S. Hedtrich, W. Friess
Manuscript writing: K. Strüver
Manuscript revision: K. Strüver, S. Hedtrich, W. Friess

5.1 ABSTRACT

Reconstructed skin models are suitable test systems for toxicity testing and for basic investigations on (patho-)physiological aspects of human skin. Reconstructed human skin, however, has clear limitations such as the lack of immune cells and a significantly weaker skin barrier function compared to native human skin. Potential reasons for the latter might be the lack of mechanical forces during skin model cultivation which is performed classically in static well-plate set-ups. Mechanical forces and shear stress have a major impact on tissue formation and, hence, tissue engineering.

In the present work, a perfusion platform was developed allowing dynamic cultivation of *in vitro* skin models. The platform was designed to cultivate reconstructed skin at the air-liquid interface with a laminar and continuous medium flow below the dermis equivalent. Histological investigations confirmed the formation of a significantly thicker stratum corneum compared to the control cultivated under static conditions. Moreover, the skin differentiation markers involucrin and filaggrin as well as the tight junction proteins claudin-1 and occludin showed increased expression in the dynamically cultured skin models. Unexpectedly, despite improved differentiation, the skin barrier function of the dynamically cultivated skin models was not enhanced compared with the skin models cultivated under static conditions.

5.2 INTRODUCTION

Safety and risk assessment procedures for drugs and the demand to improve standards and knowledge about these topics goes along with constantly high numbers of animal experiments in the European Union [1]. However, ethical standards of the modern society and low predictive power of animal models [2,3] call for the avoidance or reduction of animal experiments whenever possible. Hence, academia and pharmaceutical industry are working on the establishment of alternative test systems in accordance with the 3R's principle established in 1959: the replacement, reduction or refinement of animal experiments. To bring in line the need for powerful test systems and the avoidance of animal experiments, alternative approaches, often based on tissue engineering, are investigated and improved [4,5]. Especially for human skin a whole slew of methods is available today.

Reconstructed human epidermis and full-thickness skin models are commercially available and validated by the OECD for skin irritation and corrosion testing. Additionally, they are accepted for testing skin absorption taking into account the generally higher permeability of *in vitro* skin models [6–8]. Moreover, skin models are used for the assessment of drugs' pharmacodynamics or side effects [9] and for fundamental studies on (patho-)physiological mechanism [10–12]. Nevertheless, *in vitro* skin models clearly have limitations compared to native human skin such as lower mechanical resistance, impaired maturation and differentiation, altered skin lipid composition and organization [13,14], increased skin permeability [15] and a lack of complexity, *e.g.* missing immune cells or systemic circulation [16].

The reasons for the altered skin lipids and the weakened skin barrier function are diverse. All tissues in the human body are constantly subjected to forces such as pressure, fluid shear stress, stretch or compression. Mechanical forces are crucial for normal tissue homeostasis and remodeling and influence fundamental cellular events such as cell division [17–19]. These basic principles depict the importance of mechanical forces also for tissue engineering. Various publications have described beneficial effects of mechanical forces when applied on reconstructed tissue such as artificial cartilage or lung tissue [19–22]. Additionally, responses of human skin cells to electrical field stimulation, such as an accelerated alignment of fibroblasts, has been

described [23]. Thus, the lack of specific biophysical and biochemical signaling or mechanical forces and shear stress during cultivation under static conditions in well plates may considerably contribute to the less efficient barrier function of skin models [24,25]. Furthermore, skin models do not have an active nutrient supply through capillaries and they lack the effect of convection and dependent on nutrient supply by diffusion.

Hence, to improve the quality of *in vitro* skin models and to investigate the impact of mechanical forces on skin homeostasis, a perfused bioreactor was constructed allowing the cultivation of skin models at the air liquid interface and providing a continuous flow of cultivation medium at the basal side. Following development of the bioreactor optimized medium flow rates and velocities were determined followed by investigating their impact on skin differentiation and maturation, the expression of skin barrier and tight junction proteins was investigated, and the skin barrier function was determined.

5.3 MATERIALS AND METHODS

5.3.1 CONSTRUCTION OF PERFUSION PLATFORM

The perfusion platform was constructed for Falcon 6-well cell culture inserts (VWR, Darmstadt, Germany). The design drawing was performed using 3D CAD Design Software SolidWorks (Dassault Systèmes S.A., Vélizy-Villacoublay, France). The test systems were manufactured at research workshop of the Faculty of Chemistry and Pharmacy, LMU Munich. The platform is composed of polytetrafluoroethylene (PTFE) to allow steam sterilization.

5.3.2 CELL CULTURE

Primary human fibroblasts and keratinocytes were isolated from juvenile foreskin according to standard procedures (approved by the ethics committee of the LMU Munich, with written consent) [26]. Briefly, epidermis and dermis were separated after overnight incubation with Dispase II (1.2 U/mL in PBS, Roche Diagnostics, Mannheim, Germany). The separated epidermis was treated with trypsin/EDTA (2,5 mg/mL trypsin, 1 mmmol/L EDTA, Biochrome, Berlin, Germany) for 5 min at 37°C to singularize keratinocytes. To cultivate primary keratinocytes, keratinocyte growth medium (Lonza, Cologne, Germany) was used. After outgrowth from the dermis, fibroblasts were further cultivated in DMEM (Sigma-Aldrich, Taufkirchen, Germany) containing 5 mM L-glutamine and 10% FBS (Biochrome, Berlin, Germany). Media was changed every other day and the cells were used at passage 2 or 3.

5.3.3 CONSTRUCTION OF SKIN MODELS

In vitro skin models were generated according to previously published procedures [27,28]. Briefly, bovine collagen (3 mg/mL, Cellsytems, Troisdorf, Germany) was mixed with 10-fold Hanks balanced salt solution (Thermo Scientific, Darmstadt, Germany) and brought to neutral pH. Afterwards, 2.5 x 105 fibroblasts (per skin model) were added and 2.5 ml of the mixture was poured into 6-well cell culture inserts (pore size: 3 µm, surface area 4.2 cm2, 2x106 pores/cm2, PET membrane, VWR, Ismaning, Germany). After solidification at 37° C for 2h, 4.2 x 106 normal keratinocytes were added on top of the collagen matrix. 24h later, the skin models were lifted to the air-liquid interface and the medium was changed to a differentiation medium. At this stage,

the skin models were transferred to the perfusion platform and grown for six more days. Skin models cultivated in static 6-well plates served for reference.

5.3.4 HEMATOXYLIN-EOSIN (H&E) STAINING

Skin models were punched and immediately embedded in tissue freezing medium (Leica Microsystems, Nussloch, Germany). The embedded models were shock-frozen using liquid nitrogen and stored for 12h at -80°C. Vertical 7 µm thick cryosections (at an angle of 90°) were prepared using a cryotome (Leica Microsystems, Nussloch, Germany). A standard H&E staining procedure was performed for histological analysis. The skin sections were analyzed using the microscope BZ-8000 (Keyence, Neu-Isenburg, Germany).

5.3.5 THICKNESS MEASUREMENTS

The thickness of the stratum corneum was measured from the top of the skin models to the beginning of the viable epidermis, directly below the straum corneum. Viable epidermal thickness was measured from below the stratum corneum to the beginning of the dermal equivalent in three H&E stained sections (per skin equivalent). Dermal thickness measurement was performed from the beginning of the dermis equivalent to the beginning of the cell culture insert. In total, ten measuring points were evaluated in each section using BZ image analysis software, respectively (Keyence, Neu-Isenburg, Germany).

5.3.6 REAL-TIME POLYMERASE CHAIN REACTION (QPCR)

Skin models were punched to discs of 10 mm diameter. The epidermis was peeled-off and immediately frozen in liquid nitrogen. The frozen epidermis was subsequently milled with a CryoMill (RETSCH GmbH, Haan, Germany). RNA was isolated using the NucleoSpin® RNA II kit (Macherey-Nagel, Düren, Germany) according to the manufacturer's instructions. RNA was treated with DNase 1 (Sigma-Aldrich, Taufkirchen, Germany). For cDNA synthesis, RevertAidTM First Strand cDNA Synthesis Kit (Thermo Scientific, Waltham, MA, USA) was used. For relative gene expression quantification, quantitative PCR was performed using the Power SYBR® Green PCR Master Mix (Thermo Scientific, Darmstadt, Germany) and the qTower 2.2

PCR cycler (Analytik Jena AG, Jena, Germany). The primer sequences (Tib Molbiol, Berlin, Germany) are listed in Table 5-1. YWHAZ served as house-keeping gene.

Table 5-1 *Primer sequences for PCR.*

Gene	Primer sense 5'-3'	Primer antisense 5'-3
YWHAZ	AGACGGAAGGTGCTGAGAAA	GAAGCATTGGGGATCAAGAA
FLG	AAGGAACTTCTGGAAAAGGAATTTC	TTGTGGTCTATATCCAAGTGATCCAT
IVL	TCCTCCAGTCAATACCCATCAG	CAGCAGTCATGTGCTTTTCCT
CLDN-1	GCGCGATATTTCTTCTTGCAGG	TTCGTACCTGGCATTGACTGG
OCLN	TGCATGTTCGACCAATGC	AAGCCACTTCCTCCATAAGG

5.3.7 WESTERN BLOT

For Western blot analysis of filaggrin, involucrin, claudin 1 and occludin the epidermis of skin models was shock frozen in liquid nitrogen and milled using a CryoMill (Retsch GmbH, Haan, Germany). The milled epidermis was then lysed in RIPA buffer containing protease inhibitors (New England Biolabs, Frankfurt/Main, Germany), centrifuged for 30 min at 14,000 × g and the supernatant was subsequently stored at -80°C until use. The protein amount was quantified by a BCA protein assay (Thermo Scientific, Waltham, USA). 30 µg of each protein sample was incubated at 95°C in standard SDS-PAGE buffer and separated via 10% SDS polyacrylamide gel electrophoresis (Bio-Rad, Munich, Germany). Gels were blotted onto Immobilon P nitrocellulose membranes (Carl Roth, Karlsruhe, Germany) via Trans-Blot® Turbo™ Transfer System (Bio-Rad, Munich, Germany). After blocking with 5% non-fat dry milk in tris-buffered saline -Tween 20 (0.1%) for 1h, the membranes were incubated with primary antibodies (anti-filaggrin antibody ab81468, anti-involucrin ab53112, Abcam, Cambridge, UK, CLDN1 monoclonal antibody (clone 1C5-D9), OCLN monoclonal antibody (clone 1G7), Abnova, Taipeh, Taiwan) overnight. Subsequently, the membranes were washed and incubated with anti-rabbit or anti-mouse horseradish-peroxidase-conjugated secondary antibody (Cell Signaling, Frankfurt/Main, Germany) at room temperature for 1h. All blots were developed with SignalFire™ ECL reagent

(Cell Signaling, Frankfurt/Main, Germany) and visualized by a PXi/PXi Touch gel imaging system (Syngene, Cambridge, UK). Protein expression was semi-quantified by densitometry and normalized to β-actin levels using ImageJ version 1.6 (National Institutes of Health, Bethesda, USA).

5.3.8 SKIN PERMEABILITY TESTING

The permeability of the skin models was evaluated according to validated test procedures [8]. Briefly, stock solutions of testosterone (40 µg/ml, 2% [v/v] Igepal® CA-630) and caffeine (1 mg/ml) were spiked with an appropriate amount of the radiolabeled compound to achieve a total radioactivity of 2 µCi/ml. Permeation studies were performed at day 7 of tissue cultivation using a Franz diffusion cell setup (diameter 15 mm, volume 12 ml, Permegear, Bethlehem, USA).

5.3.9 STATISTICAL ANALYSIS

The data were statistically analyzed using ANOVA and one-sample or two-sample t-test. $p \leq 0.05$ was defined as the level of significance.

5.4 RESULTS

5.4.1 SET-UP AND ESTABLISHMENT OF A PERFUSED BIOREACTOR

In a first step, a perfusion platform was constructed where standard 6-well inserts fit in (Fig. 5-1). To ensure a laminar and continuous flow of the cultivation medium, the perfusion platform was equipped with two orifices to connect with the tubing. From the orifices, the medium got distributed by a hemicycle deepening and was transported in a laminar flow by introducing parallel channels into the PTFE platform right underneath the cell culture insert membrane. To ensure that the amount of medium entering the platform is identical with the amount which leaves the platform, both orifices were connected to the same peristaltic pump by silicon tubing ending in the medium reservoir (Fig. 5-1).

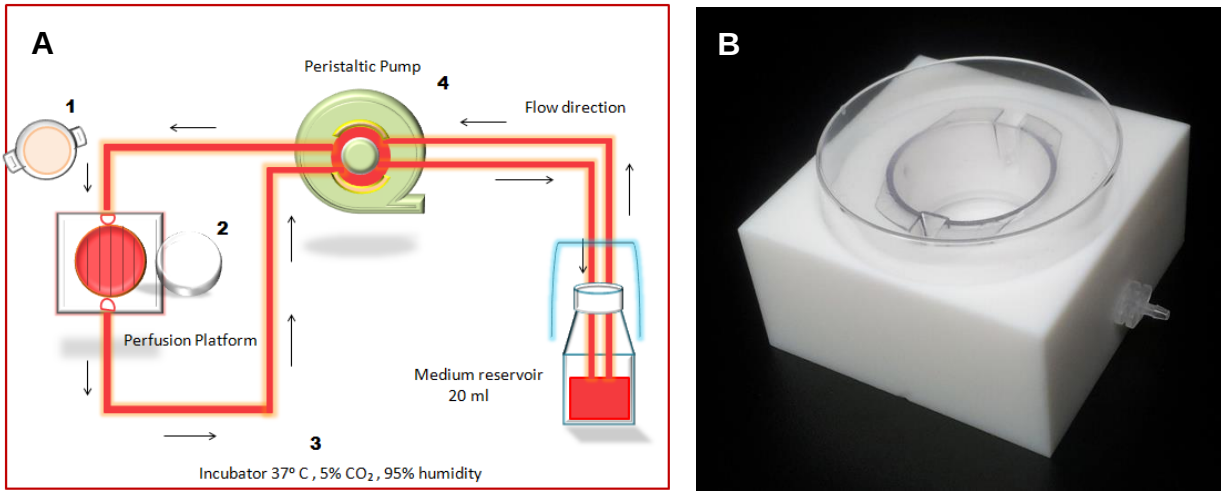

Figure 5-1 *(A) Scheme of the perfusion bioreactor. (B) Image of the perfusion platform equipped with cell culture insert, lid and tubing connectors.*

(1) transfer of the skin models in the cell culture inserts into the perfusion platform after performing the air lift at day 1 of tissue cultivation, (2) capping of the platform, (3) transfer of the entire setup into the incubator at 37°C, 5% CO2 and 95% humidity until day 7 of tissue cultivation, (4) peristaltic pump for continuous flow of the skin model differentiation medium.

5.4.2 HISTOLOGICAL ANALYSIS

Following establishment of the perfusion platform, different medium flow rates were applied, ranging from 1.25 to 10 ml/h (Fig. 2). In general, all dynamically cultivated skin models developed a significantly thicker stratum corneum, the keratinocytes aligned to the direction of medium flow and a significantly thinner but more compact dermis equivalent was observed (Fig. 2; Fig. 3). No significant differences in epidermal maturation or differentiation were overserved (Fig. 3). The viable epidermis showed similar dimensions for all flow rates compared to the static control model.

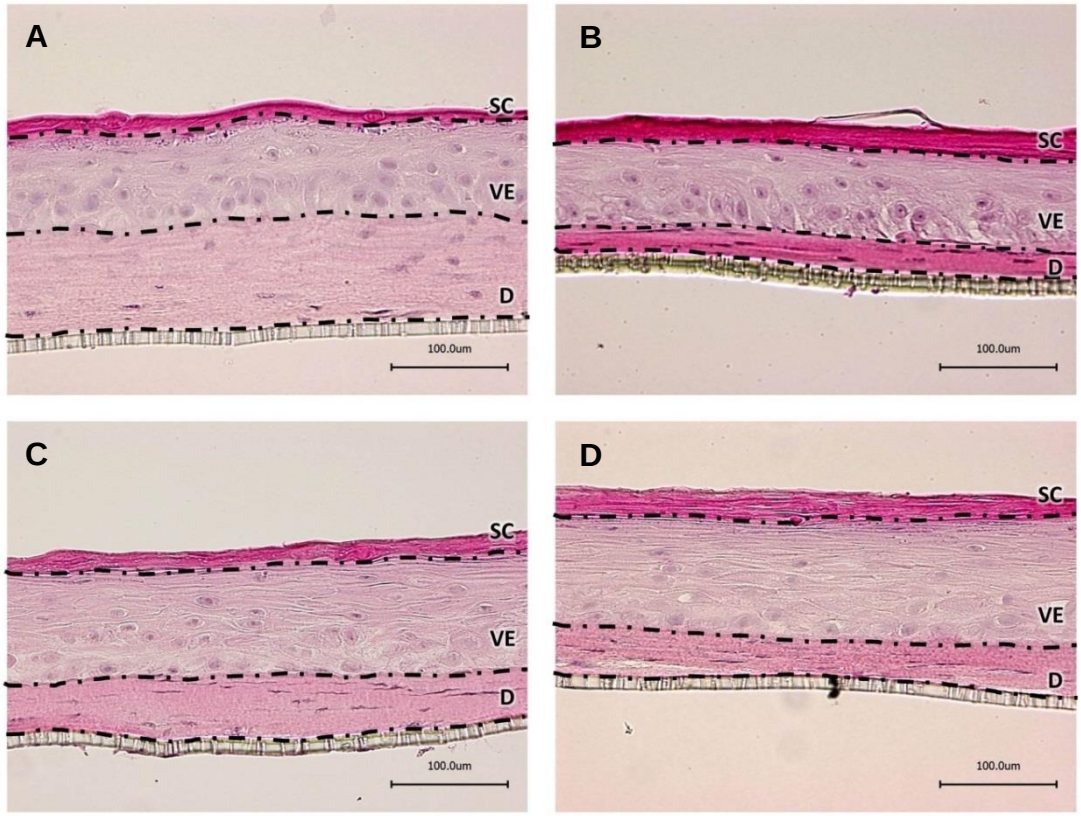

Figure 5-2 *Representative histological pictures of (A) a skin model cultivated under static condition, (B) in the perfusion platform with a flow rate of 1.25 ml/h, (C) flow rate of 2.5 ml/h or (D) flow rate 7.5 ml/h after 7 days of cultivation, SC: stratum corneum , VE: viable epidermis, D: dermis, 20x magnification, scale bar = 100 µm.*

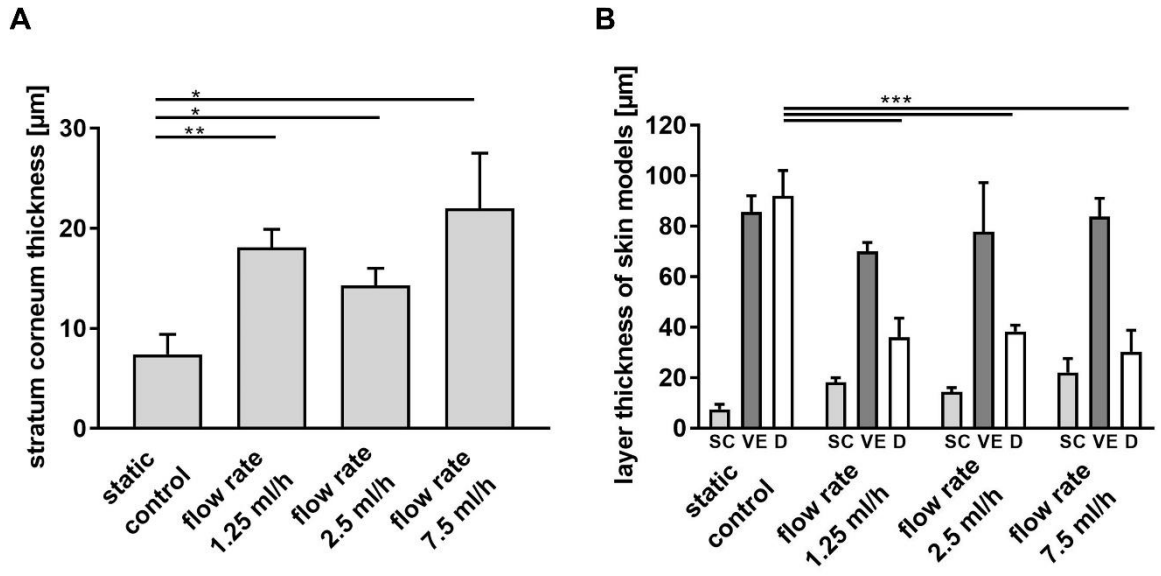

Figure 5-3 *(A) Thickness of the stratum corneum after skin model cultivation of 7 days under static conditions or in the perfusion platform with flow rates of 1.25 ml/h, 2.5 l/h or 7.5 ml/h; (B) thickness of the stratum corneum (SC, light grey), viable epidermis (VE, dark grey) and dermis (D, white) after skin model cultivation of 7 days under static conditions or in the perfusion platform with flow rates of 1.25 ml/h, 2.5 l/h or 7.5 ml/h. Mean ± SEM; n = 4; *p ≤ 0.05, **p ≤ 0.01, ***p ≤ 0.001.*

5.4.3 Gene and protein expression of skin barrier and tight junction proteins following dynamic tissue cultivation

Western blot analysis revealed higher expression of the intermediate and late-stage skin differentiation markers involucrin and filaggrin indicating improved epidermal differentiation as well as increased expression of the tight junction proteins occludin and claudin-1 in the dynamically cultivated skin models (Fig. 4). Unexpectedly, cultivation at 7.5 ml/h showed a trend towards reduced expression of involucrin and occludin (Fig. 4 B; D). On mRNA level, there was a clear trend towards reduced expression of filaggrin, involucrin, claudin-1 and occludin after cultivation at 7.5 ml/h (Fig. 5):

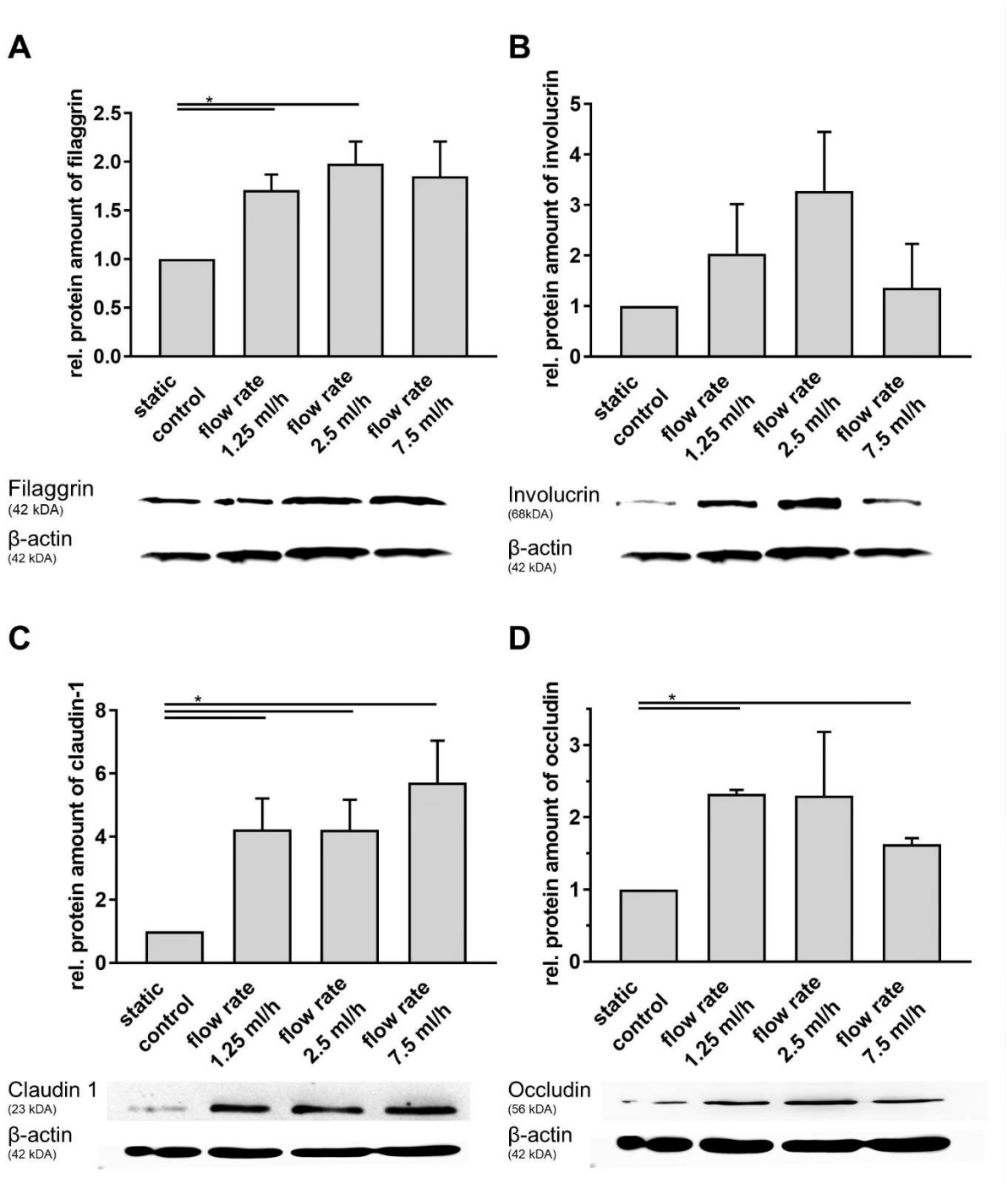

Figure 5-4 *Impact of tissue cultivation in the perfusion platform on expression of (A) filaggrin, (B) involucrin, (C) claudin 1 and (D) occludin after 7 days of cultivation. Western blots and relative protein expression were semi-quantified by densitometry. Mean ± SEM, n = 4, *p ≤ 0.05.*

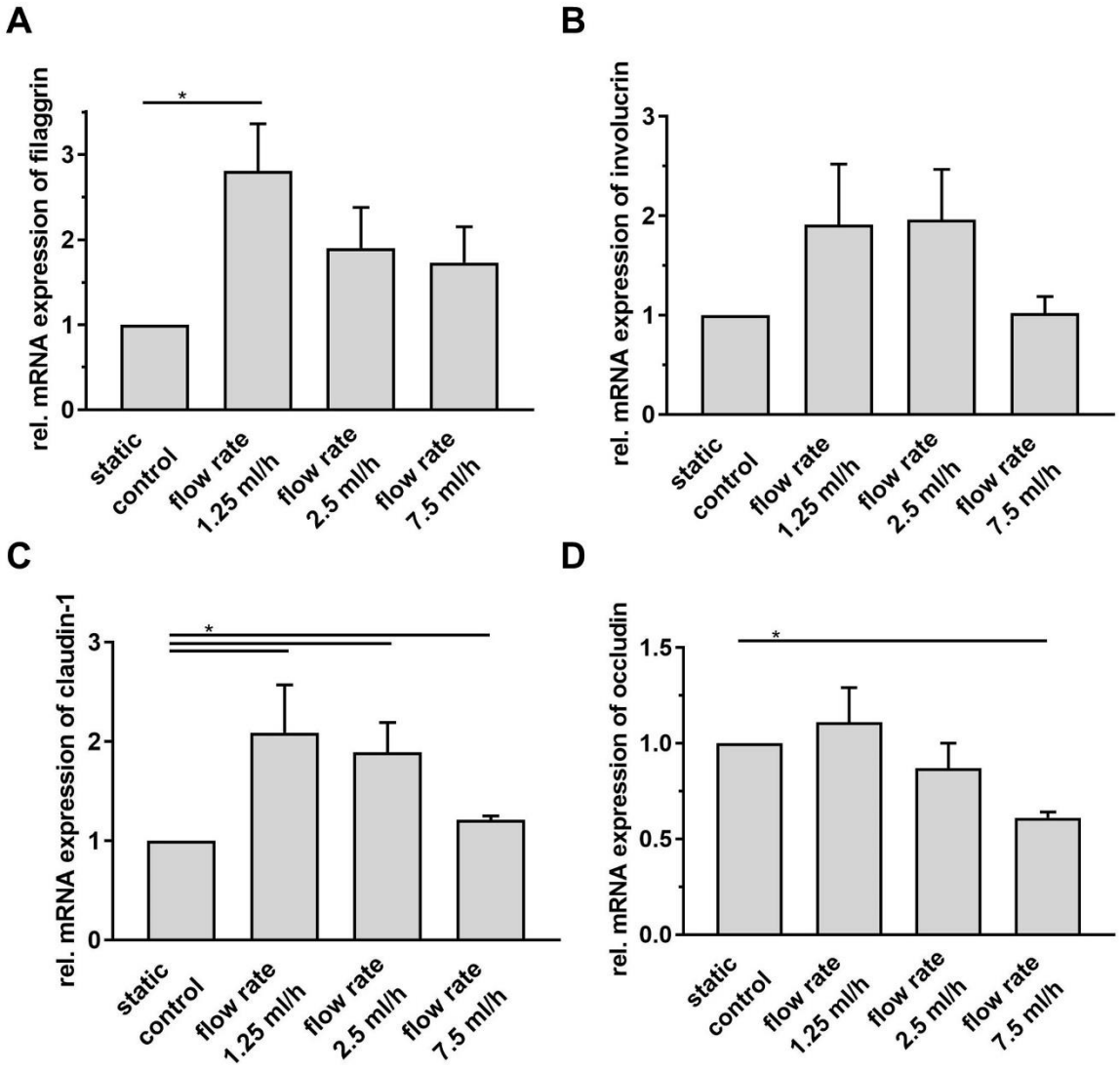

Figure 5-5 *Relative mRNA expression of (A) filaggrin, (B) involucrin, (C) claudin 1 and (D) occludin in skin models cultivated for 7 days under static or dynamic conditions. Mean ± SEM, n = 4, *p ≤ 0.05.*

5.4.4 SKIN PERMEABILITY STUDIES

To assess the barrier function of the skin models and potential positive effects of dynamic culture condition, skin absorption studies using the OECD reference substances testosterone and caffeine were performed. The testosterone flux was significantly increased in the skin models cultivated in the perfusion platforms (Fig. 6A; Tab. 2). No difference in skin permeability between statically or dynamically cultured skin models was detected for the more hydrophilic test compound caffeine (Fig. 6B).

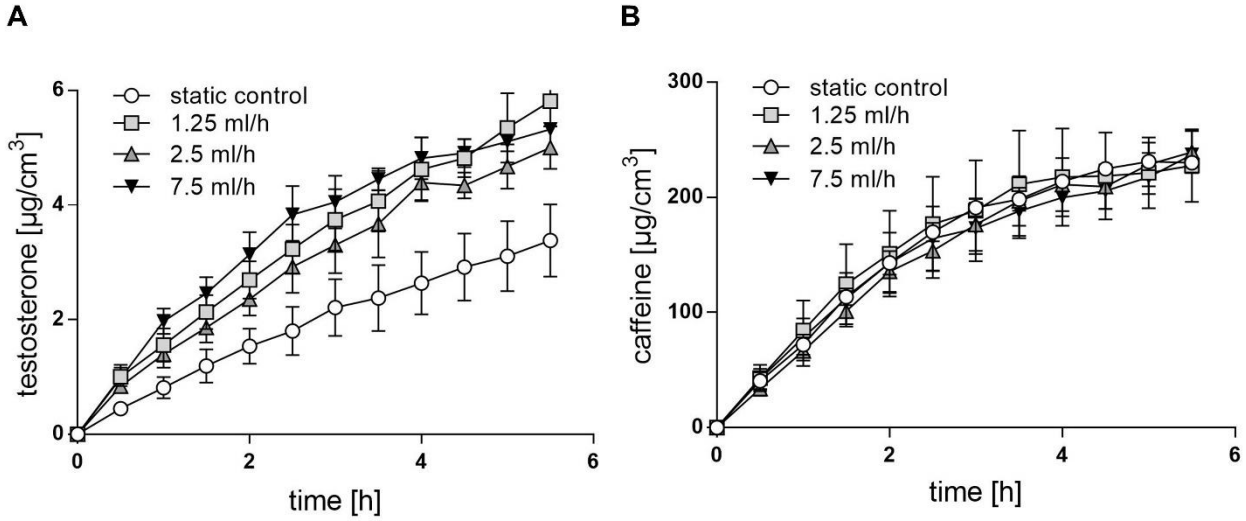

Figure 5-6 *Cumulative amounts (mean ± SEM, n=3) of radioactively-labeled permeated (A) testosterone and (B) caffeine following topical application on skin models cultivated under static control or dynamic (1.25, 2.5, 7.5 ml/h) conditions.*

Table 5-2 *Apparent permeability coefficient (Papp) of radioactively-labeled testosterone and caffeine (mean ± SD, n=3).*

P_{app} (cm/s)	Static control	1.25 ml/h	2.5 ml/h	7.5 ml/h
testosterone	$4.0\pm1.8\times10^{-06}$	$8.4\pm1.3\times10^{-06}$	$7.5\pm1.0\times10^{-06}$	$9.4\pm2.2\times10^{-06}$
caffeine	$4.4\pm0.2\times10^{-04}$	$4.4\pm1.3\times10^{-04}$	$4.3\pm0.7\times10^{-04}$	$4.4\pm0.8\times10^{-04}$

5.5 DISCUSSION

Over the past 20 years, the interest in reconstructed human skin is constantly growing since *in vitro* skin models enable the reduction and replacement of animal experiments and help to avoid interspecies-related differences which are major reasons for the often discussed low predictive power of animal models [3,29]. Although the versatility of skin models is widely recognized today, skin models still have clear limitations such as increased permeability compared to native human skin [15,30,31]. This drawback may result from non-physiological cell culture medium, a lack of cellular crosstalk or tissue complexity and/or tissue cultivation under static conditions in well-plates.

Since the impact of shear stress and mechanical forces on tissue homeostasis and regeneration *in vivo* and *in vitro* is well established [17,32,33], we constructed a PTFE-based perfusion platform enabling continuous flow of skin model differentiation medium underneath the skin model. Following construction of the skin models in well-plates, they were transferred to the perfusion platform at day 1 of tissue cultivation and were further cultivated under dynamic conditions for 7 days. At first, the impact of the flow rate on skin model differentiation and maturation was investigated. Clear detrimental effects on epidermal differentiation resulted from the highest flow rate of 10 ml/h which was therefore excluded from further studies (data not shown). Slower flow velocities between 1.25 ml/h and 7.5 ml/h resulted in a significant thickening of the stratum corneum. This effects was comparable to previously published data, where the maintenance of the EpiDermFT skin model in a dynamic set-up led to a more pronounced stratum corneum compared to the static control [24]. Additionally, higher compaction of the dermis equivalent was observed likely due to detachment of collagen gel as a result of the media flux.

Moreover, we observed significantly increased expression of the important skin barrier protein and differentiation marker filaggrin and a clear trend for increased involucrin expression following dynamic tissue cultivation (Fig. 4). Filaggrin is an important structural protein which contributes to the integrity of the epidermal barrier and the alignment of keratin bundles [34,35] and is disturbed in common skin diseases such as atopic dermatitis [36]. The intermediate-stage differentiation marker involucrin is part of the cornified envelope and reinforces the skin barrier [37]. Interestingly, a trend

for reduced mRNA and protein expression was observed for cultivation at 7.5 ml/h flow rate which may indicate detrimental effects of high velocities on skin differentiation and demonstrates the importance of flow rate adjustment. In line with the epidermal barrier proteins, claudin-1 and occludin expression was increased after dynamic tissue cultivation. Again, slightly reduced expression was observed for the models cultivated at 7.5 ml/h.

Based on the positive effects of the dynamic setting on skin differentiation and maturation, an improved barrier function of dynamically cultivated skin models was expected. Surprisingly, no improved skin barrier function was determined. An even increased permeability was determined for the lipophilic test compound testosterone in the dynamically cultured skin models in contrast to the static cultures. This stands in contrast to the significantly thicker stratum corneum as well as the increased expression of epidermal and tight junction proteins in the dynamically cultivated skin models. One can speculate about potential reasons such as detrimental effects of shear stress on the skin lipid organization or detrimental impact of the collagen detachment from the dermis equivalent, but this requires further evaluation. Interestingly, improved epidermal differentiation is clearly achieved (Fig. 4). Potential explanations, which need to be investigated further, are, for example, an increased release of specific growth factors as a direct result from the shear stress or improved nutrient supply due to introducing active mass transfer by convection as previously demonstrated in hollow fiber membranes used for graft cell cultivation or blood cell oxygenators [38–40]. Overall, the data once more highlight the complex setting of skin physiology and are first indications that simple perfusion of skin models might be not sufficient to improve the skin barrier function.

5.6 ACKNOWLEDGEMENTS

The authors would like to thank Frida Gorreja (University of Padova) for the help with the graphical visualization of the perfusion bioreactor set-up and Ramona Kleeberger (Technical University Munich) for the assistance with the histological analysis of the skin models.

5.7 REFERENCES

1 European Commission: Seventh Report on the Statistics on the Number of Animals used for Experimental and other Scientific Purposes in the Member States of the European Union. 2013. DOI: 10.1017/CBO9781107415324.004

2 Seok J, Warren HS, Cuenca AG, Mindrinos MN, Baker H V, Xu W, et al.: Genomic responses in mouse models poorly mimic human inflammatory diseases. Proc Natl Acad Sci U S A 2013 Feb 11; DOI: 10.1073/pnas.1222878110

3 Perrin S: Preclinical research: Make mouse studies work. Nature 2014 Mar 27;507:423–5.

4 de Vries RBM, Leenaars M, Tra J, Huijbregtse R, Bongers E, Jansen JA, et al.: The potential of tissue engineering for developing alternatives to animal experiments: a systematic review. J Tissue Eng Regen Med 2015 Jul 15;9:771–778.

5 Reisinger K, Hoffmann S, Alépée N, Ashikaga T, Barroso J, Elcombe C, et al.: Systematic evaluation of non-animal test methods for skin sensitisation safety assessment. Toxicol Vitr 2015;29:259–272.

6 OECD: OECD Guideline No. 431 for the Testing of Chemicals: In Vitro Skin Corrosion: Reconstructed Human Epidermis (RhE) Test Method. 2004;

7 OECD: OECD Guideline No. 439 for the Testing of Chemicals: In Vitro Skin Irritation: Reconstructed Human Epidermis Test Method. 2010;

8 OECD: OECD Guideline No. 428 for the Testing of Chemicals: Skin Absorption: In Vitro Method. 2004;

9 Zöller NN, Kippenberger S, Thaçi D, Mewes K, Spiegel M, Sättler A, et al.: Evaluation of beneficial and adverse effects of glucocorticoids on a newly developed full-thickness skin model. Toxicol In Vitro 2008 Apr;22:747–59.

10 Hönzke S, Wallmeyer L, Ostrowski A, Radbruch M, Mundhenk L, Schäfer-

Korting M, et al.: Influence of Th2 Cytokines on the Cornified Envelope, Tight Junction Proteins, and β-Defensins in Filaggrin-Deficient Skin Equivalents. J Invest Dermatol 2016 Mar;136:631–639.

11 van Drongelen V, Haisma EM, Out-Luiting JJ, Nibbering PH, El Ghalbzouri A: Reduced filaggrin expression is accompanied by increased Staphylococcus aureus colonization of epidermal skin models. Clin Exp Allergy 2014 Dec;44:1515–24.

12 Berroth A, Kühnl J, Kurschat N, Schwarz A, Stäb F, Schwarz T, et al.: Role of fibroblasts in the pathogenesis of atopic dermatitis. J Allergy Clin Immunol 2013 Jun;131:1547–54.

13 Ponec M, Boelsma E, Gibbs S, Mommaas M: Characterization of reconstructed skin models. Skin Pharmacol Appl Skin Physiol 2002 Jan;15 Suppl 1:4–17.

14 Vávrová K, Henkes D, Strüver K, Sochorová M, Skolová B, Witting MY, et al.: Filaggrin deficiency leads to impaired lipid profile and altered acidification pathways in a 3D skin construct. J Invest Dermatol 2014 Mar;134:746–53.

15 Schäfer-Korting M, Bock U, Diembeck W, Düsing H-J, Gamer A, Haltner-Ukomadu E, et al.: The use of reconstructed human epidermis for skin absorption testing: Results of the validation study. Altern Lab Anim 2008 May;36:161–87.

16 Küchler S, Strüver K, Friess W: Reconstructed skin models as emerging tools for drug absorption studies. Expert Opin Drug Metab Toxicol 2013 Oct 5;9:1255–63.

17 Shiu Y-T: Mechanical Forces on Cells; in : Tissue Engineering and Artificial Organs - CRC Press Book. 2006.

18 Hronik-Tupaj M, Kaplan DL: A review of the responses of two- and three-dimensional engineered tissues to electric fields. Tissue Eng Part B Rev 2012 Jun 1;18:167–80.

19 Huh D, Matthews BD, Mammoto A, Montoya-Zavala M, Hsin HY, Ingber DE: Reconstituting organ-level lung functions on a chip. Science 2010 Jun

25;328:1662–8.

20 Ingber DE: Tensegrity II. How structural networks influence cellular information processing networks. J Cell Sci 2003 Apr 15;116:1397–1408.

21 Davisson T, Kunig S, Chen A, Sah R, Ratcliffe A: Static and dynamic compression modulate matrix metabolism in tissue engineered cartilage. J Orthop Res 2002 Jul;20:842–8.

22 Zhang X, Wang X, Keshav V, Wang X, Johanas JT, Leisk GG, et al.: Dynamic culture conditions to generate silk-based tissue-engineered vascular grafts. Biomaterials 2009 Jul;30:3213–23.

23 Hronik-Tupaj M, Kaplan DL: A review of the responses of two- and three-dimensional engineered tissues to electric fields. Tissue Eng Part B Rev 2012 Jun;18:167–80.

24 Ataç B, Wagner I, Horland R, Lauster R, Marx U, Tonevitsky AG, et al.: Skin and hair on-a-chip: in vitro skin models versus ex vivo tissue maintenance with dynamic perfusion. Lab Chip 2013 May 14; DOI: 10.1039/c3lc50227a

25 Griffith LG, Swartz MA: Capturing complex 3D tissue physiology in vitro. Nat Rev Mol cell Biol 2006;7:211–24.

26 Gysler A, Lange K, Korting HC, Schäfer-Korting M: Prednicarbate biotransformation in human foreskin keratinocytes and fibroblasts. Pharm Res 1997 Jun;14:793–7.

27 Eckl K-M, Alef T, Torres S, Hennies HC: Full-thickness human skin models for congenital ichthyosis and related keratinization disorders. J Invest Dermatol 2011 Sep;131:1938–42.

28 Küchler S, Henkes D, Eckl K-M, Ackermann K, Plendl J, Korting H-C, et al.: Hallmarks of atopic skin mimicked in vitro by means of a skin disease model based on FLG knock-down. Altern Lab Anim 2011 Oct;39:471–80.

29 Leist M, Hartung T: Inflammatory findings on species extrapolations: humans are

definitely no 70-kg mice. Arch Toxicol 2013 Apr;87:563–7.

30 Ponec M: Skin constructs for replacement of skin tissues for in vitro testing. Adv Drug Deliv Rev 2002 Nov 1;54 Suppl 1:S19-30.

31 van Smeden J, Boiten WA, Hankemeier T, Rissmann R, Bouwstra JA, Vreeken RJ: Combined LC/MS-platform for analysis of all major stratum corneum lipids, and the profiling of skin substitutes. Biochim Biophys Acta 2014 Jan;1841:70–9.

32 Mammoto T, Ingber DE: Mechanical control of tissue and organ development. Development 2010 May;137:1407–20.

33 Mammoto A, Mammoto T, Ingber DE: Mechanosensitive mechanisms in transcriptional regulation. J Cell Sci 2012 Jul 13;125:3061–3073.

34 Proksch E, Brandner JM, Jensen JM: The skin: An indispensable barrier. Exp Dermatol 2008;17:1063–1072.

35 McAleer MA, Irvine AD: The multifunctional role of filaggrin in allergic skin disease. J Allergy Clin Immunol 2013;131:280–291.

36 Cabanillas B, Novak N: Atopic dermatitis and filaggrin. Curr Opin Immunol 2016 May 17;42:1–8.

37 Candi E, Schmidt R, Melino G: The cornified envelope: a model of cell death in the skin. Nat Rev Mol Cell Biol 2005;6:328–40.

38 Nagy E, Hadik P: Analysis of mass transfer in hollow-fiber membranes. Desalination 2002;145:147–152.

39 Wickramasinghe SR, Garcia JD, Han B: Mass and momentum transfer in hollow fibre blood oxygenators. J Memb Sci 2002 Oct 1;208:247–256.

40 Bridge MJ, Broadhead KW, Hitchcock RW, Webb K, Tresco PA: A simple instrument to characterize convective and diffusive transport of single hollow fibers of short length. J Memb Sci 2001 Mar 1;183:223–233.

6 FINAL SUMMARY

Reconstructed *in vitro* skin disease models are a sound tool to enlighten pathophysiological factors and correlations. They enable to study isolated aspects of diseases and can lay the foundation for new therapeutic strategies. Although the link between FLG mutations and AD is well established, the overall impact is not completely understood. In the first section**,** it was shown that the skin surface pH is maintained at the physiological range around pH 5.5 independently of the FLG status. The missing UCA and PCA, acidic degradation products of FLG, correlated with the upregulation of NHE-1 and sPLA2 IIA in a time dependent manner. While the higher expression of NHE-1 has a direct impact on the proton concentration at the skin surface, the higher activity of sPLA2 enzymes leads to higher amounts of FFA. Both seem to compensate the missing acidic degradation products of FLG, even if FLG degradation products are descripted as an inferior contributor to the acid mantle in the literature. The higher amounts of FFA lead to an impaired skin lipid formation and consequently contribute to the weaker barrier function found in AD patients.

In general, the acidic skin surface pH is crucial for correct skin homeostasis. Common skin diseases often come with increased skin surface pH values. To further investigate the dependencies of the individual contributors to the acidic pH of the skin surface, an NHE-1 KD model and an FLG/NHE-1 KD model was established in the second section. The NHE-1 KD model showed a moderately but significantly elevated surface pH. This is in concordance with animal studies in the literature. The combined lack of FLG and NHE-1 did not lead to further pH increase. Consequently, it was confirmed that the FLG to histidine to UCA/PCA pathway is clearly less important regarding skin acidification. The lack of FLG is not the underlying main cause for higher pH values found in patients suffering from AD. Other, so far undiscovered, pathways may well be involved. In conclusion, it was shown that RNA interference can be used to knock down two genes simultaneously in skin constructs and that *in vitro* skin constructs are a suitable tool to investigate complex phenomena like pH regulation in skin.

Besides the characterization of the previously and newly established models, this thesis focused on improvement and further development of *in vitro* skin models. Reconstructed full-thickness skin models are already a suitable tool for toxicity testing and investigations of skin physiology and pathophysiology. Nevertheless, skin models demonstrate clear limitations. They neither include immune cells nor vasculature and

they exhibit a weaker barrier function and less mechanical resistances compared to *in-vivo* or *ex-vivo* skin. Especially, mechanical resistance and barrier function are strongly related to the growing conditions of *in vitro* skin models. The lack of mechanical forces and shear stress during cultivation have a distinct impact on tissue formation. To overcome some of those obstacles, a perfusion platform for skin cultivation was developed in the third section. The dynamic platform allows for a constant laminar medium flow below the dermis and still growth of the skin constructs at an air-liquid interface. The impact of different medium flow rates was investigated regarding histology, expression of skin differentiation factors and tight junction proteins as well as skin barrier function. The skin models grown in the dynamic bioreactor exhibit a two-fold thicker stratum corneum compared to conventionally grown control models. Expression of the skin differentiation markers FLG and involucrin, as well as the tight junction proteins claudin-1 and occludin is significantly increased in dynamical grown skin models. Unexpectedly, despite improved skin differentiation, the skin barrier function was not improved. Overall, the results highlight the complex setting of tissue engineering and could serve as a starting point for further improvements.

The overall results of the thesis provided new aspects of pathophysiology mechanisms of AD with the help of *in vitro* skin models. Furthermore, it was shown that the dynamic growing conditions of *in vitro* skin models have a significant influence on skin differentiation and generation.

7 APPENDIX

7.1 Filaggrin Deficiency Leads to Impaired Lipid Profile and Altered Acidification Pathways in a 3 D Skin Construct

Table 7-1 *Ct values for NHE-1 and sPLA2-isoforms in the skin constructs (mean ± SEM, n= 8).*

Gene	Ct-values
NHE-1	25.07 ± 0.74
$sPLA_2$ IB	32.66 ± 0.40
$sPLA_2$ IIA	37.92 ± 0.68
$sPLA_2$ IIF	30.80 ± 0.65
$sPLA_2$ V	31.11 ± 0.50
$sPLA_2$ XIIA	23.89 ± 0.43

Table 7-2 *Primer sequences for PCR.*

Gene	Primer sense 5'-3'	Primer antisense 5'-3
YWHAZ	AGACGGAAGGTGCTGAGAAA	GAAGCATTGGGGATCAAGAA
FLG	AAGGAACTTCTGGAAAAGGAATTTC	TTGTGGTCTATATCCAAGTGATCCAT
NHE-1	AGATCCAGGCTTCTCCCGGAC	CCATGTGCCTGGTACCCCTGGT
$sPLA_2$-IB	GCAATCACCTGTAGCAGCAA	GTCCAGGTTCTTGTGTGCCT
$sPLA_2$-IIA	ACCCTCCCTCCCTACCCTAAC	AATCTGCTGGATGTCTCATTCTGG
$sPLA_2$-IIF	GACCCACACCCTCTCTCC	GATGCTCTCCCTGCTTACG
$sPLA_2$-V	CTGCCTGGTTCCTGAGAGAG	CAACCCTGAGTTGGAGGAGA
$sPLA_2$-XIIA	TAGCTGTCGGCATCTCCTTT	GGCATGTGAAACAACAGTGG

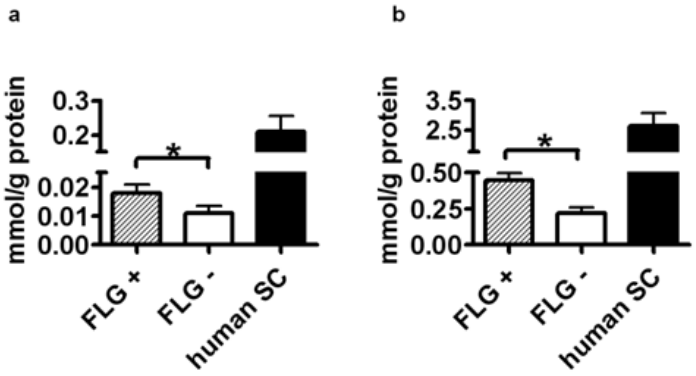

Figure 7-1 *FLG degradation products UCA (a) and PCA (b) concentrations after 14 days cultivation in FLG+, FLG- constructs and human samples determined using HPLC analysis. n=5, mean ± SEM, *p ≤ 0.05*

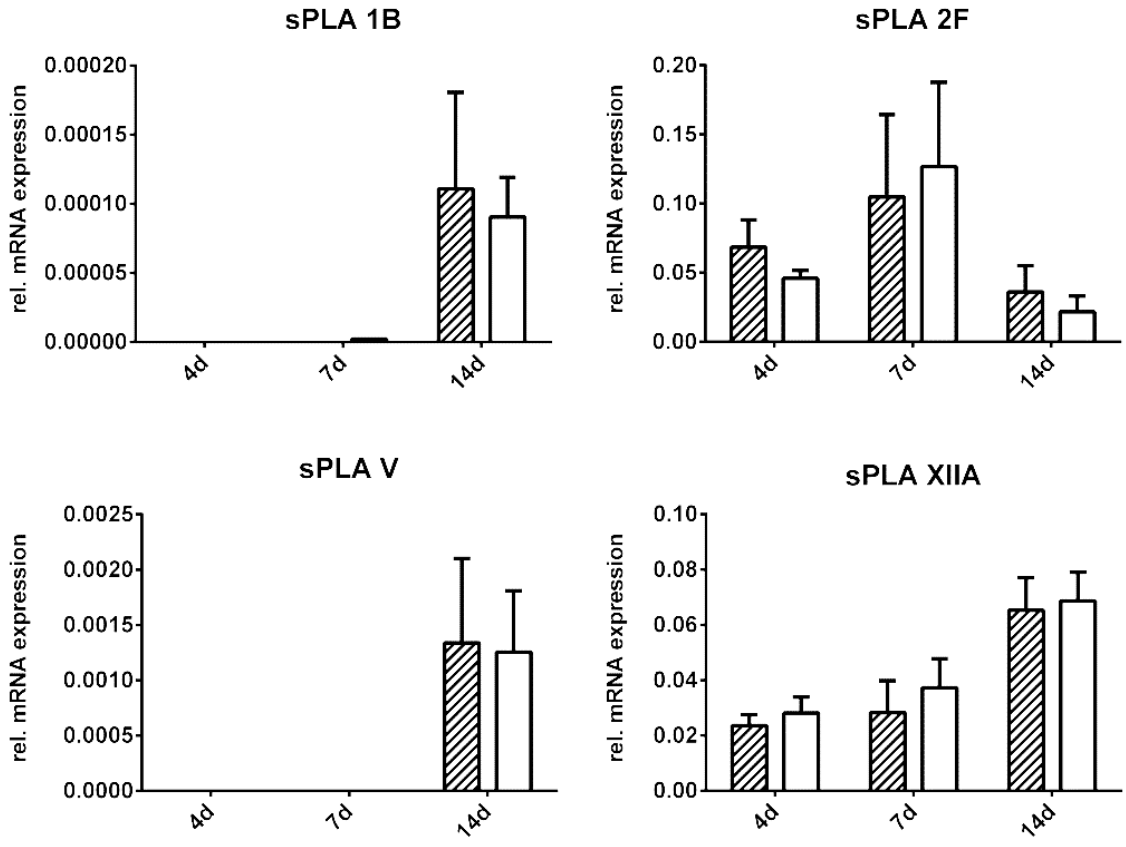

Figure 7-2 *Time dependent expression of sPLA 1B, 2F, V and XIIA in FLG+ (grey bars) and FLG- (white bars).*

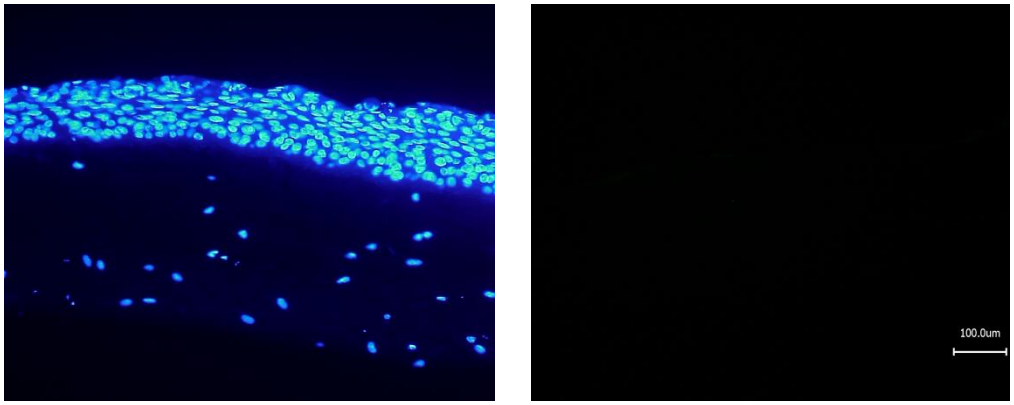

Figure 7-3 *Negative Control of NHE-1 immunostaining with (a) and without (b) DAPI staining of the nuclei.*

The skin samples were incubated without the primary antibody to ensure that the fluorescently labeled secondary antibody does not stain the samples unspecifically. These controls were run for sPLA2 immunostaining, too. No unspecific staining was detected, respectively.

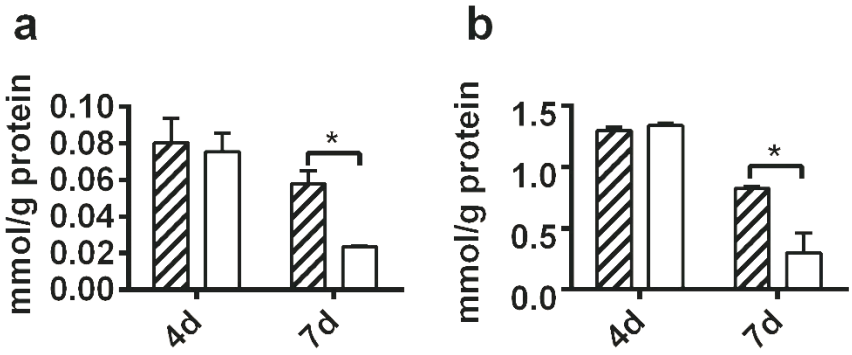

Figure 7-4 *FLG degradation products UCA (a) and PCA (b) concentrations after 4 and 7 days cultivation in FLG+ (striped bars) and FLG- constructs (blank bars) determined by HPLC analysis. n=2, mean ± SEM, *p ≤ 0.05*

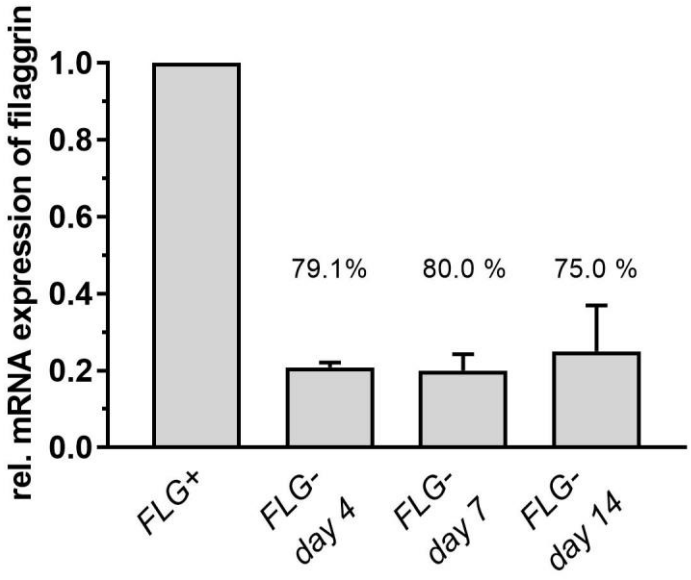

Figure 7-5 *Knock down efficiency in FLG- skin constructs at day 4, 7 and 14. n=4, mean ± SEM*

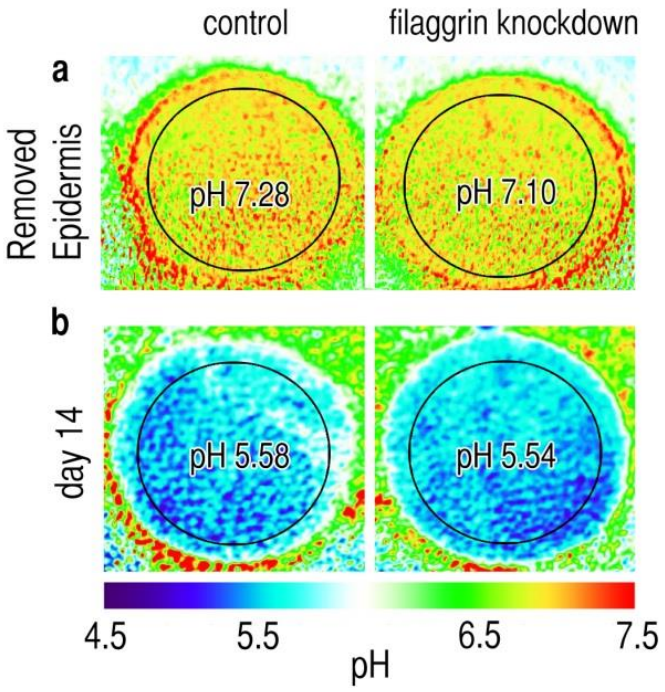

Figure 7-6 *pH measurement controls. To ensure that our pH measurement method can detect pH differences in skin constructs when present, we removed the epidermis from the skin constructs after the pH measurement of the skin surface. As expected, we detected a neutral pH proving that the method we are using detects pH differences when present.*

7.1.1 Supplementary Methods

7.1.1.1 Determination of PCA and UCA Levels

For PCA analysis, SC samples were incubated with 0.1 M KOH for 2 h at 25 °C. The extracts were neutralized, diluted with mobile phase and centrifuged for 10 minutes at 10.000 rpm. Isocratic elution with 20 mM ammonium formate containing 1.5 mM tetrabutylammonium hydroxide at pH 7.3 and 1 % acetonitrile was performed with a flow-rate of 0.4 ml/min. The concentration of PCA was quantified at 210 nm [2].

For UCA analysis, the SC samples were treated with 1 M KOH for 10 minutes. The supernatant was acidified, and the samples were diluted with the mobile phase. Isocratic elution with 20 mM potassium dihydrogen phosphate containing 5 mM heptanesulphonic acid at pH 3.7 and 7 % acetonitrile was performed with a flow-rate of 0.4 ml/min [3]. UCA concentration was measured at 270 nm. For analysis, a 5 µm reversed-phase end-capped C18 HPLC column (Phenomenex, Aschaffenburg, Germany) was used.

7.1.1.2 sPLA$_2$ activity assay

To assess the sPLA$_2$ activity in *FLG*+ and *FLG*- constructs, an sPLA$_2$ activity kit (Enzo Life Sciences, Lause, Switzerland) was used. The assay was performed according to the manufacturers' protocol (http://static.enzolifesciences.com/fileadmin/files/manual/ADI-907-002_insert.pdf). A standard curve was run for each assay. R^2 was at least 0.99, respectively.

7.1.1.3 Skin pH Measurements

The pH-indicator fluorescein isothiocyanate (FITC, λ_{ex} 507 nm, λ_{em} 542 nm) was covalently linked to aminoethylcellulose to form sensor particles (FITC-AC). The reference dye ruthenium(II)-tris(4,7-diphenyl-1,10-phenanthroline) was incorporated in oxygen-impermeable polyacrylonitrile particles (Ru(dpp)$_3$-PAN; λ_{ex} 468 nm, λ_{em} 605 nm). For further details, we refer to our methods papers [4,5].

FITC-AC and Ru(dpp)$_3$-PAN were mixed in a ratio of 3/1 (w/w) and dispersed in solution (15 mg particles per mL) consisting of polyurethanehydrogel (type D4; 5% w/v)

in ethanol/water (90/10 v/v). This mix was spread on a transparent PVdC foil (thickness 12.5 µm) with a knife-coating device to form a 120-µm-thick film. After evaporation of the solvent, the sensor layer was 6-µm thick. For RGB imaging, a 460-nm LED array was mounted on a commercial camera and served to excite the luminescent sensor. Emitted light was filtered by an OG510 glass filter (Schott, Mainz, Germany) and collected by the RGB-chip of the camera. pH-dependent signals are stored in the green channel, and pH-independent reference signals are stored in the red channel of the RGB image [1]. The green/red ratio (*R*) of luminescence intensities provides a referenced pH signal for each pixel. Foils were calibrated, and a five-parametric sigmoidal fit was performed. The resulting equation was then solved for pH, thus enabling us to calculate pH (for every pixel) based on *R*. Sensor foils were preconditioned in Ringer´s solution for 15 min prior to use. The foils were then gently applied to the skin constructs and allowed to slowly adapt to tissue surfaces by adhesion forces. Luminescence intensity ratios *R* were obtained for every pixel on the skin construct surfaces. Means of pH-dependent luminescence intensity ratios *R* within anular regions of interest (ROI; each comprising 6,249 pixels in the center of the image) were then computed. From the respective mean *R* value, mean pH for the ROI was calculated. Calculations and pseudocolor image processing were done with ImageX software (Microsoft Corporation) and ImageJ (http://rsbweb.nih.gov/ij/). For *in vitro* skin constructs, pH measurements using the glass electrode are not possible as the procedure would cause serious damage the skin models and, thus, no accurate measurement of the surface skin pH is possible.

The validation of the method for skin surface pH measurement is described in detail in the paper of Schreml *et al*., "*2D luminescence imaging of pH in vivo"* 2011 in *Proceedings of the National Academy of Sciences of the United States of America*.

Briefly, it was demonstrated that by increasing the depth of measurement (done by removing the epidermis layer-by-layer by tape-stripping) the pH of the skin increases in deeper dermal layers. The pH data were compared to values obtained by classic flat-bottom glass electrode measurements without detecting significant differences. In general, a high precision was achieved for measuring the normal skin pH (n = 10) with the *in vivo* setting: relative standard deviation of luminescence imaging 4.32 ± 1.35 %, relative standard deviation of glass electrode 4.53 ± 2.04 %. A Bland–Altmann mean

difference plot (see: Bland JM, *et al.,* 1986) was created for method comparison, showing an excellent concordance (96 % of the measurements were within the 95% confidence interval; Krippendorf coefficient K = 0.98). Hereby, it was proven that the pH sensor can be reliably used *in vivo* and, thus, also gives reliable results for the skin constructs. In general, this technique can visualize pH differences with a resolution of ≤ 5 µm [5]. Furthermore, the method is able to provide 2D mappings of pH values, showing distinct spatial differences. Compared to the values obtained with the one-spot measurement technique (the glass electrode), the ROI is defined as the whole wound area [5].

7.1.2 REFERENCES

1 Martin Bland J, Altman D: STATISTICAL METHODS FOR ASSESSING AGREEMENT BETWEEN TWO METHODS OF CLINICAL MEASUREMENT. Lancet 1986 Feb;327:307–310.

2 Kezic S, O'Regan GM, Yau N, Sandilands A, Chen H, Campbell LE, et al.: Levels of filaggrin degradation products are influenced by both filaggrin genotype and atopic dermatitis severity. Allergy 2011 Jul;66:934–940.

3 Schwarz W, Langer K, Haag A: High-performance liquid chromatographic determination of (Z)- and (E)-urocanic acid in human skin. J Chromatogr B Biomed Sci Appl 1984 Jan;310:188–192.

4 Meier RJ, Schreml S, Wang X, Landthaler M, Babilas P, Wolfbeis OS: Simultaneous photographing of oxygen and pH in vivo using sensor films. Angew Chem Int Ed Engl 2011 Nov 11;50:10893–6.

5 Schreml S, Meier RJ, Wolfbeis OS, Maisch T, Szeimies R-M, Landthaler M, et al.: 2D luminescence imaging of physiological wound oxygenation. Exp Dermatol 2011 Jul;20:550–4.

7.2 Publications and Poster Presentations associated with the Thesis

Küchler S, Strüver K, Friess W: Reconstructed skin models as emerging tools for drug absorption studies. Expert Opin Drug Metab Toxicol 2013 Oct 5;9:1255–63.

Vávrová K, Henkes D, Strüver K, Sochorová M, Skolová B, Witting MY, et al.: Filaggrin deficiency leads to impaired lipid profile and altered acidification pathways in a 3D skin construct. J Invest Dermatol 2014 Mar;134:746–53.

Strüver K, Meier RJ, Schreml S, Friess W, Küchler S; Filaggrin Deficiency Modulates Skin Acidification Pathways in a 3D Skin Construct, 9th World Meeting on Pharmaceutics, Biopharmaceutics and Pharmaceutical Technology, Lisbon, Portugal, March 31 - April 3, 2014

Strüver K, Meier RJ, Schreml S, Friess W, Küchler S; Filaggrin Deficiency is not the Underlying Cause for Elevated pH Values in Patients with Atopic Dermatitis, 14th International Conference Perspectives in Percutaneous Penetration, La Grande Motte, France, April 23-25, 2014

Strüver K, Kleeberger R, Gorreja F., Friess W., Hedtrich S; Dynamic Cultivation of 3D Skin Models in a Perfusion Chamber, 9th World Congress on Alternatives and Animal Use in the Life Science, Prague, Czech Republic, August 24-28, 2014

Strüver K, Friess W, Hedtrich S: Development of a Perfusion Platform for Dynamic Cultivation of in vitro Skin Models. Skin Pharmacol Physiol 2017;30:180–189.